BUSITEMA UNIVERSITY
Pursuing Excellence

ANALYSIS OF THE RADIOLOGICAL CONTENT IN SELECTED FLOOR TILES AND CEMENT BRANDS COMMONLY USED IN BUILDING CONSTRUCTION IN TORORO, UGANDA

BY

WAISWA SAMILU (BSc ED)

BU/GS20/MPS/10

A RESEARCH DISSERTATION SUBMITTED TO THE DIRECTORATE OF GRADUATE STUDIES, RESEARCH AND INNOVATIONS IN PARTIAL FULFILLMENT OF THE REQUIREMENTS FOR THE AWARD OF THE DEGEREE OF MASTER OF SCIENCE IN PHYSICS OF BUSITEMA UNIVERSITY

AUGUST, 2024

DECLARATION

I **Waiswa Samilu**, declare that this dissertation is entirely my original work except when proper acknowledgment and reference has been made for other people`s work, I certify that this work has never been submitted to this university or any other organization for funding or for any award.

Name: Waiswa Samilu

Registration Number: **BU/GS20/MSP/10.**

Signature: 

Date: 15th / 08 / 2024

APPROVAL

This study titled **"Analysis of the Radiological Content in Selected Floor Tiles and Cement Brands commonly used in Building Construction in Uganda"** was conducted under our guidance and hereby recommend it for examination in partial fulfillment of the requirements for the award of Degree of Masters of Science in Physics of Busitema University.

1. **Assoc. Prof. Saphina Biira**
   Department of Physics,
   Faculty of Science and Education,
   Busitema University
   Signature..... Date..30/08/2024.....

2. **Dr. Rashidah Akoba**
   Department of Physics,
   Faculty of Science and Education,
   Busitema University
   Signature..... Date..30th/08/2024.....

DEDICATION

I give all credit for this research to God Almighty, who is also my powerful support system, inspiration, knowledge, and understanding. In this program, He has been the source of my strength, and it is only on His wings that I have succeeded. This work is also dedicated to my parents Mr. Mukoova Bakaali and Mrs. Nabirye Lukiya Mukoova. To my friends, Mrs. Tracy Pirnack Hess and Dr. Carl Hess, to my spouse, Mrs. Namukobe Fazira, and our children, God bless you.

ACKNOWLEDGEMENT

First and foremost, I thank God , the Almighty for endowing his immense blessing that is helping me in each step of my progress towards the successful completion of my research work. I am deeply grateful to my research supervisor Assoc. Prof. Saphina Biira and Dr. Akoba Rashidah for the canalized guidance, dedication, constant inspiration, innovative ideas and encouragement which led me in the right path in doing this research work.

I convey my heartfelt thanks to my friends Dr. Carl Hess, Applied physics Stanford University and Mrs. Tracy Pirnack, MS Industrial Engineering Stanford University for the kind financial support and for providing me with their valuable suggestions to complete the work successfully. I wish to express my deep sense of appreciation to Musana Community Development Organization (MCDO) for the financial support and encouragement in this study.

Last I wish to express my sincere thanks to all my family members, Mr Ibanda Shafic and Ms Nalubowa Daphalini and friends, Mr Ekenyai John, Mr Jingo Benjamine, Mr Waibi Rogers and Fr. Kajubi Henry for their timely help, moral support and encouragement.

TABLE OF CONTENTS

ABSTRACT

In this study, cement and floor tiles that are frequently used in building construction were investigated using a NaI (TI) detector in gamma ray spectrometry to identify the gamma ray emitting radionuclides of Ra-226, Th-232, and K-40 as well as radiological parameters of radionuclide activities concentration, radium equivalent activity, absorbed gamma dose, annual effective dose, external and internal hazard indices, excess lifetime cancer risk, and annual gonadal equivalent dose. In the study, samples of cement and floor tiles from different cement and tile manufacturers were evaluated. Using the NaI (TI) detector, naturally occurring radionuclides of radium (Ra-226,), thorium (Th-232) and Potassium (K-40) were found in all the analyzed samples. The radionuclide activity concentration of Ra-226, Th-232, and K-40 in cement were in the range of 10.2± 0.7 $Bqkg^{-1}$ to 86.1± 4.3 $Bqkg^{-1}$, 28.9± 1.3 $Bqkg^{-1}$ to 105.3± 2.5 $Bqkg^{-1}$ and 334.2± 6.4 $Bqkg^{-1}$ to 508.5± 7.9 $Bqkg^{-1}$, with average values of 31.2± 1.7 $Bqkg^{-1}$, 61.9± 1.9 $Bqkg^{-1}$ and 463.1± 7.5 $Bqkg^{-1}$ respectively. Save for Ra-226 whose average activity concentration was less than 40 $Bqkg^{-1}$ the global average value, the activity concentrations of Th-232 and K-40 recorded were higher than 35 $Bqkg^{-1}$ and 400 $Bqkg^{-1}$, the global recommended dose limits respectively. The average value of the absorbed dose rate, annual effective dose, radium equivalent activity, external and internal indices in the analyzed cement samples were 71.1± 2.2 $nGyhr^{-1}$, 0.349± 0.011 $mSvy^{-1}$, 155.3± 5.1 $Bqkg^{-1}$, 0.42 and 0.50 below the maximum permissive dose limit of 84 $nGyhr^{-1}$, 1.0 $mSvy^{-1}$, 370 $Bqkg^{-1}$ and 1(unity) respectively. The recorded average values of the excess life time cancer risk and annual gonadal equivalent dose were $1.22x10^{-3}$ and 0.50 $mSvy^{-1}$ which are above the recommended dose limit of $0.29x10^{-3}$ and 0.3$mSvy^{-1}$ respectively.

In the floor tile samples, the concentration of radionuclide activity for Ra-226, Th-232, and K-40 ranged from 13.2± 0.8 $Bqkg^{-1}$ to 49.0± 2.4 $Bqkg^{-1}$, 38.7± 1.3 $Bqkg^{-1}$ to 149.5± 3.7 $Bqkg^{-1}$, and 192.9± 2.6 $Bqkg^{-1}$ to 526.7± 8.0 $Bqkg^{-1}$, with average values of 30.8± 1.4 $Bqkg^{-1}$, 95.8± 2.3 $Bqkg^{-1}$, and 388.6± 6.2 $Bqkg^{-1}$, respectively. Th-232 was found to have average activity concentration above the global recommended dose limits of 35 $Bqkg^{-1}$, with the exception of Ra-226 and K-40, whose average activity concentrations were less than the global average value of 40 $Bqkg^{-1}$ and 400 $Bqkg^{-1}$, respectively. In the examined floor tile samples, the average values of the absorbed dose rate, annual effective dose, radium equivalent activity, external and internal indices were 88.3± 2.3 $nGyh^{-1}$, 0.43± 0.011 $mSvy^{-1}$, 197.7± 5.2 $Bqkg^{-1}$, 0.534, and 0.458,

respectively, which are below the maximum permissive dose limit of 84 $nGyhr^{-1}$, 1.0 $mSvy^{-1}$, 370 $Bqkg^{-1}$ and 1(unity). The average reported values of the excess life-time cancer risk and the annual gonadal equivalent dose were $1.52x10^{-3}$ and 0.619 $mSvy^{-1}$, respectively beyond the suggested dosage limit of $0.29x10^{-3}$ and 0.3 $mSvy^{-1}$. Due to some samples showing higher activity concentrations than the global average, further studies are recommended to confirm these findings and assess additional radiological parameters like alpha and gamma indices. Future research should include more types of building materials. High radionuclide activity in some samples poses significant health risks, such as increased cancer rates, radiation sickness, genetic damage, respiratory problems, reproductive issues, and cardiovascular disease, particularly for those living in buildings made with such materials.

LIST OF FIGURES

LIST OF TABLES

LIST OF ACRONYMS AND ABBREVIATIONS

AEC	Atomic energy council
AED	Annual effective dose
AGED	Annual gonadal equivalent dose
ALARA	As low as reasonably achievable
DNA	Deoxyribonucleic acid
EC	European Commission
ED	Equivalent dose
EDE	Effective dose equivalent
ELCR	Excess lifetime cancer risk
IAEA	International Atomic Energy Agency
ICRP	International Commission on Radiological Protection
NORM	Naturally occurring Radioactive Materials
NPA	National Planning Authority
SDG	Sustainable Development Goals
UBOS	Uganda Bureau Of Statistics
UN	United Nations
UNBS	Uganda National Bureau of Standards
UNSEAR	United Nation Scientific Committee on the Effect of Atomic Radiation.
WHO	World Health Organisation

CHAPTER ONE: INTRODUCTION

1.1 Background

Human beings and other living organisms are constantly subjected to ionizing radiation from radionuclides in minerals and raw materials of natural origin. Naturally occurring radioactive materials (NORM) are the radionuclides of uranium (U-238) and thorium (Th-232) decay series, and radioactive potassium (K-40), which present a radiological risk to humans (Kapanadze et al., 2019a). NORM is the result of specific human activities such as mineral extraction from under the ground, quarrying, and agriculture activities that enhance human exposure to the radionuclides that emerge from the Earth's crust. Therefore, these radionuclides can be found in water, air, food and building materials that a human body always interacts with for living (IAEA, 1989; Volume, 2006). Given that humans spend a significant portion of their lives indoors, it becomes crucial to assess the potential radiation exposure they may face from the very materials used to construct their homes and workplaces.

On average, an individual spends 80% of their time indoors (Al-Sewaidan, 2019; Smith, 2014). Therefore, it is essential to estimate how much radiation exposure from building materials an individual may experience. Building materials such as cement, tiles, bricks, and many others are normally extracted from rocks, sand, and soil and contain varying levels of radionuclides depending on the raw materials from which they are derived (Dairiki, 1982; Kapanadze et al., 2019b). The variation in the radionuclide levels in the building materials implies a variation in their radiation hazards via external and internal exposure. External exposure is related to direct gamma radiation emitted from isotopes in the Uranium and Thorium decay series, as well as from the main potassium gamma line. Internal exposure is caused by the inhalation of the radioactive inert gases radon (Rn-222), thoron (Rn-220), and their short-lived progeny radioisotopes such as polonium (Po-218), lead (Pb-214), bismuth (Bi-214), and polonium (Po-214) (J. A. Ademola & Oguneletu, 2005; Mammba et al., 2021).

Health hazards related to exposure to radiation from building materials have been studied by different researchers worldwide (J. A. Ademola & Oguneletu, 2005; Döse, 2016; Joel et al., 2019; Lyngkhoi & Nongkynrih, 2020; Mammba et al., 2021; Nalianya et al., 2022; Penabei et al., 2018; Righi et al., 2009; Vañó et al., 2015). In addition, international organizations such as

the United Nations Scientific Committee on the Effects of Atomic Radiation (UNSCEAR), the European Commission (EC), the International Atomic Energy Agency (IAEA) and the International Commission on Radiological Protection (ICRP) have produced several publications regarding limits on the activity concentrations in some building materials and have issued restrictions on materials with excessive levels of radioactivity (Commission, 2004; Mittal et al., 2016; Nations et al., 2010; United Nations (UN), 2013). These international standards and restrictions encourage local authorities and manufacturers to monitor and control the radiological content of the building materials like cement and tiles. These guidelines help ensure that building practices prioritize public health by minimizing radiation exposure. In Uganda, the radiological content of building materials like cement and tiles is a growing concern; especially as the construction industry expands, particularly in areas like Tororo. The region's natural resources, such as limestone and phosphate, are extensively mined and processed for cement production, leading to potential radiological implications.

Most published studies on the health effects of radiation from building materials over the past decades have not shown significant findings (Adewoyin et al., 2019; Meindinyo et al., 2017; UN, 2013). However, the accumulation of radioactivity from building materials over time combined with poor ventilation may increase the probability of the occurrence of cancer and other health disorders in the building occupants. Therefore, the achievement of Sustainable Development Goal (SDG) 3: "Good health and wellbeing" may be severely impacted by this effect (Janouˇ, 2016) and Vision 2040 in Uganda (National Planning Authority (NPA), 2020).

Unfortunately, some studies conducted as indicated in Table 1.1, reported that the activity concentrations of Radium-226, Thorium-232, and Potassium-40 in some selected tiles and cement types were above the recommended world average values of 40 $Bqkg^{-1}$, 35 $Bqkg^{-1}$ and 400 $Bqkg^{-1}$ for Ra-226, Th-232 and K-40 respectively (Assembly, 2016; Durusoy & Yildirim, 2017; Kapanadze et al., 2019b; Nations et al., 2013b; Vañó et al., 2015). Given the potential health risks associated with exposure to elevated levels of these radionuclides, it is important to assess whether the building materials in Tororo town meet the safety standards. This is because similar building materials are found on the Ugandan market, however very limited data exists about their radiological content. Thus this study set in to examine the radiological content of the commonly used ceramic floor tiles and cement brands in Uganda. Given this context, the rapid

growth in Uganda's construction industry further underscores the importance of understanding the radiological content of these materials.

Table 1.1: Showing the Reported Activity concentrations in studied ceramic tiles and cement types

Country	**Activity Concentration ($Bqkg^{-1}$)**			**Author(s)**	**Material**
	Ra-226	Th-232	K-40		
China	131.40	106.50	866.80	(Joel et al., 2019; Xinwei, 2004)	Ceramic
Poland	35.34±9.11	47.70±5.34	732.57±68.52	(Łukaszek-Chmielewska et al., 2018)	
Italy	59.50 ±4.20	79.00 ±8.3	940.0 ±115.1	(Joel, Maxwell, Adewoyin, Ehi-Eromosele, et al., 2018)	
Nigeria	37.50 ±3.60	101.5±8.20	670. 0 ±70.2	(Joel et al., 2019)	
Spain	30.50 ±4.10	64±4.10	650. 0 ±81.4	(Maxwell et al., 2019)	
Kenya	11. 00 ±0.55	109±5.48	1574. 0 ±78.7	(Nalianya et al., 2022)	
India	104.70	24.10	432.20	(Consultation et al., 2020)	Cement
Brazil	188.80	58.50	564.00	(H. Of & Extensions, 2008)	
Malaysia	188. 0 ±27	23. 00 ±1.0	823±69.0	(Consultation et al., 2020)	

According to (Census, 2006; NPA, 2020; Uganda Burea of Standards (UBOS), 2020), Governmental expansion of public and private structures is increasing at all levels in Uganda, and the population is growing quickly, driving up the demand for more housing and public facilities as it is indicated in Figure 1.1 particularly for the central part of Tororo town in Uganda. As a result, it is anticipated that the demand for cement, tiles, and other building materials will continue to rise. This may be one of the factors in the growth and expansion of the cement and tile industries in Uganda and perhaps elsewhere in the world (UBOS, 2022). This growth presents both opportunities and challenges. On one hand, it drives economic development; on the other, it necessitates greater scrutiny of the radiological safety of materials to protect public health.

Figure 1.1: Shows Infrastructural Development in the Central Section of Tororo Town.

Presently, the most common material tile used in Uganda dwellings is ceramic, with various new brand names entering the market, both local and imported. In addition, cement is still an essential material in the construction of houses and buildings all over the country. The cement sector in Uganda is the third largest after the food and textile industries, with a cement production capacity of over 7 million tons and a local demand of approximately 2.4 million tons (C. Of & Establishments, 2011; UBOS, 2017). In the case of ceramic tiles, the UBOS report (C. Of & Establishments, 2011) indicated that the production capacity of floor and wall tiles is estimated to be approximately 62,400 square meters per day with the capacity planned to triple to 1,872,000 square meters per day, following the increasing local and international demand.

Given the variety of uses for tiles and cement in Uganda's building and construction sector, as well as the average person's 80% indoor time (Nations et al., 2013a), understanding the radiological content and associated hazards of tiles and cement is therefore essential. The aim of this study was therefore to identify the natural radionuclide content of commonly used floor tiles and cement brands available in local markets in Uganda and estimate the potential radiological hazard to the dwellers of buildings constructed using such cements and tiles. The data from this study can be used by Ugandan authorities for the development and implementation of radiation protection guidelines for the use and management of cements and tiles in the country. The data in this work could also assist builders in Uganda in considering radiological factors when making choices for cements and tiles rather than the traditional factors of cost and availability. More so, the data obtained in this study can also add to the global database of radioactivity content in

cement and tiles as building construction materials. To achieve this, radiological technologies were used.

1.2 Problem Statement

The rising use of modern building materials like tiles and cement has increased construction with materials that may contain naturally occurring radionuclides such as Uranium, Thorium, Potassium, and their decay products. Since most people spend about 18 hours indoors daily, potential radiation exposure is significant. However, the radiation levels in these materials have not been adequately assessed. No radiological data associated with building materials commonly used in Tororo district, Uganda is available to establish the safety of using the materials for construction purposes. This study aimed to measure these radiation levels and assessed the risk of human exposure to the commonly used cement and tiles materials in this district. Tororo was selected for our study as it is reported to have higher cases of cement factories when compared with other districts of the country. The knowledge of the amount of activity of radionuclides present in building materials and the radiological hazards assessed by the radiological parameters associated with them will, therefore, serve as the basic guidelines for the use of these materials and protect the population from avoidable radiation exposure risks.

1.3 Aim of the Study

The goal of this study is to assess radionuclide concentrations and associated health hazard indices in order to determine the radiation dose levels and the health implications, in homemade and imported floor tiles and cement used in Tororo town.

1.4 Specific Objectives

This study was guided by the following objectives;

(a) Identify gamma ray-emitting radionuclides in cement and tile samples using a NaI detector.
(b) Determine the activity concentration of the identified radionuclides in the samples.
(c) Calculate the annual effective dose, Excess Lifetime Cancer Risk (ELCR), and Annual Gonadal Equivalent Dose (AGED) of the cement and tile samples.

(d) Assess radium equivalent activity and radiological health hazard indices for internal and external exposure from the cement and tile samples.

1.5 Significance of the Research

The findings of this study are poised to play a critical role in guiding key stakeholders, including the Ministry of Health, the National Environment Management Authority (NEMA), the Ministry of Housing and Urban Development, the Uganda Bureau of Standards, and the Atomic Energy Council (AEC). These results will enable these entities, along with other governmental policymakers and the general public, to implement precautionary measures against radiation exposure from cement and floor tiles used in construction. Additionally, the data generated by this research will serve as a valuable reference for assessing potential changes in environmental radioactivity resulting from nuclear activities, industrial processes, and other human interventions. The study's outcomes are also expected to prompt revisions to building codes and construction standards, mandating the testing of building materials for radiation before their approval and use. This will encourage builders to prioritize the selection of materials with lower radiation levels, particularly in residential and public structures, thereby reducing health risks associated with radiation exposure.

1.6 Justification of the Study

Building materials contain minerals naturally associated with radionuclides such as uranium, thorium, and radium. Living in buildings made of such materials can result in external and internal exposure to radiation. Radionuclides, such as radon which is a decay product of uranium ,can be inhaled and accumulate in the body, affecting sensitive tissues and organs such as the lungs, kidneys, and liver. Therefore, in addition to monitoring background radiation in the environment, it is crucial to continuously assess and monitor radiation levels in commonly used building materials. The results from these assessments can inform mitigation measures to protect the population from avoidable radiation exposure.

1.7 Scope of the Study

This study focused on determining the radiological hazard levels of gamma rays emitted by radionuclides in selected floor tiles and cement brands commonly used in Tororo town, Uganda.

Given that cement and tiles are derived from rocks and soils which are primary sources of natural radionuclides, these materials are particularly susceptible to radiological contamination. This study was conducted in Tororo town, a rapidly developing town in eastern Uganda, The research provides critical first-hand data on the radiological content of locally sourced building materials (cement and floor tiles). The study specifically identifies gamma-ray-emitting radionuclides in the samples and measures variables such as activity concentrations, absorbed dose rates, annual effective doses, Annual Gonadal Equivalent Dose (AGED), Excess Lifetime Cancer Risk (ELCR) and both internal and external radiological hazard levels. The study offers valuable insights into the safety of building materials in Uganda, aligning with global standards and addressing a significant gap in local data. It was conducted for eight (8) months from November 2022 to June 2023.

CHARPTER TWO: LITERATURE REVIEW

2.0 Introduction

The literature review for this study covered concepts related to radioactivity and materials containing radioisotopes. It described the nature and properties of naturally occurring ionizing radiation from terrestrial sources, such as soils and rocks, and the process of radioactive decay. The review examined rock types and mineral compositions in igneous rocks that contain abundant radioactive nuclides like potassium, uranium, thorium, and cesium. It also covered the disintegration and decay series of radioactive nuclides. The biological effects of ionizing radiation on the body, including ionization, excitation of body tissues, molecular damage, and DNA damage, were described. Additionally, the review discussed radiological dosimetric quantities and parameters such as absorbed dose rate, annual effective dose equivalent, and radiological hazard indices. The detection and measurement of ionizing radiation using scintillation detectors and gamma-ray spectrometry were also included in the literature review.

2.1 Nature and Properties of the Ionizing Radiations

Radiation is energy emitted from a source, propagating through space at the speed of light, and is characterized by oscillating electric and magnetic fields. Radiation can be classified as ionizing or non-ionizing based on its interaction with matter. Ionizing radiation, including gamma rays, X-rays, alpha particles, and beta particles, possesses sufficient energy to ionize atoms and molecules, leading to the formation of charged particles. Non-ionizing radiation, encompassing visible light, infrared, ultraviolet, microwaves, and radio waves, lacks the energy required to ionize atoms or molecules and instead induces excitation or vibrational changes in the medium through which it traverses (Ng, 2003).

Matter contains atoms, which may be stable or unstable. Unstable atoms with extra energy and nucleons decay by releasing ionizing radiation. These ionizing radiations include beta (β), gamma (γ), and alpha (α). Of the three types of ionizing radiation, alpha radiation is positively charged, has the most ionizing strength, and has the least penetrating power. Since they are ionizing and can ionize human cells when they enter the body, they have the potential to do significant harm. Highly energetic electrons, known as beta radiation, are released from an atom's nucleus. Beta radiation can pass through the skin more readily than alpha radiation since

it has high penetrating power. They have the least ionizing power than alpha radiation, but they are still dangerous. Gamma radiation comprises the most energetic electromagnetic waves with an extremely high frequency. It possesses the highest penetrating capability among the three types of ionizing radiation. While it is the least ionizing, it carries significant energy and can traverse thin lead and dense concrete. Due to their lack of charge, gamma rays remain unaffected by electric and magnetic fields. Natural sources of gamma radiation include radioactive minerals present in the environment and cosmic radiation.

Cosmic radiations originate from space, (Granger et al., 2013). Cosmic radiation is the minor source of external exposure to gamma radiation; the major source of natural exposure is from terrestrial sources. Cosmic radiation is composed of subatomic particles from outer space, mostly energetic protons, electrons, gamma rays, and X-rays. Cosmic rays are categorized into two types: primary and secondary cosmic rays (Strong et al., 2007). Cosmic rays are said to be primary cosmic rays if they have not interacted with matter in the earth's atmosphere, lithosphere, or hydrosphere. Primary cosmic rays are composed of protons (about 85%) and alpha particles (about 14%) with much smaller fluxes (< 1%) of heavier nuclei (Chiozzi et al., 2000). Secondary cosmic rays are produced by interactions of primary rays with the atmosphere and consist largely of subatomic particles such as pions, muons, and electrons (Granger et al., 2013). At sea level, the most detected cosmic radiation consists of secondary cosmic rays, with some 68% of the flux accounted for by muons and 30% by electrons (Elgazzar & Kazem, 2015; Shahbazi-Gahrouei et al., 2013). Less than 1% of the flux consists of protons. Primary cosmic rays are mainly positively charged and usually carry large kinetic energy of order of 2 to 30 GeV (Bhattacharjee & Sigl, 2000). These large energies of primary cosmic rays enable them to literally blast apart atoms in the earth's atmosphere upon collision. The intensity of cosmic rays increases with altitude, latitude and solar flare activities (Goodhead, 1989). When cosmic radiations interact with the earth's atmosphere a variety of radionuclides such as Sodium- 22 of half-life of 2.605 years and Carbon-14 of half-life of 5715 years are produced. However , the contributions of these radionuclides to radiation absorbed dose rate is not significant (Okello, 2013). At sea level, the average absorbed dose rate arising from exposure to cosmic ionizing radiations is 31 $nGyh^{-1}$ which is equivalent to an annual effective dose equivalent rate of 0.270 $mSvy^{-1}$ (Nations et al., 2013a). Terrestrial radiation is the major source of ionizing radiations. It arises from terrestrial or primordial radionuclides in the earth crust. Soils, rocks, air, water, food

and building materials (Mittal et al., 2016) contain primordial radioactive isotopes from which ionizing radiations originate. They are mainly Uranium-238, Thorium-232, radionuclides in their decay series and Potassium-40. Primordial radionuclides have half-lives of order of 100 million years, comparable to the age of the earth. Uranium and Thorium can initiate a chain of radioactive decay into daughter radionuclides. Although the daughter radionuclides are short lived they are distributed in the environment because they are continually being emitted by the long lived parent radionuclide. Radioactive isotopes are chemically bound to the earth's crust and can be a source of radiation exposure if exposed to the earth surface or released by natural processes such as earthquake, volcanic and human activities such as mining and construction (Matolin et al., 2003). The isotopes are present till today due to their long half-lives.

Potassium-40, Uranium- 235, Uranium- 238, Caesium- 137 and Thorium-232 and their decay products are among the radio-isotopes that produce high energy gamma rays. Several activities, practices such as use of fertilizers, use of radioisotopes in medical diagnosis, nuclear accidents, processing industries and construction industry that use large volumes of raw materials containing natural radionuclides exposes people and other radiation workers in nuclear establishments, hospitals and construction to ionizing radiations (Sidique et al., 2022).

2.2 Mineral Composition in Rocks and Soil

Soil is a three-dimensional, dynamic natural body occurring on the surface, consisting of rock and mineral particles mixed with decayed organic matter (Publications, 2007). A mineral is a naturally occurring substance with a particular composition, atomic structure, and set of chemical and physical properties. In natural form, minerals are found in rocks and soils. A typical soil is made up of 50% solids, of which 45% are minerals, 5% are organic materials, and 50% are pores (voids), of which half are filled with water and half with gas (Publications, 2007). A rock, on the other hand, is composed only of minerals and is categorized as either igneous or sedimentary rock depending on the process in which they are formed (Klaver et al., 2024; Publications, 2007).

The igneous rocks are categorized into intrusive and extrusive igneous rocks which are formed as a result of cooling and or crystallization of molten magma within the earth crust or at the surface of the earth crust. They can be coarse or fine grained. The coarse grained igneous rocks include granite, delorite, gabbro and peridotites (Klaver et al., 2024). They contain mineral ores with

abundant radioactive nuclides such as Potassium, Uranium, Caesium and Thorium that have been present since the formation of the earth 4.5 billion years ago (Alnour et al., 2012). Granite and sedimentary rocks in Uganda contain U-238, Th- 232 and K-40 radionuclides in addition to the heavy accessory minerals such as Monazite, and Zircon (Baguma, 2009). Uranium in form of euxenite, microlite, and kasolite exists in pegmatite rocks and Thorium exists in monazite formed by weathering of granite rocks containing quartz-rutile ilmenite nodules in the biotite gneisis. Traces of these radioactive nuclides are always present in the bedrock.

Natural radioactivity occurs at varying proportions in all forms of rocks and soils around the world and accounts for external gamma dose rates that humans receive from the environment. Due to weathering and other physical and chemical processes, radionuclides in rocks and soils accumulate in sediments. Therefore the building materials obtained from such rocks and soil are contaminated by the radionuclides. The use of these materials contaminated by radionuclides of high activity concentration can be a health hazard to the dwellers (Goodhead, 1989; Youk et al., 2024).

A study was carried out on concentration levels of radon in mines, industries and dwelling in Tororo and Busia districts (Biira et al., 2014). It was found out that the selected areas were contaminated by radon gas and its concentration levels were found to vary from 28±1 to 97±5 Bqm^{-3} and the effective dose varied from 0.71±0.03 to 2.44±0.13 $mSvy^{-1}$. A similar study was carried to determine the radioactivity levels and dose rates due to natural radionuclides in rocks from selected mining areas in eastern Uganda, the activity concentration for Radium-226 ranged from 13.95 ± 0.31 to 698.02 ±3.38 $Bqkg^{-1}$, 98.68 ± 1.30 to 239.78 ± 19.64 $Bqkg^{-1}$ for Thorium-232 and 45.97 ± 2.48 $Bqkg^{-1}$ to 2183.80 ± 17.89 $Bqkg^{-1}$ for Potassium-40 (A.Mugaiga, 2016). This still left room for studies to be done in Tororo town in particular with regards to the common building materials of cement and tiles.

2.3 Radioactive Nuclide Nature and Disintegration

Atomic nuclei that are unstable undergo radioactivity and release ionizing radiations such as gamma rays, beta and alpha particles. The chain of decay continues until the nucleus reaches the state of stability. The unstable atoms decay by releasing a particle that changes the nucleus into another nucleus or into a lower energy state. When ionizing radiation's energy surpasses the

ionization potential of matter, then it has sufficient energy to ionize matter either directly or indirectly.

As an atomic nucleus spontaneously changes into a different nuclide, it can produce particles only, photons only, or particles followed by photons. This process is known as radioactive decay (Scherer, 2017). According to statistical rules, radioactive nuclide decay is a random process and simple linear differential equation (2.1) known as the decay law describes the decay rate or activity of a radioactive source. The decay law states that the number of atoms decaying per unit of time is proportional to the number of atoms N that remain undecayed at the current time, t.

$$A_t = \frac{dN}{dt} = -\lambda N_t \qquad 2.1$$

Where; A_t is the activity and λ is the decay constant.

The daughter nuclides that arise from beta decay, in particular, and alpha decay, are frequently seen in an excited energy state. The nucleus releases a high energy photon, which releases the energy attached to this excited state. The gamma ray is typically released 10^{-12} seconds after the particle is released. The mass and atomic numbers of the radionuclide are unaffected by the production of gamma ray photons.

Three types of naturally occurring radioactive decay series exist: the Thorium, Actinium, and Uranium decay series (Doroudiani et al., 2012; Sheppard et al., 1980). The Uranium decay series as shown in Figure 2.1 starts from Uranium-238 which decays by alpha emission to Thorium-234 which is itself unstable, it further decays by beta emission to produce Protactinium -234 (Pa-234) and this process goes on until stable Lead-206 (Pb-206) is produced. The Actinium decay series as indicated in Figure 2.3 starts from Uranium-235 (U-235) and decays by emission of alpha particle to Thorium-231 (Th-231). Thorium -231 is also unstable and further decays to produce Protactinium (Pa-231) by beta emission. The process goes on until stable Lead-207 (Pb-207) is produced. Thorium decay series as shown in Figure 2.2 begins from Thorium-232 (Th-232). It decays by alpha emission to produce Radium-228 (Ra-228). Radium-228 decays by emission of beta particles to produce Actinium (Ac-228) and this process goes on until stable Lead-208 (Pb-208) is obtained. The three natural radioactive decay series contains a radioactive daughter nuclide which is in gaseous state, that is Radon- 222 (Radon in U-238 decay series), Rn-219 (Actinon in the 235U decay series) and Rn-220 (Thoron in the Th-232 decay series).

Radium-226 decays by alpha emission to Radon, Rn-222 which is a radioactive inert gas. Radon decays by alpha emission to give a progeny of radioactive daughters (Mapping Using Gamma Ray, 2003; Sharma et al., 2015; Sheppard et al., 1980). The main cause of the public health concerns regarding naturally occurring environmental radioactivity is the presence of radon and thorium in the decay chain. As the gas diffuses into the air from the rocks and soils, it can gather in public buildings, underground water, and residences with inadequate ventilation. The amount of Thorium and Uranium present in rocks, soils, and building materials determines the amount of Radon gas present.

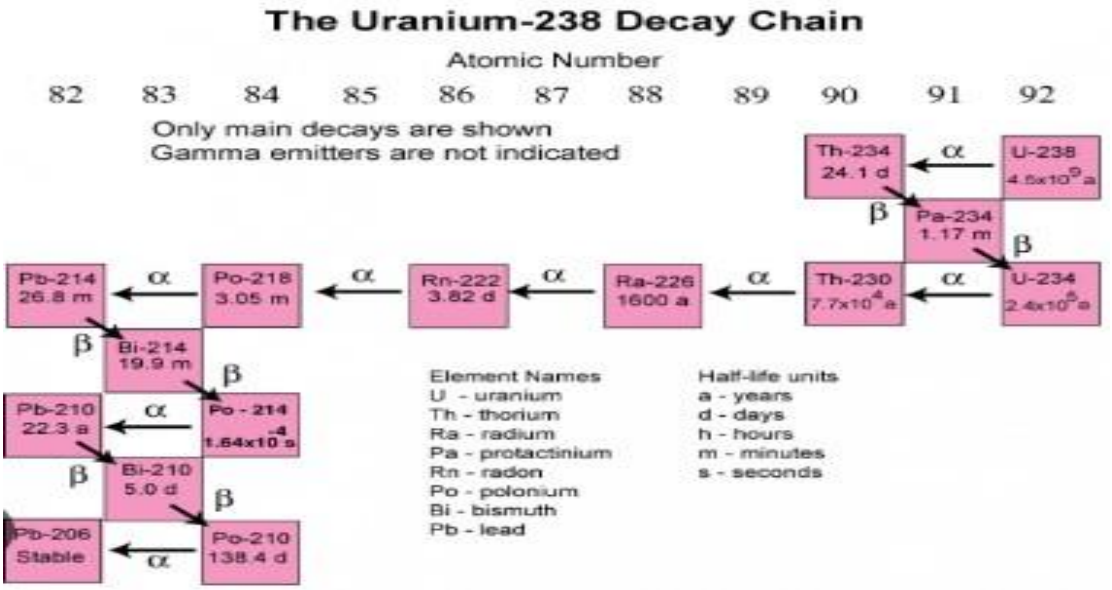

Figure 2.1: Uranium-238 decay chain (https://www.google.com/search?q=uranium+decay)

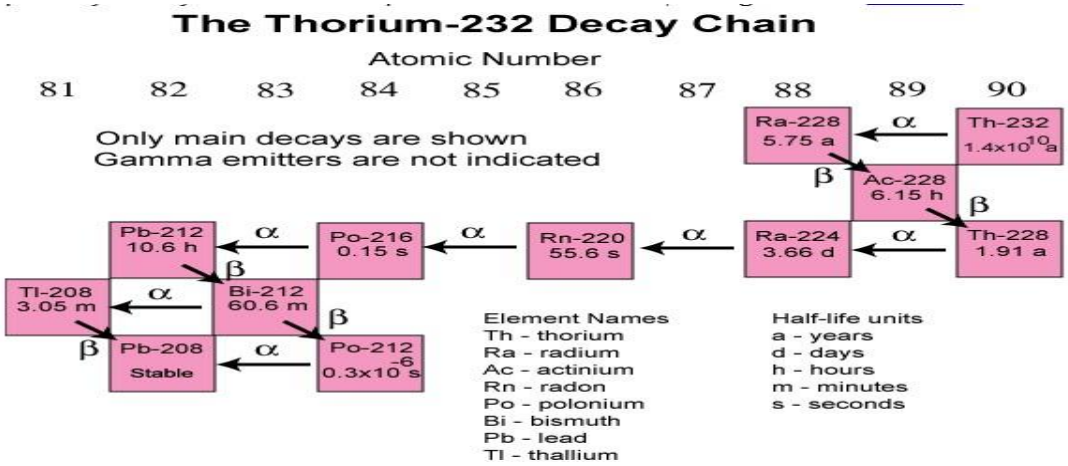

Figure 2.2: Thorium-232 decay series (https://pubs.usgs.gov/of/2004/1050/thorium.htm)

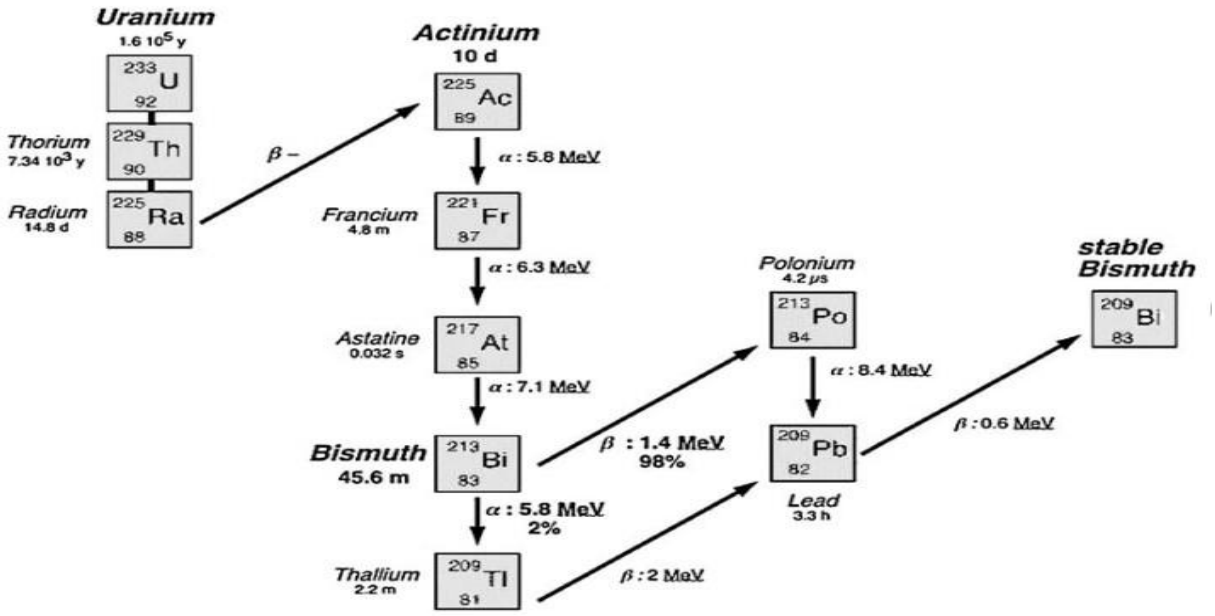

Figure 2.3: Actinum-225 decay series (https://www.researchgate.net/figure/Decay-of-actinium-225)

2.4 Biological Effect of Ionizing Radiation

These are the consequences that ionizing radiation exposure has on the human body (Elgazzar & Kazem, 2015). Radiation has the advantage that more information about the health dangers it poses is known than about any other harmful chemical that has effects on the body that are comparable. By evaluating the dangers associated with radiation, regulatory bodies can set guidelines and dose limits that maintain exposure at a level of risk that is manageable and unlikely to result in adverse effects.

When radiation falls on normal cell, it causes a change in deoxyribonucleic acid (DNA) of the cell and affects the cell. The radiation damages the cell and tissue of human body (Elgazzar & Kazem, 2015; Sjostedt & Bezak, 2010). The conditions of exposure, such as the type, energy, and quantity of radiation received, determine the potential biological consequences and damages induced by radiation. There are two main categories of ionizing radiation's biological effects. Deterministic effects are the potential results of receiving a high radiation dose in a short time. Stochastic effects are the potential long-term effects of lower radiation doses acquired over an extended period of time (White & Mallya, 2012).

2.4.1 Deterministic Effects

The duration, dosage, and kind of radiation all affect these type effects (White & Mallya, 2012). There is a dose threshold that must be reached for the effect to manifest; however, this threshold may differ for different individuals. For example, at dosages less than 1Sv, no immediate effects are seen in the average person. Responses that get stronger when the dosage is increased are known as deterministic effects. Deterministic effect includes;

a) **Acute Radiation Sickness**: These effects are mainly brought on by significant doses of radiation delivered quickly (Elgazzar & Kazem, 2015; White & Mallya, 2012). These effects happen immediately following exposure or within a day of exposure. They are simple to treat and manage. Radiation illness, including headache, nausea, vomiting, diarrhea, fever, and burns to the skin and tissue, can happen within a few hours of exposure above the threshold dose. If the dosage is not regulated, the effects worsen, start earlier, and last longer as the dose rises.

b**) Chronic Radiation Sickness:** Chronic radiation sickness originates as a result of repeated irradiation by small doses, or as a result of overcoming acute form of the disease (Elgazzar & Kazem, 2015). These side effects are harmful, difficult to treat, and potentially fatal. These impacts could have long-term effects because they are not immediately noticeable. Examples of long-term effects include genetic mutations, cataracts, and cancer. Infertility and both temporary and persistent sterility are other chronic effects (Sjostedt & Bezak, 2010; White & Mallya, 2012).

2.4.2 Stochastic Effects

The effects that arise from a high dosage of radiation are known as stochastic effects. As the dosage is increased, the likelihood of these consequences happening increases. It is not possible to determine a threshold dose below which a stochastic impact cannot arise. The severity is independent of the amount of absorbed dosages (White & Mallya, 2012). Occurrence of stochastic effect is probabilistic in nature and is proportional to dose received. Stochastic effect is of two types;

a) Somatic stochastic effect: These are radiation-related consequences that are specific to the individual exposed, and they are not to be confused with hereditary impacts. The more exposed cells there are, the higher the dose, and the greater the likelihood that one of those cells will

survive and eventually develop into cancer. Because of this, the dose and the likelihood of these effects are related. Cancer is the only stochastic somatic effect (Blackadar, 2016).

b) Genetic or hereditary effect: Generation after generation is impacted by the damage that ionizing radiation causes to reproductive cells' genetic material. Through the initiation of changes in the DNA of the cell nucleus, ionizing radiation has the ability to both kill and damage cells (Prise et al., 2002; Sjostedt & Bezak, 2010; UN, 2013). If the damage is not repaired and the cell remains viable and able to reproduce, it can initiate the development of cancer (White & Mallya, 2012). Furthermore, if the damaged cell is a part of the genetic line, such as an ovum or sperm-generating cell, it may cause genetic disorders in the progeny. X-ray photons interact with water to produce reactive radicals and recoil electrons, which in turn cause DNA damage. When ionizing radiation breaks the double stranded backbone (in dark grey) in multiple places, the damage cannot be repaired. Such damage may lead to cancer.

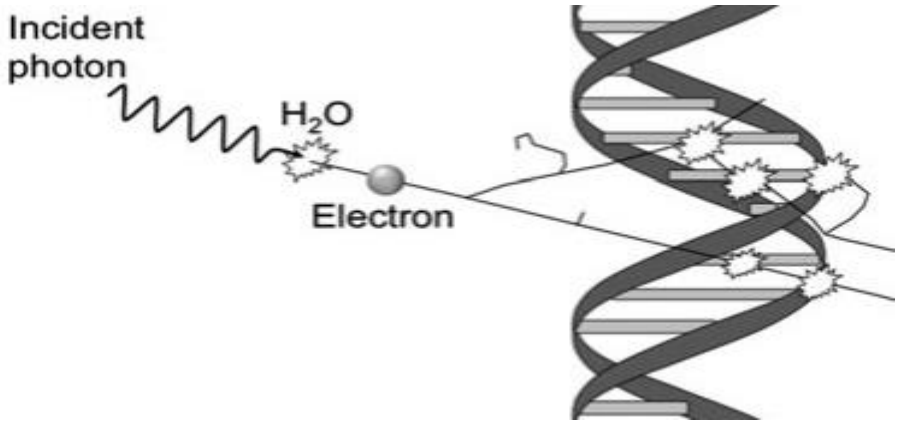

Figure 2.4: Schematic drawing of a DNA molecule and damage that may result from one X-ray photon(White & Mallya, 2012)**.**

2.5 Radiation Dosimetry

In the fields of radiation protection and health physics, radiation dosimetry refers to the measurement, computation, and evaluation of the amount of ionizing radiation that is absorbed by an object, usually the human body (IAEA., 2018; Senthamizhchelvan et al., 2010).This applies internally, due to ingested or inhaled radioactive substances and externally due to irradiation by sources of radiation.

2.5.1 Radiation Quantities and Units

Radiation Exposure; Is a measurement of the quantity of electric charge produced in an air mass by photons (Akhtar et al., 2005). The electric charge comes from the production of ion pairs, which can be collected by the detector and measured as a current. When it comes to sources that emit radiation continuously, like x-ray tubes, it can be quantified as a rate (exposure per unit time), or as a total integrated exposure.

The roentgen (R) is the traditional exposure unit. The radiation needed to release one electrostatic unit of charge in one cubic centimeter of air at standard temperature and pressure (STP) is equal to one R. This is equivalent to 2.08 x 10^9 ion pairs. One R equals 2.58×10^{-4} C/kg in SI units (Doroudiani et al., 2012; IAEA, 1989). Exposure does not apply to charged particle ionization or photons with energy greater than three (3) million electron volts (MeV) and it is only measured in air. "Air kerma," which is not yet widely used and will not be defined for the time being, is progressively replacing the idea of exposure.

Absorbed Dose: This is a measurement of the energy that all forms of radiation deposit in a substance. The radiation absorbed dose (rad), is the tradition unit of measurement for absorbed dose and is equivalent to 100 ergs/gram. The gray (Gy), or one joule per kilogram, is the SI unit for absorbed dosage. One Gy is equal to 100 rad (Petoussi-Henss et al., 2010).

Since it can be difficult to assess the absorbed dose directly, it is usually determined using other parameters, such as exposure and the conversion coefficients of the materials of interest. For instance, the steps in equation 2.2 are taken to convert exposure to the absorbed dosage in air (Higley et al., 2012; Petoussi-Henss et al., 2010)

$$D_{air}(rad) = 0.88(rad/R) \times X(R) \qquad 2.2$$

Where, D_{air} is the absorbed dose in the air, $X(R)$ exposure in air and 0.88 is the conversion factor in the air. However to convert exposure to absorbed dose in the tissue, the following equation 2.3 is applied (Clement et al., 2012; Yoder et al., 2022).

$$D_{Tissue}(rad) = 0.93(rad/R) \times X(R) \qquad 2.3$$

Where, D_{Tissue} is the absorbed dose in the tissue, $X(R)$ exposure and 0.93 is the conversion factor in the tissue.

It should be noted that because rad and roentgen are almost the same in tissue, they are frequently used interchangeably in radiation protection. However, the roentgen only applies to gamma or x-ray radiations and is a unit of exposure.

Equivalent Dose/ Dose Equivalent(ED): Is a radiation quantity calculated from the absorbed dose that takes into account that some types of radiation are more harmful to biological tissues than others (Clement et al., 2012; Mapping Using Gamma Ray, 2003). It is a dose in Sieverts (Sv) that expresses the health effects of the specific type of radiation. ED is the total of all the radiation types present, which is equal to the absorbed dose in a tissue from each type of radiation multiplied by the radiation weighting factor (W_R) for each type of radiation (Higley et al., 2012; Vañó et al., 2015) as shown in equation 2.4.

$$ED = \sum W_R \times D_R \qquad 2.4$$

The S.I unit of ED is the Sievert (Sv). The traditional unit of ED is the "rem" which stands for "roentegen equivalent man" and $1Sv = 100rem$. Radiation weighting factor (W_R) is a dimensionless factor by which the organ or tissue absorbed dose component of a radiation type R is multiplied to reflect the relative biological effectiveness of that radiation type (Higley et al., 2012). It is used to derive the organ equivalent dose from the mean absorbed dose in an organ or tissue. According to (Higley et al., 2012),each type of radiation has a particular radiation weighting factor that is internationally reorganized. The Table 2.1 indicates the radiation weighting factors for different types of radiation emitted from the radioactive source.

Table 2.1: Radiation weighting factors of the different types of radiation.

Type of radiation	**Weighting factor**
x-rays	1
Gamma rays	1
Beta particle	1
Slow neutrons	5
Fast neitrons	10
Alpha particles	20

Effective Dose Equivalent / Effective Dose (EDE); This is a dose weighing the differences in the sensitivity among body organs and tissues and sums them up to express the radiation effect of

the whole body (Clement et al., 2012; Kapanadze et al., 2019a; Petoussi-Henss et al., 2010; Yoder et al., 2022). The EDE accounts for the fact that the human body's tissues and organs react to radiation in different ways. EDE compares the risk of stochastic effects associated with a non-uniform radiation dose with that of a uniform whole-body exposure. It is primarily used in radiation protection or exposure control.

A stochastic effect is a health effect that happens at random and for which the probability of the effect happening is a linear function of the dose rather than the effect's severity, such as developing cancer (White & Mallya, 2012). The EDE is not meant to be used for determining doses for individual users; instead, it is intended for assessing risk mainly for radiation protection purposes. The equivalent dose (ED) to each organ or tissue is multiplied by the tissue weighting factor (W_T) for that organ or tissue, and the result is the EDE, which is then added together for all the organs and tissues in the body (Kapanadze et al., 2019a) as indicated in equation 2.5.

$$EDE = \sum W_T \times ED \qquad 2.5$$

Table 2.2: Tissue weighing factor of the different body organs and tissues.

Body Tissue/ organ	Tissue weighting factor	Absorbed dose (mGy)	EDE(mSv)
Colon	0.12	1.21	0.145
Lung		19.22	2.307
Breast		13.91	1.669
other tissue		10.35	1.242
Stomach		15.57	1.868
Gonads	0.08	0.26	0.021
Bladder	0.04	0.23	0.009
Esophagus		3.00	0.120
Liver		18.25	0.730
Thyroid		0.86	0.035
Brain	0.01	0.12	0.001
Salivary glands		0.62	0.006
Lung surface	0.01	10.84	0.108
Other organs	0.01	0.26	0.003
Effective dose			8.260

An estimate of the proportion of the risk of stochastic effects arising from the irradiation of an organ or tissue to the overall risk of stochastic effects when the body is irradiated uniformly is known as the tissue weighting factor (W_T). Thus, a high W_T indicates a high level of risk. Each bodily tissue or organ has a unique tissue or organ weighting factor since they all absorb radiation in different ways. According to (Vañó et al., 2015), the table 2.2 indicates the tissue weighting factors of different body tissues or organs. The International Commission on Radiological Protection (ICRP) recommends the annual effective dose equivalent limit of $1mSvy^{-1}$ for the members of the public and $20mSvy^{-1}$for radiation workers (Clement et al., 2012; UN, 2013).

2.5 Radiation Hazard Indices

Radiation sickness, or skin burns, can result from acute exposure to high radiation levels, such as being near an atomic explosion. It may also have long-term adverse effects on health, like cancer and cardiovascular (Elgazzar & Kazem, 2015; Sjostedt & Bezak, 2010). Radiation exposure and human life are inextricably linked. The human body is constantly exposed to natural radiation sources, apart from manmade radiation sources that humans can control and limit the radiation levels absorbed (IAEA., 2018; UN, 2013).

Assessment of radiation hazard index due to irradiation from the sources and ingestion or inhalation of radionuclides in the body is necessary (Goodhead, 1989). According to UNSCEAR reports, the values obtained are compared with the global data on permitted dose limits that are already accessible (Kapanadze et al., 2019b; Özdiş et al., 2017). According to (Nations et al., 2000; UN, 2013) UNSCEAR reports, internal and external hazard indices due to radium, thorium and potassium which continuously emit alpha, beta and gamma radiation should be ≤ 1. Once the limit is exceeded, adverse health effects start showing up in the human body (Ng, 2003).

Since naturally occurring radionuclides belong to Uranium and thorium series present in soils and rocks, which usually give high radiation doses than those provided by artificial radionuclides, it should be of greater concern (Kapanadze et al., 2019b). Therefore the study of external and internal radiation hazard indices due to natural radionuclides is necessary.

2.5.1 External Hazard Index

External hazard index is a radiation hazard index used to evaluate the indoor radiation rate due external exposure to gamma radiation from natural radionuclides from the radiation sources such as building materials (Özdiş et al., 2017). External radiation hazard is as a result of gamma radiation that comes from each radionuclide. It is calculated using the following equation 2.6 (Goodhead, 1989).

$$H_{ex} = \frac{A_{Ra}}{370} + \frac{A_{Th}}{259} + \frac{A_K}{4810} \leq 1 \qquad 2.6$$

Where, A_{Ra}, A_{Th} , $and\ A_K$ are activity concentrations due Radium-226, Thorium-232 and potassium -40 radionuclides respectively.

2.5.2 Internal Hazard Index

Internal radiation hard index is as a result of radioactive ingestion and inhalation of radionuclides. It is especially due to Uranium and Thorium decay (Elgazzar & Kazem, 2015). Internal radiation is explained as the radiation which occurs if human consumes something that emits radiation. The radiation enters and radiates to human body directly and results in internal radiological hazards. According to (Goodhead, 1989; Ng, 2003), internal hazard index is calculated using the following equation 2.7.

$$H_{in} = \frac{A_{Ra}}{185} + \frac{A_{Th}}{259} + \frac{A_K}{4810} \leq 1 \qquad 2.7$$

Where, A_{Ra}, A_{Th} , $and\ A_K$ are activity concentrations due Radium-226, Thorium-232 and potassium -40 radionuclides respectively.

2.6 Radiation Safety

Ensuring the safe use of radiation is the aim of radiation protection. The regulatory agencies work to lower the risk of radiation exposure from radioactive sources by limiting the amount of radioactivity that is allowed (UN, 2013; World Health Organization, 2016). The International Commission on Radiological Protection's (ICRP) regulations serve as a basis for radiation protection principles (IAEA., 2018; Senthamizhchelvan et al., 2010; Vañó et al., 2015).The principles are;

Justification: Any decision that modifies radiation exposure ought to result in more benefits than harm. In other words, it ought to assist the exposed people or society more than it damages them.

Optimization of protection: Taking into account social and economic issues, the number of individuals exposed and the total amount of their individual doses should be kept as low as reasonably achievable (ALARA).

Application of dose limits: In planned exposure scenarios other than medical exposure of patients, the total dosage administered to any individual from regulated sources should not be beyond the authorized limitations. This principle emphasizes that no individual should be exposed to unacceptable levels of radiation danger (World Health Organization, 2016).

2.6.1 Protection against External Exposure

Although exposure to ionizing radiation has risks it poses to the human health and environment, it is impossible to completely avoid exposure to radiation especially the background radiation. One can avoid unnecessary exposure by the following three fundamental methods or measures: **Time:** The radiation dose will be proportionate to the length of time spent in close proximity to the source since radiation is emitted from it at a nearly constant rate. As such, it is best to minimize the amount of time spent dealing radioactive materials.

Distance; According to the inverse square, the radiation dose due to gamma and X-rays decreases with distance from the source. The potential dose decreases as the exposure potential does. Another highly useful strategy for lowering the dose from alpha and beta radioisotopes is distance. Because of the absorption of alpha and beta particles in air, the consequent decrease in dose is considerably more than in the case of gamma and X-ray sources.

Shielding: One can lower their radiation dose by placing an appropriate shield material between them and the source of radiation. Lead and concrete barriers shield against harmful radiations like X-rays and gamma rays.

2.6.2 Protection against Internal Radiation

All types of radiation become more hazardous once inside the human body. Alpha radiation is the least hazardous while it is outside the body, but it poses the worst internal threat. Protection against internal radiation is the same as with other biological or chemical hazardous materials (IAEA., 2018; World Health Organization, 2016). It is essential to use safety gear, appropriate handling measures, and appropriate operating practices. It is prohibited to eat, drink, or even store food or beverages within any designated radioactive laboratory or source. Disposable gloves and lab coats are required when working with radioactive materials. When working with open sources of radioactive materials, it's also advised to use eye or facial protection (goggles or a plastic face shield).

2.7 Cement as a Building Material

Cement is a binder, a chemical substance used for construction that sets, hardens, and adhere to other materials to bind them together. Different building materials can be combined with cement being an adhesive and cohesive bonding agent, to make compacted assemblies (Engineer & Chemicals, 2015; "Portl. Cem. Third Ed.," 2011). Cement is made from calcareous and argillaceous rocks that are taken out of quarries. Consequently, the majority of the chemical composition of cement is composed of silicates and carbonates. The Table 2.3 list the main minerals or raw materials required to make cement (Engineer & Chemicals, 2015; Eštoková & Palaš, 2013). Depending on how the cement will be used, different ratios of these fundamental raw components are mixed.

Table 2.3: The raw calcareous and argillaceous materials of cement

Raw material	**Remark**
The raw calcareous materials of cement	
Lime stone	$CaCO_3$, sedimentary rock formed by accumulation of shales or corals
Cement rock	Sedimentary rock with composition similar to industrial cement.
Chalk	Soft lime stone
Marl	Loose deposit consisting mainly $CaCO_3$
Alkali waste	Obtained from chemical plants.
Raw argillaceous materials of cement	
Clay	Hydrous aluminum silcate

Shale	Consists of clay, mud and silt, maincy aluminum silicates.
Slate	Dense fine grained rock containing mainly clay.
Ash	Contains silicates

2.7.1 Active Chemical Components of Cement

There are four chemical components that are active constituents in the composition of cement. These ingredients provide the cement additional desirable properties, such as setting response and compressive strength(Engineer & Chemicals, 2015; Notation & Compounds, 1824). Compounds such as dicalcium and tricalcium silicates are used to effect the setting reactions. When calcium silicate and water come into contact, the silicates combine to generate calcium hydroxide and calcium hydrate. The cement's active chemical components are listed in the Table 2.4. A range of additives, such as retarders, dispersants, extenders, and fluid loss additives, can be added to cement to alter its compressive strength and setting time, depending on the intended use.

Table 2.4: Active chemical components in the cement formulation.

Component	**Formula**	**Remarks**
Tricalcium silicate	$3CaOxSiO_2$	Responsible for strength in all stages.
Dicalcium silicate	$2CaOxSiO_2$	Responsible for final strength.
Tricalcium aluminate	$3CaOxAl_2O_3$	Hydrates quickly, responsible for strength of cement in the early stages. Setting time can be controlled by addition of gypsum.
Tetracalcium aluminoferrite	$4CaOxAl_2O_3xFe_2O_3$	Responsible for long term gain of strength of the cement.

2.7.2 Classification of Cement

(a) Port land cements (OPC): This is made of chalk (lime) and clay, which solidifies in water and takes on a grey color like that of Portland stone. When standard soil conditions are present and special qualities are not needed, Portland cement is utilized for conventional building. It is typically utilized for pavements, bridges, reinforced concrete buildings, and other structures (Notation & Compounds, 1824; “Portl. Cem. Third Ed.,” 2011). The general minerals (raw materials) used to produce cement contain chemicals which are mixed in the ratios shown in Table 2.5 to make ordinary Portland cement (OPC).

Table 2.5: Chemical compositions in a mass of the Portland cement

Compound	Percentage
CaO	60 -69
SiO_2	18 -24
Al_2O_3 + TiO_2	4 -8
Fe_2O_3	1 – 8
MgO	<5
K_2O, Na_2O	<2
SO_3	<3

(b) Portland Pozzolana Cement (PPC) is made by mixing pozzolana material with Portland cement. Pozzolana should make up between 15 and 40 percent of the cement's mass composition, according to the American Society of Testing and Materials (ASTM). Like OPC, the primary raw ingredients for Portland pozzolana cement are limestone ($CaCO_3$) and clay (SiO_3, Al_2O_3, and Fe_2O_3). To create clinkers, these ingredients are mixed and fired to a very high temperature in the kiln.("Portl. Cem. Third Ed.," 2011; UNBS, 2017). A pozzolana material is an aluminous, siliceous substance that, at room temperature and in the presence of moisture, chemically interacts with calcium hydroxide to generate compounds with cement-like properties. Volcanic powder, burnt clay, fly ash, rice husk, and blast furnace slag are a few types of pozzolana materials.

2.7.3 Cement Grades

The hydration properties of Cement are dependent on its chemical composition. It suggests that by varying the proportion of raw materials, cement of different types or grades can be produced (Engineer & Chemicals, 2015). According to ASTM, the different grades of cement are;

Ordinary Portland cement (OPC), Type- I: This is the most popular grade of cement for general concrete building, particularly in situations where there is no exposure to sulfates in the groundwater or soil. Dicalcium and tricalcium silicates must make up at least two thirds of the clinker composition in order to generate type-I (Engineer & Chemicals, 2015; Notation & Compounds, 1824; UNBS, 2017).

Modified cement , type –II; This grade of cement is obtained by mixing OPC and additives such as fly ash, slag up to a maximum of 35% of the cement mass (Bediako & Amankwah, 2015; Engineer & Chemicals, 2015). Type II cement grade combines a strength growth rate that is

comparable to OPC with a rate of heat development that is higher than that of low heat Portland cement. Constructions with a moderate risk of sulfate attack and a desirable amount of heat generation are advised to use this grade.

Rapid Hardening Portland Cement (RHPC), Type-III: This grade of cement is produced by combining OPC and blust furnace slag to accelerate strength development and reduce setting time. According to Blaine method, indicates that it is consists of tricalcium silicate (C_3S) and tricalcium aluminate (C_3A), with C_3S > 55%, and has a greater fineness of 450–600m^2kg^{-1} (Buregyeya et al., 2018; Engineer & Chemicals, 2015).This grade is used when rapid strength development is desired and for construction at low temperatures to prevent the frost damage of the capillary water.

Low Heat Portland Cement (LHPC), Type –IV; LHPC contains < 5% of C_3S and C_3A percentages and high percentages of C_2S of about 46% in comparison with OPC. It has a lower early strength and its fineness is not less than 3200cm^2g^{-1} (Engineer & Chemicals, 2015). LHPC is used in massive concrete operations where it's important to control internal heat accumulation and stress during hydration to lower the chance of thermal cracking.

Sulfate Resistance Portland Cement (SRPC), Type- V; SRPC contains lower percentage of C_3A ($\leq$ 3.5%) and C_4AF which are considered to be most affected compounds by sulfate. It however contains a high percentage of silicates in comparison with OPC (Engineer & Chemicals, 2015; Notation & Compounds, 1824). It has a lower early strength due to C_2S representing a high percentage of silicates and its resulted heat of hydration is not much higher than that of LHPC. SRPC is used in concrete products where extreme sulfate resistance is necessary such as coastal structures, piers under water tunnels, foundation and road ways.

2.7.4 Physical Properties of Cement

Fineness, setting time, soundness, standard consistency, and compressive strength are among cement's key physical characteristics. High quality cement should have a consistent color and be lump free. Must be cool to the touch when held in the hand and sink when dropped in little amounts into the water. As shown in Table 2.6 , Portland cements are categorized in accordance with BS 12: 1991 (Mittal et al., 2016; UNBS, 2017) according to the compressive strength attained after 28 days of setting. Considering the Table 2.6, the class names 32.5, 42.5, 52.5, and

62.5 as indicated above based on the 28-day minimum strength in MPa. There are maximum and minimum strengths for each class of cement. The class with a high early strength is indicated by the letter R, which stands for cement that hardens quickly.

Table 2.6: Compressive strength requirements of cement.

Class	Min strength (MPa) at the age of;			Maximum strength (MPa) at the age of ;
	2days	7days	28day	28days
32.5N	----	16	32.5	52.5
32.5R	10	----		
42.5N	10	----	42.5	62.5
42.5R	20	----		
52.5N	20	----	52.5	------
52.5R	30	----		
62.5N	20	----	62.5	-----

2.8 Tiles as Building Material

A tile is a piece of flat or curved fired clay, stone, or concrete that is used for roofing, baths, kitchen countertops, and flooring in homes. The technologies and raw materials used in their production, for example, determine how different the tiles are from one another (Patrick et al., 2015).

2.8.1 Classification of Tiles

Tiles are classified according to the raw materials used to make them for instance;

Ceramic tiles; these are manufactured from mineral raw materials such as clays, silica, fluxes, and coloring. They are made of ceramic materials, which are silica and alumina compounds bound by strong covalent and ironic bonds (Ochen et al., 2021; Patrick et al., 2015; Tiles et al., n.d.). Given their attractiveness and durability, ceramic tiles have become popular for usage on practically all walls and floors in both busy business spaces and residential settings.

Porcelain tile; these are formed of quartz, feldspar, and kaolin clay, which are ceramic elements. Because of its excellent flexural strength (>30MPa) and minimal water absorption (≤0.5%), porcelain tiles are a good choice for flooring (Michele et al., 2019; Nalianya et al., 2022). Each raw element in a porcelain system has a distinct function. For example, after burning, kaolin

combines with feldspar to form mullite crystals, which are dipyrimidal minerals made of Al, O2, and Si (Michele et al., 2019; Panzi Mukhokosi et al., 2023; Patrick et al., 2015). The interlocking of the millute needles increases the flexural strength, and quartz maintains dimensional and thermal stability to help avoid warping.

2.8.2 Chemical Composition of Tiles

Generally, the raw material used in the manufacturing of tiles such as quartz sand, kaolin clay, feldspar, lime stone, soda ash, natural gas and petroleum coke contain chemicals which are mixed in appropriate ratios (%) in a mass of tiles as indicated in the Table 2.7 (Michele et al., 2019; Patrick et al., 2015).

It is evident from the aforementioned literature that raw materials that are naturally found in rocks and soils, such as clay, shale, slate ash, feldspar, and quartz sand, are used to make both cement and tiles. These materials naturally contain potassium, thorium, and uranium radionuclides (., 2016; Biira et al., 2021). This suggests that even if we value the benefits of modern building materials, we also need to be concerned about learning about the radiation exposure these materials may cause.

Table 2.7: Chemical composition in a mass of a tile.

Constituents	**Percentage by mass**
Silicon dioxide(SiO_2)	66.57
Aluminum oxide (Al_2O_3)	21.60
Iron oxide (Fe_2O_3)	1.41
Calcium oxide (CaO)	2.41
Sodium oxide (Na_2O)	1.41
Potassium Oxide (K_2O)	2.79
Zirconium oxide (ZrO_2)	1.49

2.8.3 Physical Properties of Tiles

Tiles are made of clay, feldspar and flint or quartz. The quantity and the quality of the clay that ceramic tile contains play a key role in the final properties of the materials. The properties of the

tile can be improved by varying the composition of the main ingredients in the formulation of tiles (Michele et al., 2019; Patrick et al., 2015). Some of the physical properties of tiles include;

Water absorption; this measures how much moisture a specific type of tile is likely to absorb on an ongoing basis. Some types of tile may crack if the moisture penetration is too high. An easy way to test tiles absorption is to drop little amount of water on the backside of the tile. If water is absorbed quite quickly, the tile is considered to be normal absorbent type. Vitreous porcelain tile absorbs water at a rate of 0.5-3 percent, ceramic at 3-7 percent, and impervious porcelain tile at less than 0.5 percent. Water absorption in tiles is determined using the following equation 2.8 (Patrick et al., 2015).

$$W = \left(\frac{M_2 - M_1}{M_1}\right) x100 \qquad 2.8$$

Where; W is the water absorption of the specimen tile, M_1 mass of the dry specimen tile and M_2 is mass of the specimen tile after 24 hours submerging in the clean water.

Bulk density, in g/cm^3, of a specimen tile is the ratio of its dry mass to the exterior volume, including pores. Due to the difficulty of measuring ceramic tile porosity, bulk density is the physical magnitude that is actually measured to control the pressing stage. Bulk density of tile is determined using the following equation 2.9 (Patrick et al., 2015).

$$B = \frac{M_1}{V} \qquad 2.9$$

Where; B is the Bulk density of the specimen tile, $M_1$is the mass of the dry specimen tile and V is the exterior volume.

Compressive strength measured in MPa; is the ratio of the failure load to the surface area covered by the specimen tile (Patrick et al., 2015). It is determined using the following equation 2.10.

$$C = \frac{Failure\ load}{surface\ area\ of\ the\ tile} \qquad 2.10$$

Where; C is the compressive strength. According to (Patrick et al., 2015) study report on physics properties of tiles, for ceramic tiles, the maximum average Modulus of rupture is 482 kgcm^{-2}.

Modulus of capture (Flexural strength) of a material; is the maximum bending stress that can be applied to that material before it yields. Modulus of rupture test is performed by placing a tile

on two supports and applying a load at the center of the tile until it breaks. This test is essential to ensure that tiles can withstand the stresses they will experience in real-world applications such as floors and walls. It is calculated using the following equation 2.11 (Panzi Mukhokosi et al., 2023; Patrick et al., 2015)

$$\delta = \frac{3FL}{2bh^2} \qquad 2.11$$

Where; δ is the modulus of rupture in Nmm^{-2} , F is the load required to break the tile in N, L is the length between the support rods in mm, b is the width of the tile in mm and h is the thickness of the test tile. According to (Patrick et al., 2015) study report on physics properties of tiles, for ceramic tiles, the maximum average Modulus of rupture is 487.5 $kgcm^{-2}$.

Breaking strength; this is the ability of a material to withstand a tensile or pulling force. The break strength of a tile is a numerical measurement of how much weight it can bear. This is based on subjecting unsupported tile to a loading stress to determine its resistance to breaking under certain loading conditions. It is obtained using the following equation 2.12.

$$S = \frac{FL}{b} \qquad 2.12$$

Where; S is the break strength, F is the load required to break the tile in N, L is the length between the support rods in mm, and b is the width of the tile in mm.

2.9 Radionuclide Contamination in Building Materials

The public may be exposed to radiation since radionuclides are present in materials like cement and tiles, which among others are used in building and construction. Therefore, to limit the public's exposure to ionizing radiation from building materials, a systematic and graded approach is needed (IAEA., 2018; Protection, Minerals, et al., n.d.). Since rocks and soils are considered to be the main sources of naturally occurring radionuclides of potassium, uranium, and thorium, they are used to make the majority of building materials.

2.9.1 Radionuclide Contamination in Cement

Cement as one of the major building materials is vulnerable to contamination by minerals in the rocks and soils from which it is made. These contaminants may include radioactive materials and as a result emit gamma radiations. A study on radiological safety of cements used in Kenya

(Mulwa et al., 2023) ,found out that cement was contaminated by radionuclides such as U-238, Th- 232 and K-40. The average activity concentrations of Th-232, U-238, and K-40 were found to be 52.70±3.3, 35.88±4.3, and 432.31±50.7 $BqKg^{-1}$ respectively which are above the recommended global dose limit of 30 $BqKg^{-1}$, 40 $BqKg^{-1}$ and 400 $BqKg^{-1}$ respectively according to ICRP, UNSCEAR and IAEA reports (Higley et al., 2012; Nations et al., 2013b; Protection, Basic, et al., n.d.; *UNSCEAR 1993 Report.Pdf*, n.d.; Volume, 2006). The absorbed dose rate in some cement samples studied was higher than the world average of $84nGyh^{-1}$. The radium equivalent activity, annual effective dose rates, and indoor and outdoor hazard index values were all within the acceptable global safety limits (IAEA ANNUAL REPORT 2016 IAEA Annual Report 2016, 2016; Report, 2011). There is no significant radiation danger associated with the use and handlings of the cements used in Kenya because these radiation hazard indicators measured were within safety bounds.

Similar study carried out by Mammba et al (2021) (Mammba et al., 2021) to assess Natural Radioactivity and Radiation Hazards of Building Materials including cement in Kinondoni District, Dar es Salaam, Tanzania using gamma spectrometry, the activity concentrations of Ra-226, Th-232, and K-40 in $Bqkg^{-1}$ were measured. The average activity concentrations of Ra-226, Th-232, and K-40 were found to be 15.62, 21.51, and 237.99 $Bqkg^{-1}$, respectively. In the examined samples, the activity concentrations were all less than the global average values, which are 40 $Bqkg^{-1}$ for Ra-226, 30 $Bqkg^{-1}$ for Th-232, and 400 $Bqkg^{-1}$ for K-40. The radium equivalent activity (Raeq), external hazard index (H_{ex}) , internal hazard index (H_{in}) and gamma activity concentration index($I\gamma$) were calculated to assess the radiological hazards due to presence of natural radionuclides in the building materials. The results showed that the average values of Raeq, H_{ex}, and $I\gamma$ were 64.7 $Bqkg^{-1}$, 0.17, 0.21 and 0.24, respectively (Trevisi et al., 2012). These values were lower than the world criteria values 370 for Raeq, ≤ 1 for H_{ex}, ≤ 1 for H_{in} and ≤ 1 for $I\gamma$, respectively. The obtained results indicated that all the investigated building materials were safe for inhabitants in Kinondoni District, Tanzania.

A study was also carried out to assess the natural radioactivity in cements used as building materials in Turkey (Özdiş et al., 2017). In the study, it was found out that cement samples contained Ra-226, Th-232 and K-40 radionuclides that are emitters of gamma rays. The radioactivity concentrations of Ra-226, Th-232 and K-40 in the cement samples from different

types of cements produced in Turkey were measured using gamma-ray spectrometer. The activity concentrations were in the range of 18–143 Bq kg^{-1} for Ra- 226, 5–66 Bq kg^{-1} for Th-232 and 142–540 Bqkg-1 for K-40K. It is noted from the results that most of the cement samples analyzed had activity concentration above the recommended dose limit of 40, 30 and 400Bqkg^{-1} for Ra-226, Th-232 and K-40 respectively. However, apart from absorbed dose rate whose maximum value was recorded to be 158 nGy h^{-1} above the dose limit of 84 nGy h^{-1} in building material, the calculated radiological hazard parameters such as annual effective dose, radium equivalent activity, the external hazard, activity and alpha indices were found to be in the range of 0.19–0.78 $mSvy^{-1}$, 41–182 Bq kg^{-1} , 0.11–0.49, 0.15– 0.65 and 0.09–0.71, respectively below the world recommended average values according to the reported data values given by European Commission and UNSCEAR (Assembly, 2016; UN, 2013).

Also a study was carried out to assessment natural radioactivity levels in Cement samples commonly used for construction in Lagos and Ogun State, Nigeria by A.K. Ademola (2017) (A. K. Ademola et al., 2017). He measured the activity concentrations of natural radionuclides U-238, Th-232 and K-40 in the cement samples by gamma spectrometry using NaI(Tl) detector type. Radiological hazard assessments due to these natural radionuclides were also carried out. The average activity concentrations of U-238, Th-232 and K-40 in the cement samples were found to be 2.16, 7.82 and 114.3 Bqkg^{-1} respectively. The mean absorbed dose rate, the mean annual effective dose, excess lifetime cancer risk and annual gonadal equivalent dose in the samples analyzed were 9.59 $nGyh^{-1}$, 17.66 μSvy^{-1}, 67.99 $(MPY)^{-1}$ and 69.07 μSvy^{-1} respectively. Additionally, estimates of the gamma activity concentration index (Iγ), radium equivalent activity (Ra_{eq}), and external and internal hazard indices (H_{ex} and H_{in}) were made. In every instance, the outcomes are significantly lower than the global average value. As a result, cement made in this region of the country is safe and regarded to have less radioactive effect on anybody who comes into contact with it.

2.9.2 Radionuclide Contamination in Tiles

One building material that is subject to contamination by minerals found in the rocks and soils it is made of is tile. These contaminants may release gamma radiation because they contain radioactive elements. A study on the natural radioactive content of tiles used in Bungoma County, Kenya was carried out using gamma ray spectroscopy. The amounts of certain

radioisotopes found in 20 samples of decoration tiles used in Bungoma County, Kenya were determined using a NaI(Tl) detector. The average activity concentrations of Ra-226, Th-232, and K-40 for the tiles were determined to be 11±0.55, 109±5.85, and 1574±78.7 $Bqkg^{-1}$ respectively. The activity concentration of Thorium and potassium in most samples analyzed samples was above the world recommended dose limit of 30 $Bqkg^{-1}$ and 400 $Bqkg^{-1}$ save for radium whose average was less than 40 $Bqkg^{-1}$, the recommended dose limit (IAEA ANNUAL REPORT 2016 IAEA Annual Report 2016, 2016). Consequently absorbed dose rate was 140±7.03 $nGyh^{-1}$ higher than the global dose limit of 84 $nGyh^{-1}$ in building materials. Other Radiological hazard indices such as radium equivalent activity, external Hazard Index (Hex), internal Hazard Index (Hin), Indoor and outdoor Annual Effective Dose, were found to be 288±14.44 $Bqkg^{-1}$, 0.7±0.03, 0.8±0.04 , 0.5±0.02$mSvy^{-1}$ and 0.3±0.01$mSvy^{-1}$ respectively which are below the dose limit globally. Compared to the global reference value of 370 $Bqkg^{-1}$, the mean radium equivalent activity obtained in the study was lower and so are other radiological indices. Because of this, there is no risk to the public's health when using tiles for decoration in Bungoma County, Kenya.

A study carried out by Christiana O. et al (2019) (Christiana O. et al., 2019) to evaluate radiological hazards in ceramic tiles used in Jos-South, plateau state, Nigeria, found out that the samples were contaminated with gamma emitting natural radionuclides of K-40, Ra-226 and Th-232 using a NaI(Tl) gamma ray spectrometer. The ceramic tiles had mean activity concentrations of 44.5, 59.6 and 417.4 Bq kg^{-1} for Ra-226, Th-232 and K-40 respectively. The mean activity for each radionuclide was slightly above the set dose limits of 40, 30 and 400 $Bqkg^{-1}$ respectively. The average radium equivalent activity was found to be within the recommended limit of 370 Bq kg^{-1} for building materials. The radiological hazard indices such as the gamma absorbed dose rate, annual effective dose, external radiation index (H_{ex}), internal radiation hazard index (H_{in}), Alpha index ($I\alpha$), Gamma index ($I\gamma$), excess lifetime cancer risk, and annual gonadal dose equivalent were evaluated. The results obtained show that the radiological parameters do not exceed the recommended safety limits and hence pose no significant radiological hazard when used as building material.

A study on radioactivity level in Chinese building ceramic tiles was carried to determine activity concentrations of Ra-226,Th-232 and K-40 using gamma ray spectrometry by Xinwei(2004) (Xinwei, 2004) . He found out that the concentrations of Ra-226, Th-232 and K-40 ranged from

63.5 $Bqkg^{-1}$ to 131.4 $Bqkg^{-1}$, 55.4 $Bqkg^{-1}$ to 106.5 $Bqkg^{-1}$, and 386.7 $Bqkg^{-1}$ to 866.8 $Bqkg^{-1}$ for ceramic tile, respectively. The measured activity concentrations for these radionuclides were compared with the world values dose limits of 40, 30 and 400 $Bqkg^{-1}$.The result in the study showed that in all the samples, the activity concentration exceeded the global dose limits and this poses health risks. The radium equivalent activities (Ra_{eq}) in most selected samples exceeded the world average value of 370 $Bqkg^{-1}$ though the average value for all the samples was found to 350.4 $Bqkg^{-1}$ slightly less 370 $Bqkg^{-1}$ limit. The absorbed dose rate, internal hazard index (H_{in}) and annual gonadal equivalent dose were calculated and found to be 161.3 $nGyh^{-1}$, 1.3 and 1.124 $Bqkg^{-1}$ respectively each above the maximum permissible dose. The annual effective dose, external hazard index (Hex) and excess life time cancer risk were found to be 0.793 $mSvy^{-1}$, 0.94 and 0.0027 respectively were below world average values recommended by ICRP.

2.10 Gamma Ray Spectrometry

Since gamma ray detection and energy measurement are crucial components of experimental nuclear physics research, gamma ray spectroscopy is one of the most advanced and significant methods in the field. The energy spectra of gamma ray sources are studied quantitatively using gamma ray spectroscopy. It is an analytical technique that makes it possible to identify and measure isotopes that release gamma rays in a range of matrices. Several gamma ray producing radionuclides in the sample can be detected by gamma ray spectrometry in a single measurement with minimal sample preparation (IAEA, 1989; IAEA ANNUAL REPORT 2010, 2010). The measurement provides a spectrum of gamma lines that can be used to calculate the energy and intensity of the gamma rays that are released.

The selection of an appropriate gamma ray spectroscopy system for measuring and detecting ionizing radiation is determined by several factors. These include detection efficiency, which establishes the source strength required for measuring a spectrum; resolution, which determines the complexity of the spectrum that can be easily analyzed; the arrangement's simplicity and ease of data accumulation; and secondary factors such as response linearity, stability, the ratio of photoelectric interactions to Compton interactions, timing accuracy, and detector availability. (Chiozzi et al., 2000; IAEA, 1989).

High purity Germanium (HpGe) spectrometers and sodium iodide (NaI) spectrometers are two principal gamma spectroscopy instrument. Moderate energy resolution and good efficiency

gamma ray detection are offered by the sodium iodide (NaI) scintillator detector. Low efficiency, high resolution energy spectra are obtained with the high-purity germanium (HpGe) semiconductor detector (Assessment, n.d.; Windows & Professional, n.d.). The crystal must be kept sealed since one drawback of the NaI detector is that it absorbs water from the surrounding air, which damages the crystal. The scintillation photons are detected by a photomultiplier tube (PMT), which is another drawback of any scintillation counter. Three main mechanisms explain how gamma rays interact with detector atoms in gamma ray spectroscopy using a NaI(Tl) detector: pair production, photoelectric absorption, and Compton scattering. The interaction mechanisms are shown in Figure 2.5.

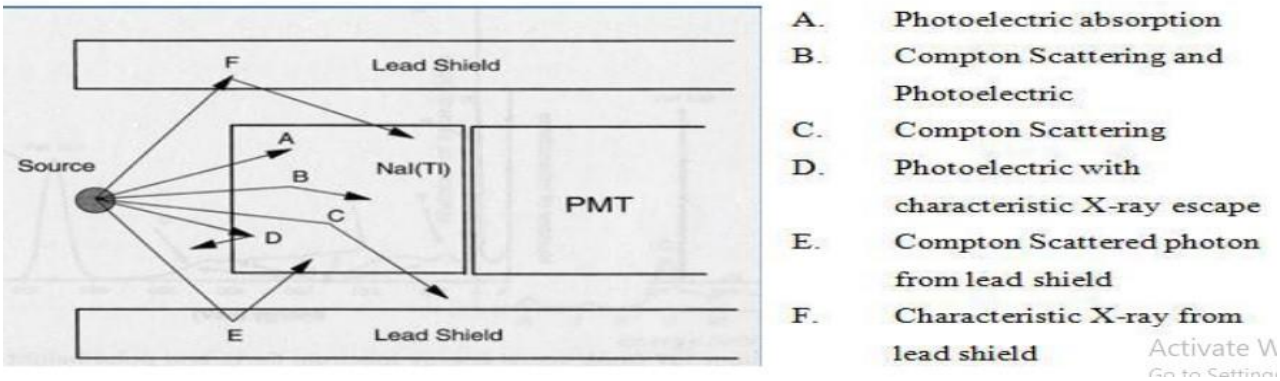

Figure 2.5: Diagram of Interaction of Gamma Rays with the detector material (Al-Kaabi & Hmood, 2019)

The primary way that low energy gamma rays interact with the detector is through photoelectric absorption. A gamma photon that hits an absorber atom undergoes complete absorption during the photoelectric absorption process. Instead, the atom ejects a powerful photoelectron from one of its bonded shells. The most tightly bound, or K shell, of the atom is most likely the source of the photoelectron for sufficiently energy-dense gamma photons. The photoelectron appears with kinetic energy given by equation 2.13.

$$E_K = E - E_B \qquad 2.13$$

Where; E_K is the kinetic energy of the ejected photoelectron, E is the energy of the incident gamma ray and E_B is the binding energy of the photoelectron in its original shell.

The energy of the released electron may be regarded as equal to that of the incoming gamma ray since the energy of the incident gamma ray (usually about 0.5 MeV) is significantly higher than the binding energy of the ion's electron (usually 10 - 100 eV) (S. Publication, 1977) . As a result, with an energy equivalent to the input gamma ray, the photoelectric effect produces a peak in the photomultiplier spectrum known as the photo peak. The photoelectric effect grows as the number of atoms in the absorber increases as well. The absorber atoms are left ionized and have a vacancy in one of the bonded electron shells as a result of this interaction. The remaining vacancy may then be filled by a free electron being drawn from the medium or by an electron transitioning from the absorber atom's higher (outer) shell. In this case characteristic X-rays are produced. The X-rays may be re-absorbed in the detector through photoelectric absorption involving electrons from less tightly bound shells and auger electrons may be produced.

The incoming gamma ray photon experiences Compton scattering when it is deflected through an angle relative to its initial direction. A fraction of the photon's energy is transferred to the electron, also referred to as the recoil electron. Since there are infinitely many different scattering angles, the energy transmitted to the electron that recoils varies from zero and is maximum when the scattering angle reaches 180^0. Figure 2.6, illustrates effect of Compton scattering.

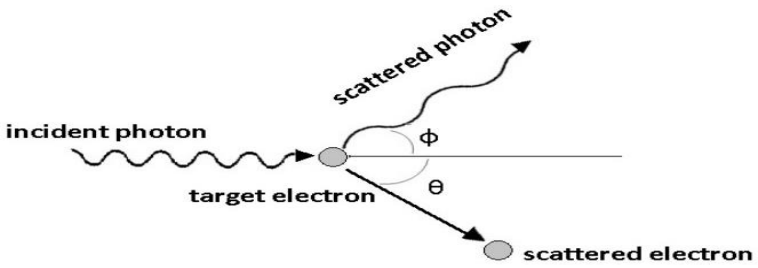

Figure 2.6, Illustrates effect of Compton scattering (https://www.researchgate.net/figure/The-geometry-of-Compton-scattering).

From Figure 2.6, the electron recoils with a speed, v, at some angle, ϕ , with the initial direction of the photon. The probability of Compton scattering per atom of the absorber depends on the number of electrons in the atom and so it linearly increases with atomic number. The gamma rays initial wavelength is given by $\lambda = \frac{hc}{E} nm$, where E is the energy of the incident gamma

ray in joules. The change in wavelength due to reduction in energy of the gamma ray increases with the scattering angle θ according to the Compton formula given by equation 2.14.

$$\Delta\lambda = \frac{h}{mc}(1 - \cos\theta) \qquad 2.14$$

Where; $h = 6.63x10^{-34}js$ is the Planck's constant, $m = 9.11x10^{-31}\,kg$ isthe mass of the electron and $c = 3.0x10^{8}ms^{-1}$ is the speed of light. A wavelength change of 0.00486 nm causes the energy of the scattered electron to change between zero and its maximum value, the Compton edge. Compton scattered electrons have a nearly constant energy distribution. A photomultiplier tube generates a Compton spectrum, which is a flat plateau from zero energy up to the Compton edge, where it suddenly drops off at a rate determined by the tube's energy resolution.

2.10.1 Mode of Operation of the '2x2' NaI Detector

A '2x2' NaI (TI) gamma-ray spectrometer, which is the appropriate for measuring gamma rays` energy, can be used to measure the concentration of radionuclides in the chosen samples. (Amakom et al., 2018; IAEA, 1989, 2013). The NaI (TI) gamma-ray spectrometer is made of NaI (TI) scintillating material called Aluminum (Al). Next to the end window is the photocathode made up of alkaline elements like calcium and Belyrium. The dynodes are made up of MgO. Next to the photocathode is the P-amplifier and linear amplifier (L - amplifier) followed by Single channel and Multichannel analyzer then to the counter or recorder.

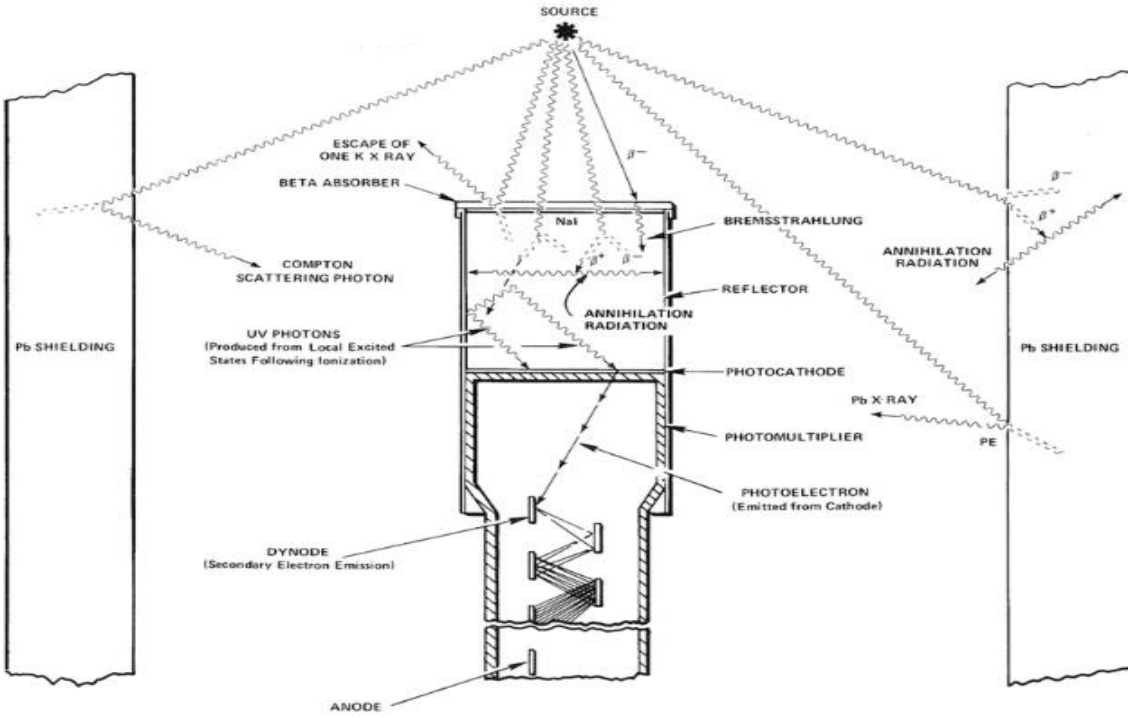

Figure 2.7: Structure of NaI (TI) gamma ray spectrometer (Source: Internet)

The NaI (TI) gamma-ray spectrometer works on the principle that when NaI (TI) interacts with the radiations from the source (samples), it produces a flash of light. The photocathode converts the flash of light into electrons. The electrons are then multiplied by the dynodes before reaching the photo anode. The photo anode collects the electrons and a current pulse is generated. The current pulse (signal) is given to P-amplifiers or L-amplifier to be amplified. The amplified signal is given to SCA or MCA and a current pulse is recorded (Chiozzi et al., 2000).

The pulse height at the preamplifier and linear amplifier outputs is proportional to the energy that the detected gamma ray deposits in the scintillator. In order to capture the energy spectrum generated by the NaI (TI) detector, the multichannel analyzer (MCA) measures the pulse heights given by the amplifier and organizes them into a histogram. Using a USB cable, the MCA is connected to the computer running ORTEC MAESTRO V7 software. To provide a hermetic seal that guards the hygroscopic NaI against moisture absorption, the detector is enclosed in an aluminum enclosure with a glass window at the interface with the photocathode. The interior of the aluminum is lined with a coating that reflects light to increase the fraction of light that

reaches the photocathode. The block diagram of the gamma-ray spectrometer used in this study is shown in the Figure 2.8 below.

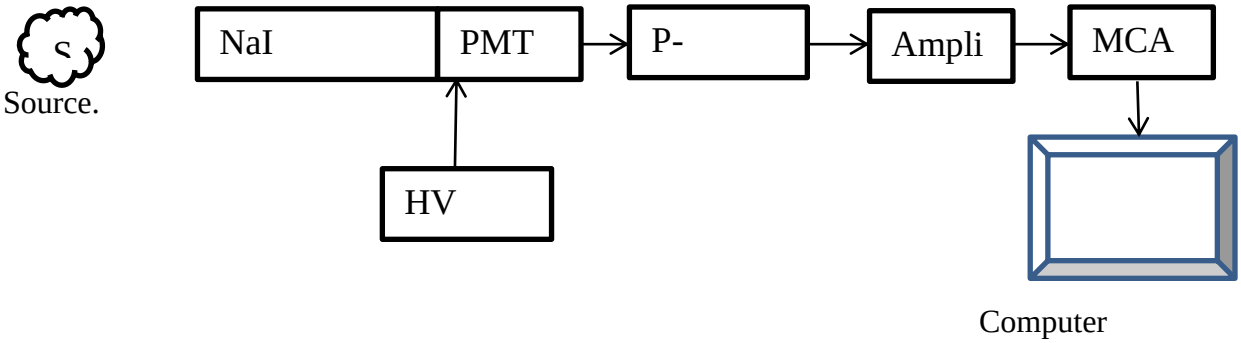

Figure 2.8: Block diagram of a NaI (TI) gamma detector

2.10.2 Calibration of the NaI (TI) Detector

The energy calibration of the detector is done using a standard source of ceasium-137 since it emits gamma rays of known energy 661.9keV and 1173.2keV. A beaker containing the standard source is placed on the detector surfaces and the system is left to run for 7200 seconds (2 hours) to obtain a new spectrum. After the background subtraction automatically done by the software, the calibration spectrum is saved for analysis. Photo peak of energy 661.9keVand 1173.2keV is analyzed using ORTEC MAESTRO V7 software to convert the channel number scale into an energy scale. (Aneke & Shabangu, 2021; Biira et al., 2021; Chiozzi et al., 2000; IAEA, 1989; Purnama & Damayanti, 2020).

The specific radionuclides in each sample are then recognized by corresponding them to their respective theoretical energies. Low gamma energies of 63 keV and 92 keV for radio nuclides of U-238 and Th-232 respectively are not matched well due to poor resolution of NaI detector (Siddeeg et al., 2018).

Efficiency calibration is conducted using reference sources with well-known activities to establish a relationship between the detected count rate and the actual activity. This calibration is crucial for quantitative measurements and is periodically repeated to account for changes in detector efficiency due to aging or environmental factors (Abbas et al., 2015; Badawi et al., 2015).

2.10.3 Background Subtraction in the NaI Detector

The background count rates are subtracted from the gross count rates by the built-in algarithism or program of the NaI (TI) detector. The software attempts least squares fit of a Gaussian function to the remaining data after subtracting the computed background channel per channel. If unsuccessful, it displays "Could Not Properly Fit Peak." If successful, the centroid is based on the fitted function (He et al., 2015; Windows & Professional, n.d.). Figure2.9 shows the spectrum components used for the background computation. The stated widths are interpolated linearly between the channels that have had their background eliminated.

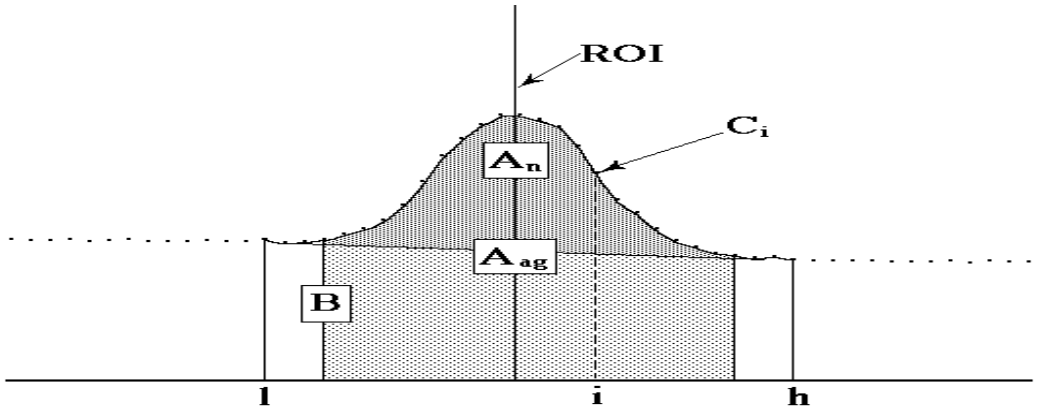

Figure 2.9: Calculation details of background count rates.

The average of the first n channels of the ROI, where n is the number of background points chosen, represents the background on the low channel side of the peak. The channel number for this background point is the midpoint fractional channel of the *n* points. The average of the final n channels in the ROI makes up the background on the high channel side of the peak. The midpoint fractional channel of the n points is also the channel number for the background point. These *(n-1)* points on each side of the peak form the end points of the straight-line background (He et al., 2015; Windows & Professional, n.d.). The background is given by the following equation 2.15.

$$\boldsymbol{B} = \left[\sum_{i=l}^{l+(n-1)} \boldsymbol{C_i} + \sum_{i=h-(n-1)}^{h} \boldsymbol{C_i}\right]\frac{h-l+1}{2n} \qquad \mathbf{2.15}$$

where: B, l, h, C_i and n is the background area, the ROI low limit, the ROI high limit , the contents of channel i and the number of background points respectively.

2.10.4 The NaI (TI) Detector Efficiency

The measure of the probability that an incident photon is absorbed in the detector is obtained using equation 2.16 below (Abbas et al., 2015; Badawi et al., 2015; IAEA, 1989; Mapping Using Gamma Ray, 2003).

$$\varepsilon = \frac{N_A}{A_s t_s} \qquad 2.16$$

Where ε is the photo peak efficiency of the detector, N_A is the net photo peak area of the calibration spectrum at a known peak energy, A_s is the activity of the standard source obtained from the manufacturer of the standard source and t_s is the counting time of the standard.

CHARPTER THREE: RESEARCH MATERIALS AND METHODS

3.0 Introduction

Using a sodium iodide detector to identify the radionuclides which emit gamma rays provided the basis for this study. Gamma-ray emitting radionuclide activity concentrations were then calculated using the raw data that were collected from the detector. The absorbed dose rates, annual effective dose equivalent, internal and external radiological hazard indices, excess lifetime cancer risk, and annual gonadal dose equivalent were all calculated using the obtained activity concentrations. Additionally, the specific methods that were used to determine activity concentrations, absorbed dose rates, annual effective dose equivalent, and levels of radiological hazard from gamma rays both internal and external have been covered. This chapter also includes a description of the research designs used in the study, the study area, and the sample preparation procedures used on the samples.

3.1 Study Area

This study was conducted in Tororo municipal council, located in Tororo district in eastern Uganda, approximately 206 kilometers east of Kampala, the capital city, and bordering Kenya to the east, as seen in Figure 3.1. Tororo was specifically chosen due to its significant industrial activity, particularly in the production of building materials. The district is rich in natural resources such as limestone and phosphate (National Planning Authority, 2020), which has led to the establishment of major industries, including Tororo Cement, Simba Cement Company, Hima cement and a phosphate fertilizer factory. These industries contribute to the local economy but also raise concerns about the potential radiological content of the materials they produce. This made Tororo an ideal case study for assessing the radiological hazards associated with cement and tile production. Tororo municipal council, covering an area of 1,196 km², had a population of 42,016 as of the Uganda Bureau of Statistics (UBOS) reports (Population & Profiles, 2017; UBOS, 2020; Uganda Bureau of Statistics, 2016). The town's population has seen periodic growth, driven by the presence of these industries and the related small and medium-sized businesses, such as hardware stores, that support the construction sector. The industrial activity in Tororo provides a relevant context for this study, as it directly aligns with the research objective of analyzing the radiological safety of locally sourced building materials.

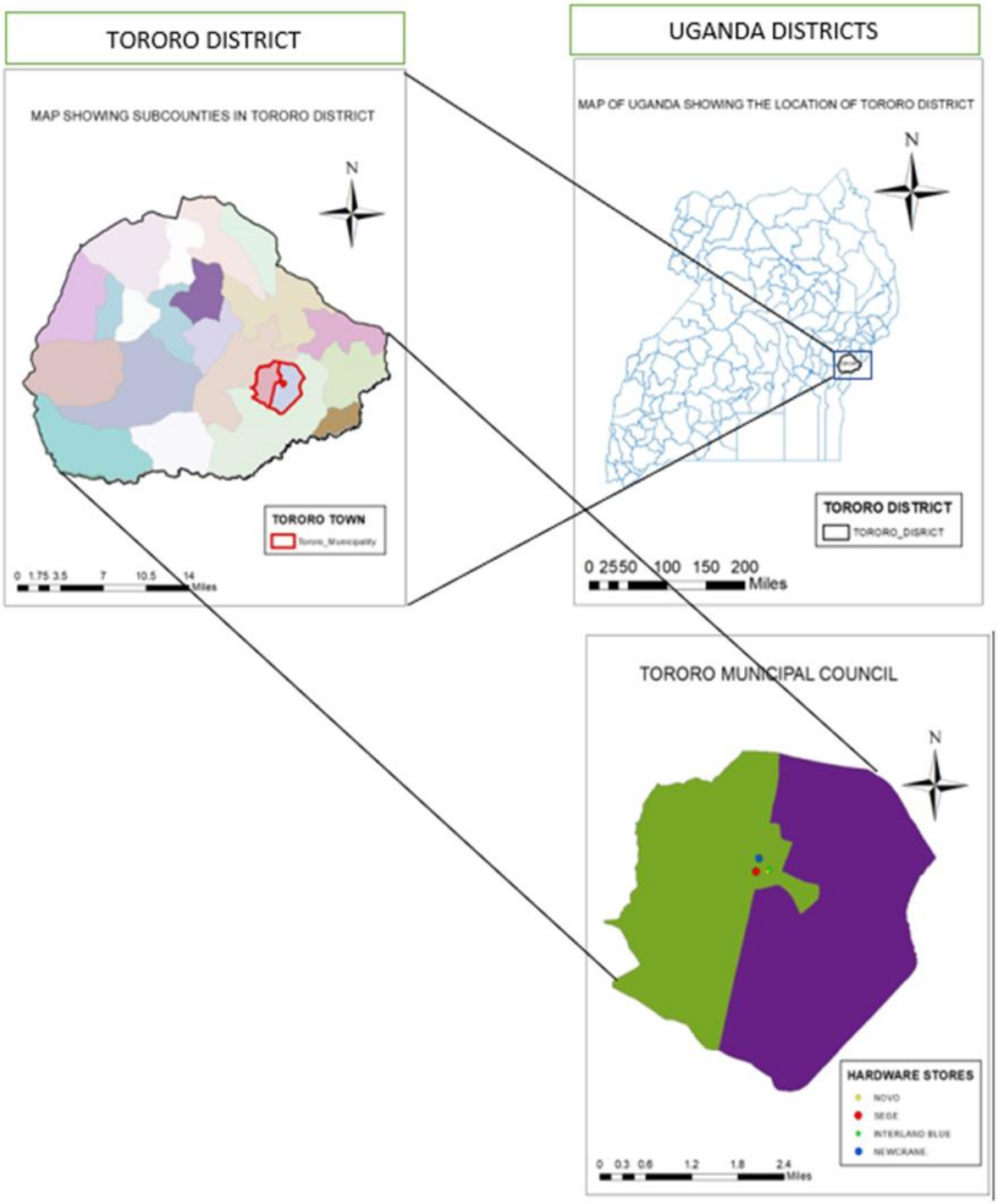

Figure 3.1: A map of the study area and sites where the samples were obtained.

The local hardware stores in Tororo Town sell different brands of cement and floor tiles that are used to build modern structures as shown in Figure 3.2. Therefore, as a representation of what is

available on the Ugandan market, the brands of cement and floor tiles that are frequently sold in hardware stores in Tororo town were carefully selected and studied.

Figure 3.2 Aerial oblique view of Tororo town with buildings constructed using modern building materials. (Source : Internet.)

3.2 Site Description

To collect cement and floor tile brands that present a fair proportion of the major cements and tiles used in Uganda, a survey was carried out. The survey included visiting the hardware stores and some construction sites in Tororo town with a guided survey questionnaire. The survey revealed that;

a) The acceptability of a particular brand of cement or tile is dictated by its availability and the cost. The availability of particular brands was closely related to the proximity to the distributor and the cost of all the packed cement and floor tiles including the imported brands found in the market by the time of the survey was almost the same.
b) CEM-II, CEM-III and CEM-IV of the cement brands had high rate of turn over for construction of ordinary buildings while CEM-I was majorly found for construction of road works and stalled building because of its strength and quick setting time.
c) Acceptance of tiles depended most on their texture and surface designs. Most of the clients use tiles that are appealing to them with less focus on other physical properties such as thickness and strength.

d) Most of the cement brands used in the area are locally produced with a few brands from Tanzania and Kenya since the study area neighbors Kenya in the West. A few imported tiles brand found in the market were of prices almost at the same level as the locally produced tiles.

3.3 Sample Selection

The study took into account the types of floor tiles and cement available in Tororo town hardware stores that are made locally in Uganda. Samples of imported cement and floor tiles from Kenya, Tanzania, Spain, china and India were also evaluated for comparability to international standards. Kenya, China, Egypt, Spain, and India are some of the exporters of building materials to Uganda, according to the UBOS, 2022 study (UBOS, 2020, 2022). As a result, imported cement and floor tiles from the countries mentioned above were given preference.

3.3.1 Sample Selection of the Floor Tiles

To assess the radiological hazard in both local and imported tiles, this study analyzed a total of nineteen (19) floor tile samples that were readily available on the market at the time of collection and commonly used for construction. The selection was limited to these samples due to accessibility issues and potential market constraints, such as the existence of a black market, particularly for imported tiles. In some hardware stores, attendants were unwilling to provide information about imported tiles, which restricted the variety of samples. Therefore, while these 19 samples provide valuable insights, they may not fully represent the broader market in Uganda, and the findings should be interpreted with this limitation in mind.

Out of the nineteen samples, nine (9) different floor tiles of comparable size that are widely utilized and produced locally by the three leading companies (that is goodwill, modern and millennium) were collected. The samples of tiles with a high rate of turnover in the hardware stores for each local producer were chosen. The names of different samples of ceramic tiles are (Goodwill: T_7, T_8, T_9. Modern: T_{10}, T_{11} ,T_{12}. Millennium: T_{13},T_{14}, T_{15}). In addition, Ten (10) distinct varieties of imported floor tiles from Kenya, Tanzania, India, Spain, and China that were found in the different stores at the time of the sample collection were taken into consideration that is (Tanzania: T_1. Kenya: T_2, T_3, T_4, T_5,T_6. Spain: T_{16}, T_{17}. China: T_{18}. India: T_{19}). The selection of samples was based on the knowledge that each type of floor tile has a distinct

chemical composition ratio that defines its strength (Evitt et al., 2000; Michele et al., 2019). The selection and specification of the samples is shown in table 3.1.

Table 3.1: The Specification of the selected floor tiles.

SN	Sample name	Sample code	Size Specifications (mm)	Country of origin
01	NM44003T	T_1	400x400x7.4	Tanzania
02	FGB44711J-1	T_2	400x400x7.9	Kenay
03	FGB44711J-2	T_3	400x400x7.9	Kenya
04	FGB44711-3	T_4	400x400x7.9	Kenya
05	FGB 44711J-4	T_5	400x400x7.9	Kenya
06	FGB44711J-5	T_6	400x400x7.9	Kenya
07	FT grade –A-1	T_7	400x400x8.0	Uganda
08	FT grade –A-2	T_8	400x400x8.0	Uganda
09	FT grade –A-3	T_9	400x400x8.0	Uganda.
10	FT premium Q-1	T_{10}	250x400x7.4	Uganda
11	SF- 4013	T_{11}	400x400x7.4	Uganda
12	SF-4015	T_{12}	400x400x7.4	Uganda
13	SF-5015	T_{13}	415x415x7.9	Uganda
14	SF-5046	T_{14}	400x400x7.4	Uganda
15	SF-5016	T_{15}	400x400x7.7	Uganda
16	SF P12	T_{16}	450x450x8.0	Spain
17	SF P13	T_{17}	450x450x8.0	Spain
18	SF romantic	T_{18}	600x600x10.0	China
19	Grazed modular FTG-A	T_{19}	300x300x8.0	India

3.3.2 Sample Selection of the Cement Brands

Thirteen (13) samples of various cement brands were selected based on their availability in the market and their common use in local construction practices. Nine (9) samples were sourced from locally produced brands, including those from major manufacturers like Tororo Cement Ltd, National Cement Company (Simba Cement), Hima Cement Ltd, and Metro Cement, as these brands dominate the Ugandan market and are widely used in construction projects. The samples included different products from these manufacturers (Tororo Cement: C_1, C_2, C_3, C_4; Simba Cement: C_5, C_6, C_7; Hima Cement: C_8; Metro Cement: C_9) to ensure a representative analysis of local production.

Additionally, four (4) samples were selected from imported cement brands, with two from Kenya (C_{10}, C_{11}) and two from Tanzania (C_{12}, C_{13}), reflecting the presence of foreign cement in the local market, as indicated in Table 3.2. However, following the results from the market survey carried out before collection of the samples, it is important to note that some imported brands may enter the market through unofficial channels, such as the black market, where traders often do not disclose details about these products. This limitation affected the comprehensiveness of the sample selection.

The chosen samples align with common construction practices in Uganda, as they represent the most widely used cement brands in the area. However, the study acknowledges that the black market for imported cement could mean that some brands were not captured in this analysis, potentially limiting the scope of the findings.

Table 3.2: The Specification of the selected cement brands.

Sample code	**Sample name**	**Specification**	**Country of origin**
C_1	Portland cem –I 42.5N –OPC	CEM I- 42.5N –OPC	Uganda
C_2	Portland pozzolana cem –II	A(P) 42.5N Purple	Uganda
C_3	Portland Pozzolana cem-II B(P)	B(P) 32.5 N Black	Uganda
C_4	Pozzolanic cem-IV	B(P) 32.5N Red	Uganda
C_5	Portland Pozzolana 32.5R	Simba cem IV- 32.5R	Uganda
C_6	Portland pozzolana	Simba Cem II- B-P 32.5N	Uganda
C_7	Ordinary Portland cement 42.5N	Simba Cem -I 42.5N	Uganda
C_8	Muiltipurpose Portland pozzolana 32.5N	Cem IV/B-P 32.5	Uganda
C_9	Metro Pozzolanic	Cem IV/B 32.5	Uganda
C_{10}	Fundi 22.5N	Fundi MC 22.5N	Kenya
C_{11}	Tembo 32.5N pozzalanic	Pozzalanic 32.5N	Kenya
C_{12}	Twiga Portland Portland	CEM II/B-M 42.5N	Tanzania
C_{13}	Huaxin power plus Portland	CEM II 42.5	Tanzania

3.4 Sample Preparation for Gamma Ray Analysis

(a) Floor tiles samples

Using a harmer, each sample was first broken up into quite small pieces. The semi-automatic uniaxial and triaxial test system, based on a semi-automatic compression machine 50-C56W02

made by the controls group shown in the Figure 3.3, was used to grind the crushed pieces for each sample into fine particles.

Figure 3.3: Semi-automatic uniaxial and triaxial test system **at** Central laboratory ministry of works and transport- Uganda

To ensure consistency in the size of the fine particles after grinding, each sample was sieved using a Setaccio Di-Prova laboratory sieve with a mesh size in the range of 250µm to 500µm. Re-sieving was done for any sample whose particle size deviated from the desired particle size range. This was to ensure that all samples meet the required standards for further testing.

Figure 3.4: Setaccio Di-Prova laboratory test sieve at Central laboratory Ministry of works and transport-Uganda

Using an electronic balance of mode I, WT10002N of precision 0.01 g, the mass of 800 g of each sample in fine particles was measured. Marinelli beakers, which are polyethylene cylindrical beakers, were used to package and seal the weighted mass. The use of polyethylene over glass was justified by the fact that less radionuclides from the samples adsorb to polyethylene compared to glass (IAEA, 1989).

Figure 3.5: Measurement of mass of the floor tile samples using digital balance.

The sealed Marinelli beakers with the weighed mass of the samples were stored for 30 days. This was to ensure that the radioactive secular equilibrium between Ra-226, U-238, Th-232, and their daughter nuclides is attained (Mammba et al., 2021; Nalianya et al., 2022; Penabei et al., 2018). The sealing of the beakers prevents the escape of radon gas and contamination of the samples as well.

(b) Cement Samples

To minimize contamination during the handling of cement samples in their fine powder form, some precautions were taken. The weighing process was conducted in a controlled environment to reduce the risk of airborne particles contaminating the samples. The electronic balance used for measuring the 800 g mass was regularly cleaned before and after each use to prevent cross-contamination between samples. Additionally, gloves and lab coats were worn during the handling process to avoid introducing external contaminants. The use of Marinelli beakers, which are polyethylene, not only helped in reducing radionuclide adsorption but also minimized

the risk of contamination from the container material itself (IAEA, 1989). After the cement was placed in the beakers, they were immediately sealed to prevent exposure to the environment.

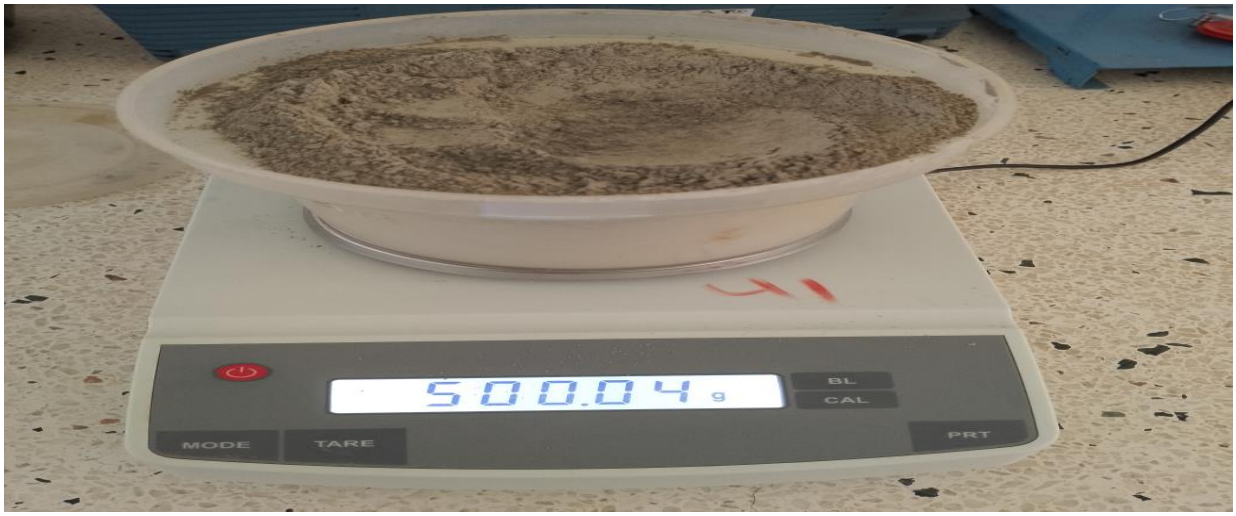

Figure 3.6: Measurement of mass of the cement samples using digital balance.

According to the guidelines in the IAEA report 2013 on rock samples (IAEA, 2013), the sealed Marinelli beakers containing the weighted mass of the samples were kept in storage for 30 days. This was done to ensure that Ra-226, U-238, Th-232, and their daughter nuclides are in radioactive secular equilibrium. The sealing was also to ensure that there is minimum escape of Radon gas from the beakers, and contamination of the samples was also prevented as shown in the Figure 3.7.

Figure 3.7: Storage of the samples in marinelli beakers

3.4 Measurement or Analysis of the Radioactivity Content of the Samples

The samples' radioactivity content was examined using a sodium iodide (NaI) “2x2” gamma-ray spectrometer. While not as precise as HPGe in terms of energy resolution (Wallbrink et al., 2007), NaI detectors have high sensitivity to gamma radiation, making them effective for detecting the presence of radioactive materials in the samples. NaI detectors are also easy to operate and maintain, requiring less complex cooling systems compared to the liquid nitrogen cooling needed for HPGe detectors (Badawi et al., 2015; Wallbrink et al., 2007).

The samples in the sealed Marinelli beakers were individually placed in contact with the detector's surface. To shield the detector and the Marinelli beaker containing the sample from background radiation and other external interferences, lead blocks were then arranged around them, secured within a rectangular iron frame. This setup minimized the impact of radiation sources present in the laboratory. The laboratory configuration of this shielding enclosure around the detector is shown in Figure 3.9.

Figure3.8: A setup of lead blocks in an iron frame around the detector.

Each sample was run in reproducible sample detector geometry for 6000 seconds live time to accumulate sufficient gamma ray counts. According to IAEA publications from 1989 and 2003 (IAEA, 1989), using a live time of 6000 seconds allows for the collection of more counts, which enhances the signal-to-noise ratio. This improved ratio reduces statistical uncertainty, thereby increasing the accuracy and reliability of radionuclide identification and quantification. The

extended measurement time also helps in clearly resolving gamma-ray peaks, particularly for low-activity samples where the signal may be weak (Badawi et al., 2015). Moreover, a 6000-second live time strikes a balance between achieving sufficient accuracy and avoiding excessive time consumption, making it suitable for routine analysis and large-scale surveys. This duration also enables the processing of a reasonable number of samples within a given timeframe, effectively balancing the need for high-quality data with practical time and operational efficiency constraints. (Aneke & Shabangu, 2021; IAEA, 1989; Mapping Using Gamma Ray, 2003).

The radioactivity data for each sample was collected from the detector cable connected to the computer that displayed and saved the spectrum of the photo peaks and channel number using ORTEC MAESTRO V7 software installed on it. The Region of Interest (ROI) reports for the selected photo peaks of each sample spectrum were generated to obtain the net count area; *Nc*, and for further analysis to determine other radiological parameters.

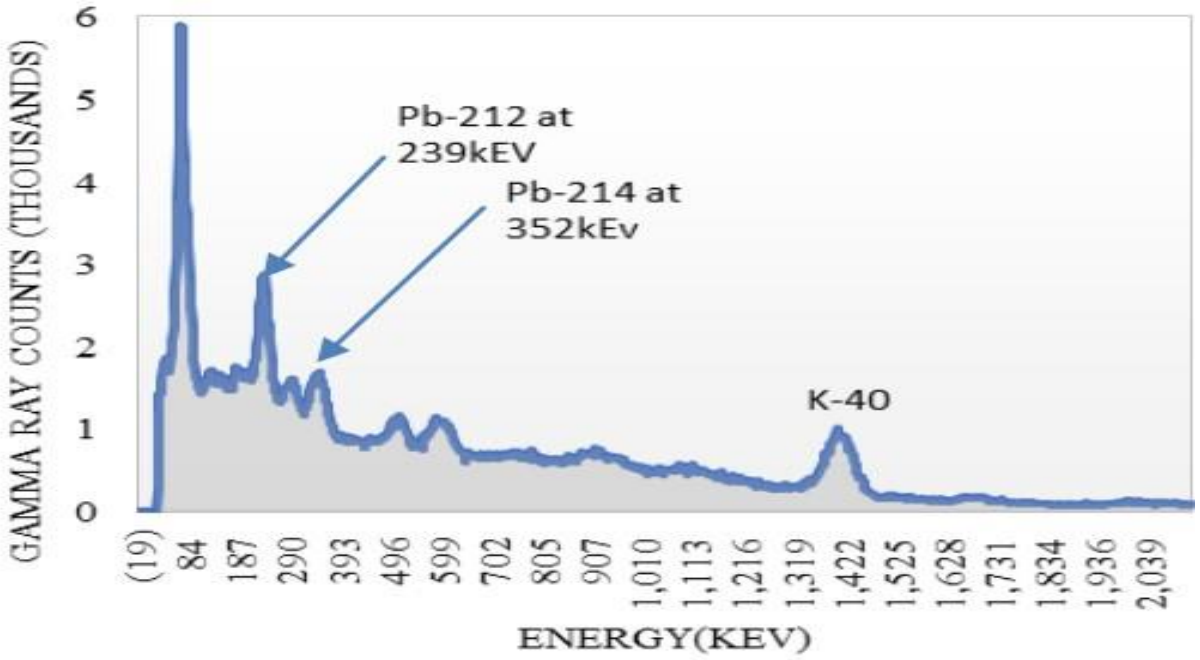

Figure 3.9: The photo peak spectrum of one of the analyzed samples.

3.4.1 Background Subtraction

The detector's surface was left open to the surroundings to determine background radiation caused by radiation from outside sources or impurity radionuclides within the detector. The system was run for 6000 seconds live time, after which a spectrum representing background

radiation was collected. The spectrum of the background radiation was stored in the computer connected to the detector. The background spectrum was always subtracted from the spectrum obtained whenever each sample of cement and tile was run for a live time of 6000 seconds. This was done to ensure that net energy spectrum of only the radionuclides present in the cement and tile samples is obtained. The net spectrum (net photo peak count) obtained after subtracting the background radiation spectrum was used for computing the basic data that included; centriod energy, Full Width at Half Maximum (FWHM), net area and the count rate for each sample (He et al., 2015).

However , to minimize deviations in the results particularly if there are significant variations in background levels across different times of day or between lab sessions, Periodic Background Monitoring was done. Background radiation was measured at regular intervals throughout the day to capture any variations. By establishing a baseline from these periodic measurements, it was possible to track and understand the natural fluctuations in background levels.

3.4.2 Efficiency Calibration of the Detector

In addition to the initial manufacturer's calibration, the detector's accuracy was maintained through regular efficiency calibrations (Abbas et al., 2015). This process involves using reference sources with well-known activities to establish a precise relationship between the detected count rate and the actual activity (Badawi et al., 2015). These calibrations are crucial for ensuring the accuracy of quantitative measurements. To account for potential changes in detector efficiency caused by aging or environmental factors, these calibrations are periodically repeated throughout the detector's operational life.

3.5 Identification of the Gamma Ray Emitting Radionuclides Present in the Cement and Tile Samples

The presence of Ra-226, Th-232, and K-40 radionuclides that emit gamma rays was examined in the cement and tile samples and the activity concentrations of these radionuclides were determined using a sodium iodide (NaI) detector, which is activated by thallium (TI). The energy efficiency calibration of the detector was already established to be 0.0255 using a standard source of cesium (Cs-137) by the detector's manufacturer. The detector operated using a cylindrical NaI(TI) crystal and the system was connected to the PC which displays a spectrum of the analyzed data for each sample. The NaI(Tl) detector system and its photomultiplier tube were

mounted in a thick iron metallic box. The detector in the metallic box was surrounded by rectangular lead blocks in order to shield it from background radiations and also to absorb characteristic X- rays generated. The hermetic seal on the detector protected the hydroscopic NaI from moisture absorption and other radiological influence. The detector was connected to the computer with a multichannel analyzer (MCA) card.

Each sample was mounted on the surface of the NaI (Tl) detector. When the gamma rays interact with the NaI crystal it produces light signal. The light was collected and converted into electrical signals/ pulses in the photo multiplier tube (PMT). The pulses are amplified and converted into digital data by the Anolog to Digital (A/D) converter. The data was then processed by the computer which presents it on the monitor as a spectrum of photo peaks of the distribution of the energy of the gamma rays. The photo peaks were then analyzed in order to determine the activity concentrations of the radionuclides present in the cement and tile samples. The energies of the photo peaks displayed on the monitor of the PC were then related to the theoretical energies from the energy window of the different radionuclides. Apart from K-40, whose gamma-ray energy can be identified directly at 1460.8 keV, Th-232 and U-238 were identified indirectly using radionuclides in their decay series.

In some regions of the spectrum, photo peaks overlapped, making it difficult to clearly distinguish them. This interference was likely caused by background radiation and sum peaks. Ambient background radiation can introduce additional peaks or elevate the baseline, complicating the identification of true photo peaks (He et al., 2015). Additionally, when two or more gamma rays are detected simultaneously, they can create a sum peak, further interfering with the accurate identification of individual peaks.

To address these challenges, regular background subtraction and the use of lead shielding around the detector were applied for each sample to minimize the impact of background radiation. Consistent background measurements ensured accurate corrections during analysis. Sum peaks were identified and accounted for using advanced spectral analysis software such as MAESTRO by ORTEC that models and corrects for these occurrences, helping to resolve the overlapping photo peaks. To minimize statistical uncertainty and for consistency in the results, a repeat of the measurement for each sample was considered.

Table 3.3: Shows the Energy Window of the Radionuclides.

Energy (Kev)	Decay series radionuclide	Parent radionuclide
>84	X-Rays	X-Rays
186	226_{Ra}	Ra-226
242	214_{Pb}	
295		
352		
609	212_{Bi}	
768		
1120		
1764		
238.6	212_{Pb}	Th-232
510.8	208_{TI}	
583.2		
2614.5		
338.3	228_{Ac}	
1188.83	40_{K}	K-40
1574.42		

3.6 Radiological Quantities

In this study, the radiological quantities which were determined include; activity concentration, absorbed dose rates, annual effective dose equivalents , radium equivalent activity, the internal and external hazard indices, excess life time cancer risk and annual gonadal dose equivalent.

3.6.1 Determination of the Activity Concentration of the Radionuclides in Selected Samples

The activity concentration (A) measured in $Bqkg^{-1}$ of Ra-226, Th-232 and K-40 in each sample was determined using the equation 3.1 (Amakom et al., 2018; Aneke & Shabangu, 2021; Biira et al., 2021; IAEA, 1989; Nalianya et al., 2022).

$$A = \frac{N_C}{\varepsilon_\gamma P_\gamma M_s t_c} \qquad 3.1$$

where , N_C is the net count rate of the sample, ε_γ is the detector photo-peak efficiency of the peak for gamma energy of interest, P_γ is the probability of transition of radionuclide (branching ratio), M_s is the mass of the sample in kg and t_c is the sample counting time.

The branching ratio, P_γ for each identified radionuclides was obtained from the standard radionuclide data table according to IAEA reports 1989, 2003 and 2007 (IAEA, 1989; Mapping Using Gamma Ray, 2003). The error in the measurement of activity concentration in a sample was obtained using equation 3.2 below (Birge, 1939).

$$\sigma = \frac{\sqrt{N_c}}{\varepsilon_\gamma P_\gamma M_s t_c} \qquad 3.2$$

where σ is the error in activity concentration in a sample , $\sqrt{N_c}$ is square root of the net count rate (net photo peak area) of the sample, ε_γ is the detector photo-peak efficiency of the peak for gamma ray energy of interest, P_γ is the probability of transition of radionuclide (branching ratio), M_s is the mass of the sample in kg and t_c is the sample counting time.

The values of activity concentrations obtained were used for finding the radiological parameters of; absorbed dose rate, annual effective dose equivalent , radium equivalent activity , internal and external radiological hazard indices, excess life time cancer and annual gonadal dose equivalent by the gamma rays in the selected samples of cement and floor tiles.

3.6.2 Determination of Absorbed Dose

The absorbed dose rate, expressed in $nGyh^{-1}$, was evaluated to ascertain whether the samples that were under investigation release radiations that have predictable consequences (deterministic effects) on the health of the body that is exposed to them and also used as a parameter while evaluating the annual effective Dose (Biira et al., 2021; IAEA, 1989; UN, 2013). The absorbed dose in air due to radiations from the materials under investigation was calculated using the following equation 3.3 (Akhtar et al., 2005; IAEA, 1989; Özdiş et al., 2017).

$$D_A = \sum A_x C_x \qquad 3.3$$

where; D_A is the absorbed dose rate , A_x are the mean activity concentrations of U-238, Th-232 and K-40, C_x are their corresponding dose conversion factors in $nGyh^{-1}$per $Bqkg^{-1}$. This study considered the dose conversion factors as $0.463,\ 0.604\ and\ 0.0417$ $nGyh^{-1}$per $Bqkg^{-1}$ for U-238, Th-232 and K-40 respectively (Durusoy & Yildirim, 2017; IAEA, 1989; Mammba et al., 2021).

3.6.3 Determination of Annual Effective Dose

The annual effective dose measured in $mSvy^{-1}$ was assessed to examine whether the radiations from the samples studied can cause the stochastic health effects to the body. The annual effective dose due to inhalation of radon gas from materials under investigation was determined using a conversion coefficient of 0.7 $SvGy^{-1}$, the absorbed dose in air and the indoor occupancy factor according to equation 3.4 (Biira et al., 2021; IAEA, 1989; Mammba et al., 2021; Penabei et al., 2018; Sharma et al., 2015).

$$D_{AE} = D_A C_f O_f \qquad 3.4$$

where; D_{AE} is the annual effective dose, D_A, C_f and O_f , are the Absorbed dose, conversion coefficient factor and indoor occupancy factor time for a year (0.8×365 d $\times$ 24 h $\simeq$ 7008 h yr^{-1}) (Higley et al., 2012; Mammba et al., 2021; Nations et al., 2000).

3.6.4 Determination of Radium Equivalent Activity

The radium equivalent activity is the sum of the activities of Ra-226, Th-232 and K-40. Natural radio nuclides in soils, rocks, plants and many other sources have non uniform distribution and this causes each area from which the samples are produced to have specific levels of background radiation (Sheppard et al., 1980; Siddeeg et al., 2018). Therefore, radium equivalent concentration index measured in $Bgkg^{-1}$ was calculated to compare the specific activities of the selected samples containing Ra-226, Th-232 and K-40 using the following equation 3.5 (Durusoy & Yildirim, 2017; IAEA, 1989; Mittal et al., 2016)

$$Ra_{eq} = A_{Ra} + 1.43A_{Th} + 0.077A_K \leq 370 \qquad 3.5$$

where; Ra_{eq} , A_{Ra}, A_{Th} and A_K are radium equivalent activity ,specific activities of Ra-226, Th-232 and K-40 respectively. The equation 3.5 is based on the fact that 370$Bqkg^{-1}$ of Ra-226, 259$Bqkg^{-1}$ of Th-232 and 4810$Bqkg^{-1}$ of K-40 give the same gamma dose equivalent

3.6.4 Estimation of External and Internal Hazard Indices

The external hazard index (E_H) evaluates the indoor radiation dose rate due to the external exposure of the dwellings to gamma radiations from the natural radionuclides in building materials. The external hazard index was calculated using the following equations 3.6 (Mammba et al., 2021; Purnama & Damayanti, 2020).

$$E_H = \frac{A_{Ra}}{370} + \frac{A_{Th}}{259} + \frac{A_K}{4810} \leq 1 \qquad 3.6$$

The internal hazard index (I_H) measures the inner exposure to radon and its daughter isotopes. It results in irradiation of critical organs such as the gastrointestinal tract, thyroid gland and bones. The internal radiological hazard index was obtained by reducing the maximum permissible concentration of radium of 370 $Bqkg^{-1}$ by a half to 185 $Bqkg^{-1}$, and was determined using the following equations 3.7.

$$I_H = \frac{A_{Ra}}{185} + \frac{A_{Th}}{259} + \frac{A_K}{4810} \leq 1 \qquad 3.7$$

where, A_{Ra}, A_{Th} , $and\ A_K$ are activity concentrations due Radium-226, Thorium-232 and potassium -40 radionuclides respectively in the selected samples of cement and tiles.

The numerical values in the denominators of equations 3.6 and 3.7 are the global maximum permissible limit of activity concentration in $Bqkg^{-1}$ of the radionuclides of radium, thorium and potassium. To avoid the expected risks, the external and internal hazard index should be less than 1, which corresponds to maximally admissible radium-equivalent activity 370 $Bqkg^{-1}$ (Kapanadze et al., 2019b; UN, 2013).

3.6.6 Estimation of the Excess Life Time Cancer Risks and Annual Gonadal Equivalent Dose

The excess life time cancer risk (ELCR), is a measure of the risk that cancer development can happen during a person`s life time. In cancer research, it is usually given as the likelihood that a person who is free of a certain type of cancer will develop or die from that type of cancer during his or her lifetime (Elgazzar & Kazem, 2015). Excess life time cancer risk (ELCR) was calculated using the following equation 3.8.

$$ELCR = D_{AE} x DL x RF \qquad 3.8$$

where EDE, DL and RF is the annual Effective Dose , duration of life (70 years) and Risk factor (Sv^{-1}) or Fatal cancer risk per Sievert. For stochastic effects, ICRP uses values of RF = $0.05x10^{-3}mSv^{-1}$ for the public . The ELCR value obtained in this study was compared with the global recommended value of $0.29x10^{-3}$ (Assembly, 2016; IAEA, 1989; Nations et al., 2013a; UN, 2013).

Annual gonadal equivalent dose(AGED); In the assessment of Annual gonadal equivalent dose, gonads, bone surface cells and bone marrow are organs of interest because they are most sensitive parts of the human body to radiation (UN, 2013). An increase in AGED has been known to affect the bone marrow, causing destruction of the red blood cells that are then replaced by white blood cells (Nations et al., 1989). This situation results in a blood cancer called leukemia which is fatal (Agbalagba et al., 2014; Biira et al., 2014; IAEA, 1989; Penabei et al., 2018). According UNSCEAR (1988) report (Agency et al., n.d.; Nations et al., 1989), the maximum permissible dose is 0.3mSv per year. The annual gonadal equivalent dose (AGED) in mSv/y due to the activity concentrations of Ra-226, Th-232, and K-40 was calculated using the following equation 3.9 (Ridha & Hasan, 2016).

$$AGDE = \frac{3.09A_{Ra} + 4.19A_{Th} + 0.314A_K}{1000} \qquad 3.9$$

3.7 Data Analysis

The main notable photo peaks which were displayed and visible on the PC screen from the detector system were used to find the fundamental data. Centroid energy, standard deviation, Full Width at Half Maximum (FWHM), the net photo peak count, acquisition time, and counting rate were among the basic data that was necessary for further measurements. The radionuclides were identified using the centroid energy, and the activity concentrations of the radionuclides in the samples were determined using the count rates. Since Ra-226, Th-232, and K-40 are the parent and daughter radionuclide emitters of gamma rays, they were the radionuclides of interest in this study. Statistical mean and range were used to examine data on radionuclide activity concentrations, absorbed dose rates, annual effective dose, radium equivalent activity, internal and external hazard indices, excess life time cancer risk and annual gonadal equivalent dose. Originlab-2019b software was used to generate graphs from the statistical data obtained for all the examined samples of tiles and cement.

CHAPTER FOUR: RESULTS AND DISCUSSIONS

4.0 Introduction

In this study, the main objectives were to identify radionuclides in cement and floor tile samples and calculate their activity concentrations, absorbed dose rates, annual effective dose, radium equivalent activity, levels of radiological hazards indices both external and internal, excess life time cancer risk and annual gonadal equivalent dose. The radionuclides detected and radiological parameters assessed for the selected samples in this study were compared with similar studies that have been conducted in different regions or countries.

4.1 Detection of Gamma Ray Emitting Radionuclides in Samples

The process of identifying the prominent photo energy peaks of the spectra formed by gamma rays from each radionuclide present in the samples provided the basis for the detection of radionuclides that emit gamma rays in the cement and tile samples. The radionuclides detected from the cement and floor tile samples and their corresponding phot peak energies are shown in Table 4.1. In the detection of gamma ray emitting radionuclides, the prominent photo peak counts were identified and their experimental energies determined which were matched with the theoretical energies from the standard radionuclide data tables. The radionuclides of Ra-226, Th-232 and K-40 were detected in all the samples of cement and tiles.

Table 4.1: Gamma Emitting Radionuclides Detected in the Samples.

Sample category	Cement	Floor tiles	Photo peak energy (keV)
Radionuclides	Bi-214 (Ra-226)	Bi-214 (Ra-226)	609.3 and 1120.28
	Pb-214 (Ra-226)	Pb-214 (Ra-226)	295.2 and 351.9
	Ac-228 (Th-232)	Ac-228 (Th-232)	911.2
	TI-208 (Th-232)	TI-208 (Th-232)	510.7 and 583.2
	K-40	K-40	1460.8

4.2 Activity Concentrations of Radionuclides in the Samples

The activity concentrations of Th-232, K-40, and Ra-226, the radionuclides that were identified as emitters of gamma rays, were calculated for each sample using equation 4.1.

$$A = \frac{N_C}{\varepsilon_\gamma P_\gamma M_s t_c} \qquad 4.1$$

where; N_C is the net count rate of the sample, ε_γ is the detector photo-peak efficiency of the peak for gamma energy of interest, P_γ is the probability of transition of radionuclide (branching ratio), M_s is the mass of the sample in kg and t_c is the sample counting time.

The activity concentration of Ra-226 was calculated from the gamma rays of photo peak energies 186.2 keV, 238.6 keV and 609.3 keV, for Ra- 226, Pb-214 and Bi-214 all corresponding to Ra-226 which is a decay daughter nuclide of U-238. The activity concentration of Th-232 was determined from the gamma rays of photo peak energies of 510.7 keV, 583.2 keV and 911.2 keV for TI-208, TI-208 and Ac-228 respectively. The activity concentration of K-40 was determined by its own gamma ray photo peak at the energy of 1460.8 keV. The evaluated activity concentrations of the parent and daughter gamma-ray emitting radionuclides, Ra-226, Th-232, and K-40 obtained in samples of this study were compared with the global average dose limit of 40 $Bqkg^{-1}$, 35 $Bqkg^{-1}$ and 400 $Bqkg^{-1}$ provided by IAEA, UNSCEAR, WHO and ICRP (IAEA, 1989; Nations et al., 2013b; Sidique et al., 2022) for Ra-226, Th-232 and K-40 respectively. These guidelines offer benchmarks for determining whether the measured values pose any health or environmental risks. By assessing the results against these international standards, it becomes possible to highlight whether the activity concentrations observed in the study exceed safety thresholds, thus making the findings more relevant to public safety and environmental protection(I. Publication, 2015).

4.2.1 Activity Concentrations of Radionuclides in the Selected Floor Tiles

Table 4.2 shows the activity concentration values of Ra-226, Th-232, and K-40 in the selected floor tile samples. Radiological parameters, including radium equivalent activity, were also calculated and compared to demonstrate how they varied between the tile samples. The activity concentrations of the radionuclides were found to vary across all the samples. For radium, thorium, and potassium, the average values of their activity concentration were 30.8 ± 1.4 $Bqkg^{-1}$, $95.8 \pm 2.3\ Bqkg^{-1}$, and $388.6 \pm 6.2\ Bqkg^{-1}$ respectively. Ra-226, Th-232, and K-40 were found to have lowest activity concentrations of $13.2 \pm 0.8\ Bqkg^{-1}$, $38.7 \pm 1.5\ Bqkg^{-1}$, and $192.9 \pm 2.6\ Bqkg^{-1}$, corresponding to tile samples T_9, T_{13}, and T_{18}, respectively, while the maximum values of $49.0 \pm 1.9\ Bqkg^{-1}$, $149.5 \pm 2.5\ Bqkg^{-1}$, and $526.7 \pm 8.0\ Bqkg^{-1}$,

corresponding to tile samples T_4, T_9, and T_{16}, respectively were obtained as indicted in the Table 4.1.

The average activity concentration of Ra-226 and K-40 in the selected samples were below the global dosage limit of 40 $Bqkg^{-1}$ and 400 $Bqkg^{-1}$ respectively whereas that for Th-232 , exceeded the world accepted average value of 35 $Bqkg^{-1}$ (Mapping Using Gamma Ray, 2003; Özdiş et al., 2017; Penabei et al., 2018; To & General, 2021; UN, 2013). Some tile samples demonstrated high activity concentration of Th-232 above the global limit. This could be due to the presence of rare earth phosphate minerals, monazite in igneous rocks which contain up to 12% thorium phosphate. Specific samples exhibiting activity concentrations of K-40 over globally accepted thresholds indicate that the source materials for these floor tile samples may have come from or were in close proximity to agricultural farms that apply potassium-rich inorganic fertilizers. Certain samples' elevated potassium levels may also be related to the presence of micas such as biotite and potash feldspar (Agbalagba et al., 2014; Nalianya et al., 2022; USGS, 2022).

Table 4.2: Activity concentrations of Ra-226, Th-232 and K-40 and radium equivalent activity in the selected samples of tiles.

Sample code	**Activity concentration ($Bqkg^{-1}$)**			**Ra_{eq}** ($Bqkg^{-1}$)
	A_{Ra}	A_{Th}	A_K	
T_1	20.3±0.8	46.6±1.3	336.8±5.2	112.9±3.1
T_2	26.6±0.9	138.7±3.7	372.3±5.8	253.6±6.7
T_3	23.9±1.1	72.3±2.0	371.9±5.5	155.8±4.4
T_4	49.0±2.1	138.0±2.8	345.3±5.3	272.9±6.5
T_5	43.2±1.9	79.1±2.2	355.2±5.6	183.6±5.5
T_6	34.1±1.4	108.2±2.5	297.4±5.1	211.7±5.4
T_7	33.2±1.3	118.1±2.4	350.8±6.0	229.1±5.2
T_8	27.3±1.2	124.7±2.2	359.9±6.1	233.3±4.9
T_9	13.2±0.9	149.5±2.5	484.2±7.7	264.2±5.0
T_{10}	25.7±1.2	55.5±1.8	478.5±7.7	141.9±4.4
T_{11}	36.8±2.4	63.8±1.9	519.7±8.0	168.2±5.8
T_{12}	31.0±1.3	111.3±2.5	334.3±5.7	216.0±5.4
T_{13}	30.5±1.3	38.7±1.5	394.2±6.2	116.2±3.9
T_{14}	22.0±1.0	86.9±2.2	487.9±7.7	183.9±4.8
T_{15}	37.9±1.4	89.6±2.3	469.9±7.6	202.2±5.3
T_{16}	18.3±1.1	44.5±1.6	526.7±8.0	122.5±4.0

T_{17}	26.8±1.6	105.7±2.5	511.5±7.9	217.3±5.7
T_{18}	40.9±1.9	110.1±2.6	192.9±2.6	213.2±5.8
T_{19}	44.8±2.0	138.3±3.1	194.0±4.9	257.5±6.8
AVR	**30.8±1.4**	**95.8±2.3**	**388.6±6.2**	**197.7±5.2**

Figure 4.1 shows that the activity concentration of Radium-226 (Ra-226) was predominantly below 40 $Bqkg^{-1}$ in the majority of tile samples, with the exceptions being samples T_4, T_5 , T_{18} and T_{19}. In contrast, the activity concentration of Thorium-232 (Th-232) exceeded the globally recognized average value of 35 $Bqkg^{-1}$ across all samples. The observed variations in the activity concentrations of Ra-226, Th-232, and Potassium-40 (K-40) among the individual samples can be attributed to different factors such as; the geological diversity of the regions from which the raw materials were sourced, the difference in mineral composition following the fact that different minerals naturally contain varying levels of radionuclides for instance, uranium and thorium are more prevalent in granite and phosphorite, while potassium is abundant in feldspar. and the differences in manufacturing processes depending on the country of origin (Kapanadze et al., 2019b; Shahbazi-Gahrouei et al., 2013). Glazing and firing process in kilns, involves heating the tiles to high temperatures, this can influence the distribution of radionuclides but generally does not alter the overall concentration significantly (Nicoletti et al., 2002). The glaze used on tiles may also contain materials with varying radionuclide levels, which could contribute to the overall radioactivity of the tiles.

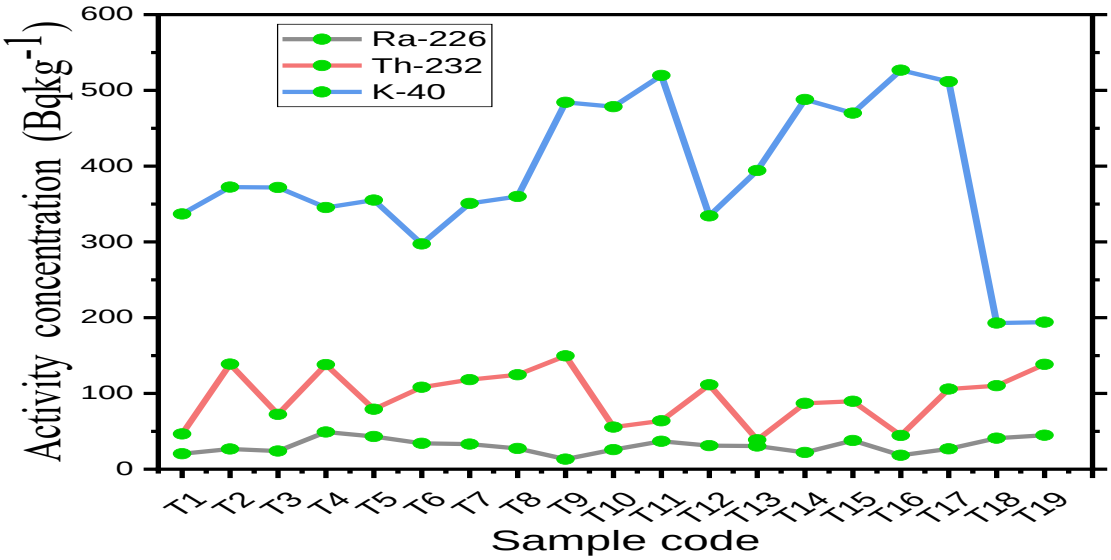

Figure 4.1: A Comparative graph showing the variation of activity concentrations of the natural radionuclides in the selected tile samples.

The average activity concentrations of Radium-226 (Ra-226), Thorium-232 (Th-232), and Potassium-40 (K-40) observed in this study were marginally lower than the values reported by Joel et al. (2018) (Joel, Maxwell, Adewoyin, Ehi-eromosele, et al., 2018), who documented concentrations of 68.2 $Bq \cdot kg^{-1}$, 173.9 $Bq \cdot kg^{-1}$, and 490.0 $Bq \cdot kg^{-1}$, respectively, in their assessment of natural radionuclides and radiological hazards in tiles. A comparable study conducted by El-Gamal et al. (2018) (El-Gamal et al., 2018), focusing on the measurement of natural radioactivity and radiological hazard evaluation in ceramic tiles, reported average activity concentrations of 46.17 $Bq \cdot kg^{-1}$ for Ra-226, 51.65 $Bq \cdot kg^{-1}$ for Th-232, and 701.62 $Bq \cdot kg^{-1}$ for K-40. In the current study, while the average activity concentration of Th-232 (95.8 $Bq \cdot kg^{-1}$) was high than previously reported, the concentrations of Ra-226 and K-40 were notably lower, measured at 30.8 $Bqkg^{-1}$ and 388.6 $Bqkg^{-1}$, respectively. These discrepancies could be due to the differences in geographic locations, analytical methods, or sample types used in each study.

4.2.2 Activity Concentrations due to Gamma Ray Emitting Radionuclides in the Selected Cement Brands

Table 4.3, shows the measured activity concentrations of the radionuclides of Th-232, Ra-226, and K-40 in the cement brands that were taken into consideration for this work. The activity

concentrations for Ra-226 ranged from $10.2 \pm 0.7\ Bqkg^{-1}$ for sample C_6 to $86.1 \pm 4.3 Bqkg^{-1}$ for sample C_1, that of Th-232 was from $28.9 \pm 1.3\ Bqkg^{-1}$, for sample C_8 to $105.3 \pm 2.5\ Bqkg^{-1}$ for sample C_{13}, and that of K-40 was from $334.2 \pm 6.4\ Bqkg^{-1}$ for sample C_7 to $508.5 \pm 7.9\ Bqkg^{-1}$ for sample C_6, respectively. Ra-226, Th-232, and 40K had mean concentrations of $31.2 \pm 1.7\ Bqkg^{-1}$, $61.9 \pm 1.9\ Bqkg^{-1}$ and $463.1 \pm 7.5\ Bqkg^{-1}$ respectively. With the exception of Ra-226, whose average value is below the globally accepted threshold of 40 $Bqkg^{-1}$, the average values of Th-232 and K-40 were above the global average of 35 and 400 $Bqkg^{-1}$ respectively. Al-Kaabi and Hmood also reported higher values (Al-Kaabi & Hmood, 2019; Volume, 2006). The differences in the raw materials' geological origin that go into making each cement brand could be the cause of the variation in the mean activity concentrations. The variation in the activity concentration can also be attributed to the processing and blending of cement. During the manufacturing of building materials, processes such as milling, firing, and chemical treatments can concentrate radionuclides (Engineer & Chemicals, 2015). For example, during the production of cement, the heating of raw materials can cause volatilization and subsequent concentration of certain radionuclides in the final product. Also during the production of these materials, processes that involve mixing with non-radioactive additives or the removal of certain components can dilute radionuclide concentrations(Engineer & Chemicals, 2015; Huntzinger & Eatmon, 2009). For instance, adding fly ash or slag, which may have different radionuclide levels compared to the base material, can significantly alter the overall activity concentrations in the final product.

In general, K-40 had the highest mean activity concentration when compared to the other two radionuclides of Ra-226 and Th-232 in the samples. For any material derived from geology, this variation is normal and expected given the relative abundance of K-40 in the natural world. (Agbalagba et al., 2014; Mammba et al., 2021; Nalianya et al., 2022).

Table 4.3: The activity concentrations of Ra-226, Th-232 and K-40 and Ra_{eq} of the cement samples.

Sample code	**Activity concentration($BqKg^{-1}$)**			
	A_{Ra}	A_{Th}	A_K	**Ra_{eq}**($Bqkg^{-1}$)
C_1	86.1±4.3	70.6±2.3	459.6±7.5	222.5±8.2
C_2	61.9±3.0	84.6±2.2	439.7±7.3	216.8±6.8
C_3	29.9±1.9	31.8±1.4	506.4±7.9	114.4±4.5
C_4	19.8±1.5	82.2±2.2	492.7±7.8	175.3±5.2
C_5	21.3±1.4	29.1±1.3	408.8±7.1	94.4±3.8
C_6	10.2±1.4	81.7±2.2	508.5±7.9	166.2±5.1
C_7	11.4±0.7	33.1±1.4	334.2±6.4	84.5±3.2
C_8	18.2±0.7	28.9±1.3	506.0±7.9	98.6±3.2
C_9	25.8±1.2	57.1±1.8	435.0±7.3	141.0±4.4
C_{10}	29.7±1.3	88.3±2.3	461.3±7.5	191.5±5.1
C_{11}	41.5±2.3	62.3±1.8	495.4±7.8	168.7±5.5
C_{12}	23.3±1.1	49.0±1.7	492.1±7.8	131.3±4.1
C_{13}	26.7±1.2	105.3±2.5	481.2±7.7	214.2±5.4
AVG	**31.2±1.7**	**61.9±1.9**	**463.1±7.5**	**155.3±4.9**
Min value	**10.2±0.7**	**28.9±1.3**	**334.2±6.4**	**84.5±3.2**
Max value	**86.1±4.3**	**105.3±2.5**	**508.5±7.9**	**222.5±8.2**
GDL	**40**	**30**	**400**	**370**

4.3 Estimation of Radium Equivalent Activity

Radium equivalent activity (Ra_{eq}) is a standardized index used to express the total radioactivity due to Ra- 226, Th- 232, and K-40 in a single value, based on their varying radiation hazards. It allows for the comparison of the radioactivity of materials containing different concentrations of these radionuclides (Mattsson & Hoeschen, 2013). Ra_{eq} is essential for assessing the potential radiological hazard of building materials. It considers the different gamma radiation emissions and their associated risks, ensuring that the combined exposure from multiple radionuclides does not exceed safety thresholds. The commonly accepted safety limit is 370 $Bqkg^{-1}$. If the Ra_{eq} of a material is below this limit, the material is generally considered safe for use in construction.

The radium equivalent activity concentration measured in $Bgkg^{-1}$ was calculated to compare the specific activities of the selected samples containing Ra-226, Th-232 and K-40 using the equation 4.2 (Durusoy & Yildirim, 2017; IAEA, 1989; Mittal et al., 2016)

$$Ra_{eq} = A_{Ra} + 1.43A_{Th} + 0.077A_K \leq 370 \qquad 4.2$$

where, A_{Ra}, A_{Th} and A_K are specific activities of Ra-226, Th-232 and K-40 respectively. Based on equation 4.2, values of 370 $Bqkg^{-1}$ for Ra-226, 259 $Bqkg^{-1}$ for Th-232 and 4810 $Bqkg^{-1}$ for K-40, give the same gamma dose equivalent were obtained.

4.3.1 Radium Equivalent Activity in the Selected Floor Tiles Samples

Table 4.2, provides the calculated values of the radium equivalent activity (Ra_{eq}) for each of the tile samples that were examined and Figure 4.2 displays the graphical representation of the radium equivalent activity concentration results. The range of values obtained varied from 112.9 ± 3.1 Bq kg^{-1} in T1 (Twyford, Tanzania) to 272 ± 6.8 Bq kg^{-1} in T4 (Twyford, Kenya). The findings indicate that Ra_{eq} values are below the UNSCEAR (2000) reported maximum permissible value of 370 Bq kg^{-1}, or 1.0 $mSvy^{-1}$ external dosage (Nations et al., 1989, 2013a).

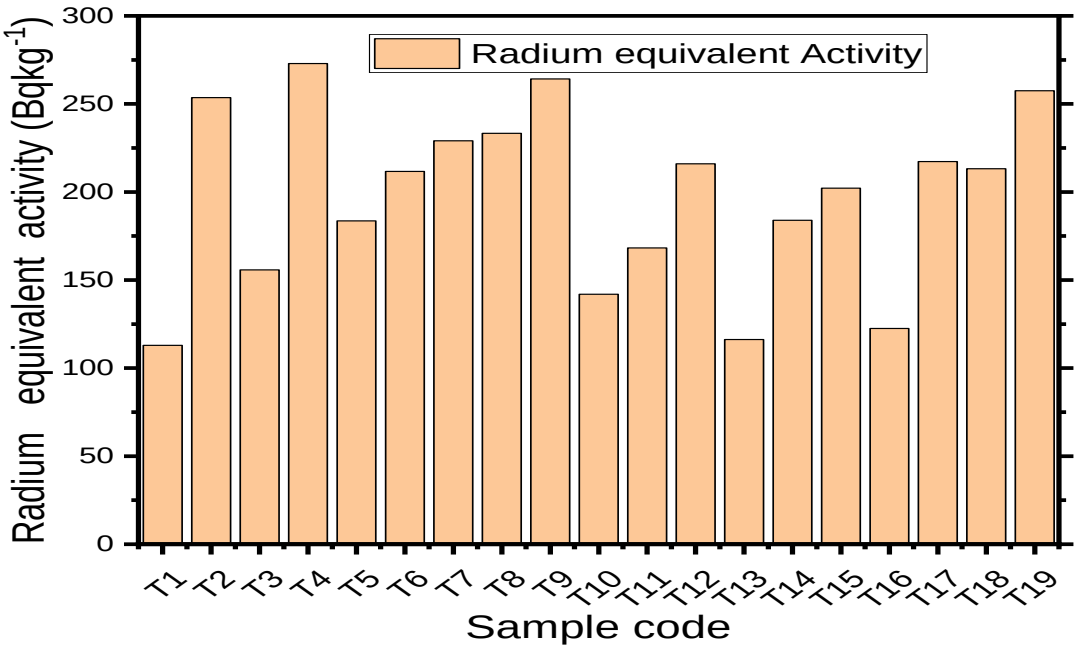

Figure 4.2: Variation of the radium equivalent activity in selected floor tile sample.

4.3.2 Radium Equivalent Activity in the Selected Cement Samples

As can be observed from Table 4.3 and Figure 4.3, the calculated values of of radium equivalent activity (Ra_{eq}) for the cement samples were found to vary from $84.5 \pm 3.2\ Bqkg^{-1}$in C7 (Simba CEM -I , Uganda) to $222.5 \pm 8.2\ Bqkg^{-1}$ in C1 (CEM I- 42.5N –OPC, Tororo uganda), with an average value of $155.3 \pm 4.9\ Bqkg^{-1}$. These values are lower than recommended criterion limit of 370 $Bqkg^{-1}$(Siddeeg et al., 2018; UN, 2013). Similar lower values were also reported by RK.Meindinyo and Ndour (Meindinyo et al., 2017; Ndour et al., 2020) .Therefore, all the cement brands examined in this study are acceptable for the use in the construction industry.

Notably from figure 4.3, Ra-226 concentrations were nearly identical in C_3 and C_{10}, Th-232 activity was comparable in C_4 and C_6, and K-40 activity concentrations were comparable in C_3, C_6, C_8, C_{11}, and C_{12}. These similarities can be attributed to the source of the raw materials or cement brands that are in the same class. This could mean that the companies that manufacture different brands of cement get their raw materials from the same or comparable locations. Variations in the concentrations of Ra-226, Th-232, and K-40 across various cement brands may be explained by the clinker composition, compression strength, and geological and geochemical background (Bediako & Amankwah, 2015; Buregyeya et al., 2018; Döse, 2016).

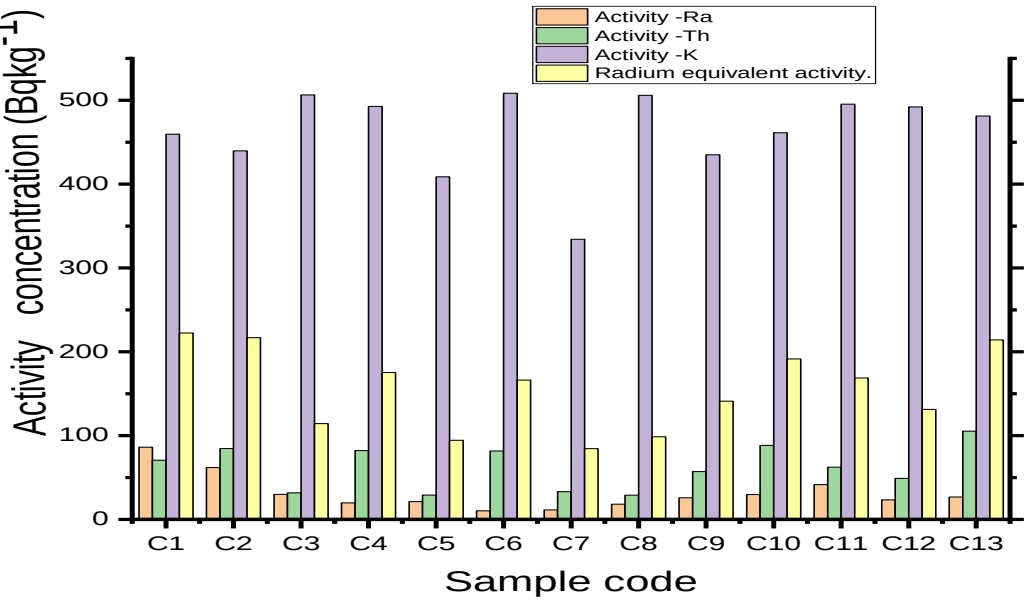

Figure 4.3: Variation of the activity concentration of the radionuclides and radium equivalent activity of the selected cement samples.

4.4 Determination of the Absorbed Dose Rate

The absorbed dose rate (D_A) is the amount of radiation energy absorbed per unit mass of a material or tissue, commonly measured in nanograys per hour ($nGyh^{-1}$). It estimates the radiation dose that individuals might receive from building materials. It is a critical factor in determining the overall exposure to gamma radiation from materials in a given environment (Al-Kaabi & Hmood, 2019; Mattsson & Hoeschen, 2013).

The absorbed dose in air due to radiation from the investigated samples was calculated using Equation 4.3 (Akhtar et al., 2005; IAEA, 1989; Özdiş et al., 2017).

$$D_A = \sum A_x C_x \qquad 4.3$$

where; D_A is the absorbed dose rate, A_x are the mean activity concentration of U-238, Th-232 and K-40, C_x are their corresponding dose conversion factors in $nGyh^{-1}$per $Bqkg^{-1}$. This study considered the dose conversion factors as $0.463,\ 0.604\ and\ 0.0417$ $nGyh^{-1}$per $Bqkg^{-1}$ for U-238, Th-232 and K-40 respectively (IAEA, 1989; Mammba et al., 2021).

4.4.1 Absorbed Dose Rate in the Selected Floor Tile Samples

Table 4.4 shows the absorbed dose rate for each tile sample and the combined average absorbed dose rate. The absorbed dose ranged from $51.6 \pm 1.4\ nGyh^{-1}$ for sample T_1 to $120.4 \pm 2.9\ nGyh^{-1}$ for sample T_4 as shown in Table 4.4 and Figure 4.4. The average absorbed dose rate was found to be $88.3 \pm 2.3\ nGyh^{-1}$ which is above the $84\ nGyh^{-1}$ global accepted indoor absorbed dose (IAEA ANNUAL REPORT 2010, 2010; Penabei et al., 2018). Similar studies carried by John Simiyu. N and E.S Joel (Joel et al., 2019; Nalianya et al., 2022) also reported high value of absorbed dose rate above the world average value.

Table 4.4: The radiation doses in the selected tile samples.

Sample code	D_A (nGy/hr)	D_{AE} (mSv)	AGED (mSv/y)
T_1	51.6±1.4	0.25±0.007	0.364±0.010
T_2	111.6±2.9	0.55±0.014	0.780±0.020
T_3	70.2±2.0	0.34±0.010	0.493±0.014
T_4	120.4±2.9	0.59±0.014	0.838±0.020
T_5	82.6±2.4	0.41±0.012	0.576±0.017
T_6	93.5±2.4	0.46±0.012	0.652±0.017
T_7	101.3±2.3	0.50±0.011	0.708±0.016
T_8	103.0±2.2	0.51±0.011	0.720±0.015
T_9	116.6±2.2	0.57±0.011	0.819±0.016
T_{10}	65.4±2.0	0.32±0.010	0.462±0.014
T_{11}	77.3±2.6	0.38±0.013	0.545±0.018
T_{12}	95.5±2.4	0.47±0.012	0.667±0.017
T_{13}	53.9±1.8	0.26±0.009	0.380±0.012
T_{14}	83.1±2.1	0.41±0.011	0.586±0.015
T_{15}	91.3±2.4	0.45±0.012	0.640±0.016
T_{16}	57.3±1.8	0.28±0.009	0.408±0.013
T_{17}	97.6±2.5	0.48±0.013	0.686±0.018
T_{18}	93.5±2.6	0.46±0.013	0.648±0.018
T_{19}	112.4±3.0	0.55±0.015	0.779±0.021
AVG	**88.3±2.3**	**0.43±0.011**	**0.619±0.016**

According to Figure 4.4, the majority of the samples had indoor absorbed dose rates that were higher than the globally accepted average of 84 $nGyhr^{-1}$(Özdiş et al., 2017; Penabei et al., 2018; UN, 2013). The tile sample T4 (Twyford, Kenya) had the highest absorbed rate of 120.4±2.9 $nGyh^{-1}$, whereas the tile sample T1 (Twyford, Tanzania) had the lowest of 51.6±1.4 $nGyh^{-1}$ These levels of absorbed dose rates are directly connected to their activity concentration. All studied Uganda - homemade tiles; from Goodwill, modern and mellinium manufacturers demonstrated comparatively low radiation levels. This could be as a result of getting raw

materials for these samples from Areas with lower background radiation levels, often due to geological stability and lack of volcanic or tectonic activity, would contribute to lower absorbed dose rates in the samples.

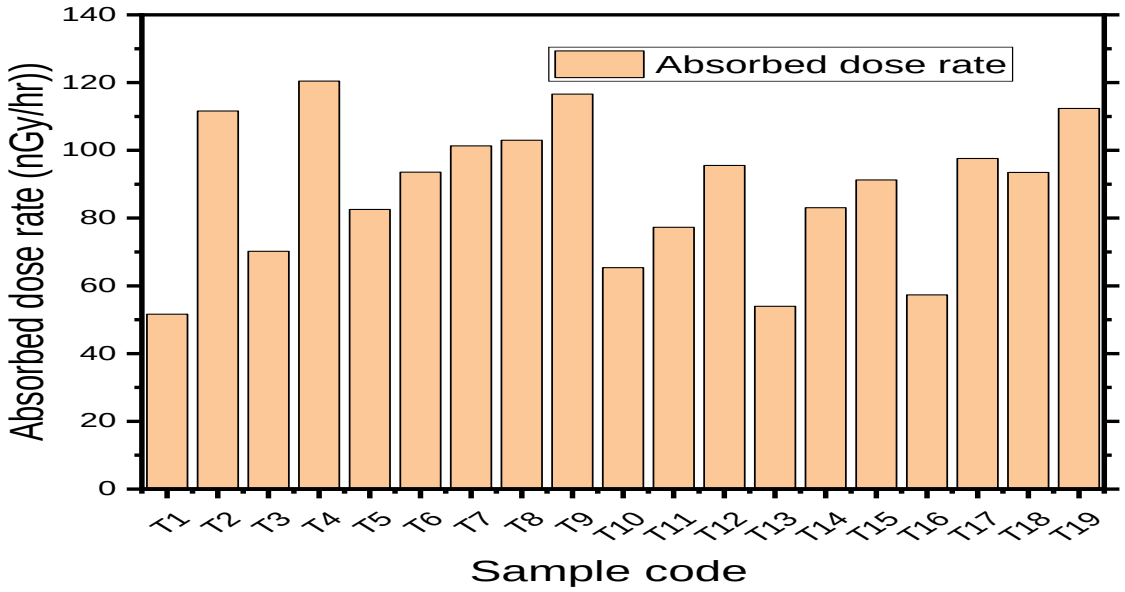

Figure 4.4: Variation of the absorbed dose rates in the selected floor tile samples

4.4.2 Absorbed Dose Rate in the Selected Cement Samples

The calculated indoor absorbed dose rates for the selected cement brands are presented in Table 4.5. The second column of Table 4.5 shows that average absorbed dosage rate indoors is $71.1 \pm 2.2\ nGyh^{-1}$, with a range of $39.2 \pm 1.4\ nGyh^{-1}$ to $101.7 \pm 3.7\ nGyh^{-1}$. This demonstrates that the acquired average absorbed dose rate data remains under the accepted $84\ nGyh^{-1}$ limit indoors. However results of the absorbed dose in C_1 sample (Portland cem –I 42.5N -OPC, Tororo-Uganda), C_2 sample (Portland pozzolana cem –II, Tororo-Uganda) and C_{13} (Huaxin power plus portland, Tanzania) were above the world agreed global value of $84\ nGyh^{-1}$ hence care must be taken while using these cement brands to avoid associated deterministic and stochastic health effects (Durusoy & Yildirim, 2017; IAEA, 1989; UN, 2013). This variation in absorbed dose also reveals the difference in elemental composition at the various geological places from where the basic raw materials for cement are sourced.

Table 4.5: The radiation doses in the selected cement samples.

Sample code	D_A (nGy/hr)	D_{AE} (mSv/y)	AGED (mSv/y)
C_1	101.7±3.7	0.499±0.018	0.706±0.025
C_2	98.1±3.0	0.481±0.015	0.684±0.021
C_3	54.2±2.1	0.266±0.010	0.385±0.014
C_4	79.4±2.3	0.389±0.011	0.560±0.016
C_5	44.5±1.7	0.218±0.009	0.316±0.012
C_6	75.3±2.3	0.369±0.011	0.534±0.016
C_7	39.2±1.4	0.192±0.007	0.279±0.010
C_8	47.0±1.4	0.231±0.007	0.336±0.010
C_9	64.6±2.0	0.317±0.010	0.456±0.014
C_{10}	86.3±2.3	0.423±0.011	0.607±0.016
C_{11}	77.5±2.5	0.380±0.012	0.545±0.017
C_{12}	60.9±1.8	0.299±0.009	0.432±0.013
C_{13}	96.0±2.4	0.471±0.012	0.675±0.017
AVG	**71.1±2.2**	**0.349±0.011**	**0.501±0.015**
Min Value	**39.2±1.4**	**0.192±0.007**	**0.279±0.010**
Max value	**101.7±3.7**	**0.499±0.018**	**0.706±0.025**

4.5 Determination of the Annual Effective Dose

The annual effective dose is the estimated radiation dose a person receives in a year, accounting for the type of radiation and the sensitivity of different tissues and organs. It is expressed in millisieverts per year ($mSvy^{-1}$). This parameter is used to assess the potential health risk to humans from prolonged exposure to radiation. The International Commission on Radiological Protection (ICRP) recommends an annual limit of 1.0 $mSvy^{-1}$ for the general public from the sources (Commission, 2004; To & General, 2021).

The Annual Effective Dose (D_{AE}) from materials (samples) which were investigated was determined using a conversion coefficient of 0.7 $SvGy^{-1}$ from the absorbed dose in air and the indoor occupancy factor of 0.8 according to equation 4.4 (Biira et al., 2021; IAEA, 1989; Mammba et al., 2021; Penabei et al., 2018; Sharma et al., 2015).

$$D_{AE} = D_A C_f O_f \qquad 4.4$$

where; D_{AE}, D_A, C_f and O_f , are the annual effective dose, Absorbed dose, conversion coefficient factor and indoor occupancy factor time for a year (0.8 × 365 d × 24 h ≃ 7008 h yr^{-1}) (Higley et al., 2012; Mammba et al., 2021; Nations et al., 2000).

4.5.1 Annual Effective Dose due to Radiations from the Selected Floor Tile Samples

Table 4.4 provides the calculated Annual Effective Dose (D_{AE}) values for all the tile samples that were studied; Figure 4.5 displays the graphical representation of these values. The average annual effective dosage is $0.43 \pm 0.011\, mSvy^{-1}$ and varies from $0.25 \pm 0.007\, mSvy^{-1}$ in T_1 (Twyford, Tanzania) to $0.59 \pm 0.014\, mSvy^{-1}$ in T_4 (Twyford, Kenya). The average indoor annual effective dosage was found to be less than the $1.0\, mSvy^{-1}$ worldwide acceptable limit (Clement et al., 2012; Nations et al., 2013b; UN, 2013).

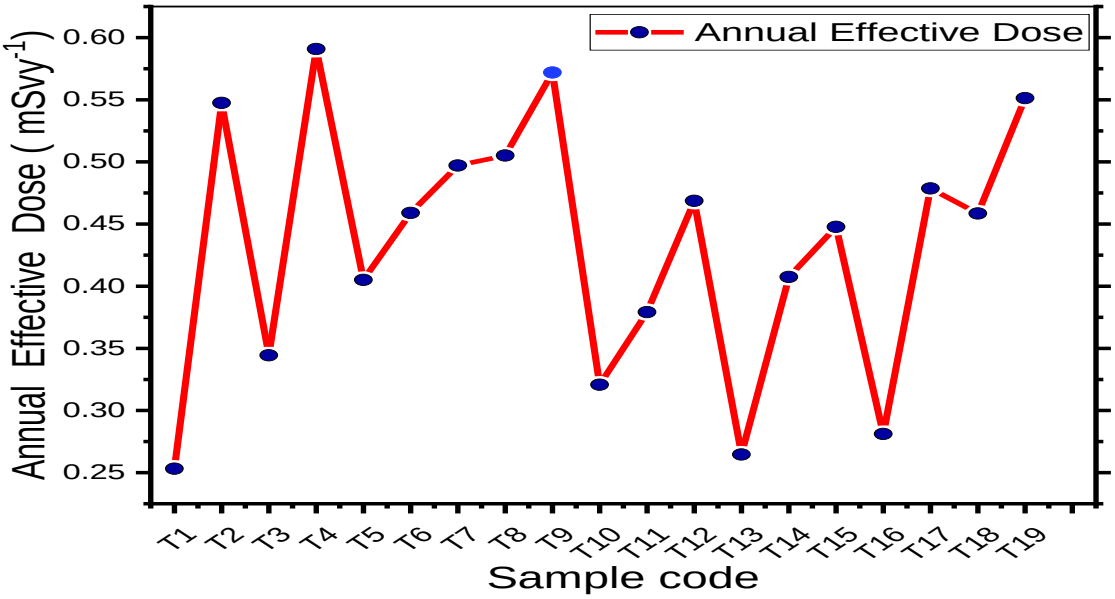

Figure 4.5: Variation of the Annual effective Dose for the selected floor tile samples.

This could be due to low activity concentration of naturally occurring radionuclides of Uranium-238 (U-238), Thorium-232 (Th-232), and Potassium-40 (K-40) in most of the samples studied. These radionuclides are the main contributors to radiation in the environment, and their reduced presence directly correlates with lower absorbed dose rates and annual effective dose. The result in this study is in agreement with E. Sidique (Sidique et al., 2022) that reported the annual effective dose in analyzed ceramic tiles sample to be 0.10 $mSvy^{-1}$.

4.5.2 Annual Effective Dose due to Radiations from the Selected Cement Samples

Table 4.5 shows the annual effective dosage values that were calculated for the thirteen (13) samples of the cement brands. The fourth column in Table 4.5 indicates the annual effective dose values, which ranged from $0.192 \pm 0.007\, mSvy^{-1}$ in C_7 (Ordinary Portland cement Cem –I 42.5N Simba, Uganda) to $0.499 \pm 0.018\, mSvy^{-1}$ in C_1 (Portland cem –I 42.5N –OPC, Tororo, Uganda), with a mean value of $0.349 \pm 0.011\, mSvy^{-1}$. It should be noted that the average value of the obtained annual effective dose for the cement samples in this study was lower than the maximum value of $1.0\, mSvy^{-1}$ stated by the ICRP report (Biira et al., 2021; Commission, 2004; Nations et al., 1989). This study's finding aligns with the reported annual effective dose values, which ranged from 0.108 $mSvy^{-1}$ to 0.718 $mSvy^{-1}$, as observed in O. Ndour's assessment of natural radioactivity and radiological hazards in various types of cement used in Senegal (Ndour et al., 2020).

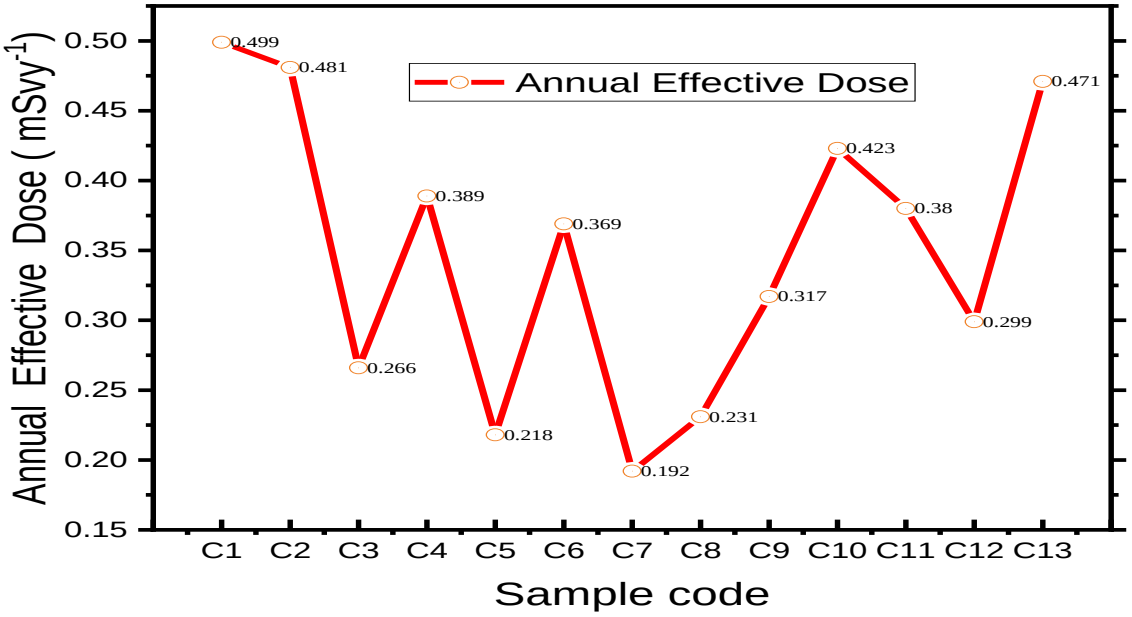

Figure 4.6: Variation of the annual effective dose in the selected cement samples

Figure 4.6 shows that across all analyzed samples, the absorbed dose remains well below 50% of the established maximum permissible dose limit of 1.0 $mSvy^{-1}$. Consequently, the specific cement brands utilized in the construction within Tororo town present a negligible radiological

health risk to the inhabitants. This finding suggests that the radiogenic contribution of these materials to the overall exposure of the population is minimal.

4.6 Calculation of the Annual gonadal Equivalent Dose

The Annual Gonadal Equivalent Dose (AGED) is a radiological parameter that estimates the radiation dose absorbed by the reproductive organs (gonads) from exposure to natural radionuclides in building materials. It is part of the broader concept of assessing the radiological impact on the human body, focusing on sensitive tissues (Mattsson & Hoeschen, 2013; Yoder et al., 2022). AGED is crucial for evaluating the potential long-term genetic and reproductive health risks posed by radiation exposure from building materials. By quantifying the dose to the gonads, this parameter helps assess whether the use of certain materials might increase the risk of genetic mutations or reproductive issues over time. A lower AGED value below 0.3 $mSvy^{-1}$ indicates a safer material from a radiological perspective.

The annual gonadal equivalent dose (AGED) in $mSvy^{-1}$ due to the activity concentrations of Ra-226, Th-232, and K-40 in the samples investigated was calculated using equation 4.5 (Ridha & Hasan, 2016).

$$AGDE = \frac{3.09A_{Ra} + 4.19A_{Th} + 0.314A_K}{1000} \qquad 4.5$$

where; $A_{Ra}, A_{Th}\ and\ A_K$ are the activity concentrations of Ra-226, Th-232 and K-40 in the analyzed samples, 3.09, 4.19 and 0.314 are the associated radiation conversion factors in the body organs or tissues.

4.6.1 Annual Gonadal Dose Equivalent due to Radiation in the Tiles Samples

The values of annual gonadal equivalent dose (AGED), with a mean value of $0.619 \pm 0.016\ mSvy^{-1}$ are shown in Table 4.4 and Figure 4.6. They varied from $0.364 \pm 0.010\ mSvy^{-1}$ in T_1 (Twyford from Tanzania) to $0.838 \pm 0.021\ mSvy^{-1}$ in T_4 (Twyford from Kenya). This mean value exceeded the globally accepted mean value, which ranges from 0.317 to 0.416 mSv y^{-1} (Agbalagba et al., 2014). However, it is noted that every tile sample analyzed had a distinct AGED value that was higher than the global mean value of 0.3 $mSvy^{-1}$, indicating that the possible negative effects of the radiation in these samples are not

negligible. For this reason, these tiles require extra radiological care. Similar high value of AGED was reported by J.S Nalianya (Nalianya et al., 2022). The high average value of the annual gonadal dose in the analyzed sample tiles could be due to the presence of naturally occurring radioactive materials (NORM) in the raw materials used to manufacture the tiles. These materials, such as clay, feldspar, and certain minerals, may contain elevated activity levels of radionuclides of uranium, thorium, and potassium as it was noticed in some samples. An increase in AGED affects the bone marrow and destroys the red blood cell which can result in a blood cancer of the type Leukemia (Commission, 2004; Nations et al., 1989). These values obtained in tile samples show that their rock sources could be of high radioactive rock most probably from igneous rock (Michele et al., 2019; UN, 2013).

From figure 4.6, there is a positive correlation between annual effective dose and AGED. This result could be due uniform distribution of radioactive elements. If the tiles contain naturally occurring radioactive materials (NORM) like uranium, thorium, or potassium-40, which are uniformly distributed throughout the material, both the effective dose (which considers the overall impact on the body) and the gonadal dose (which specifically considers the impact on reproductive organs) would increase together.

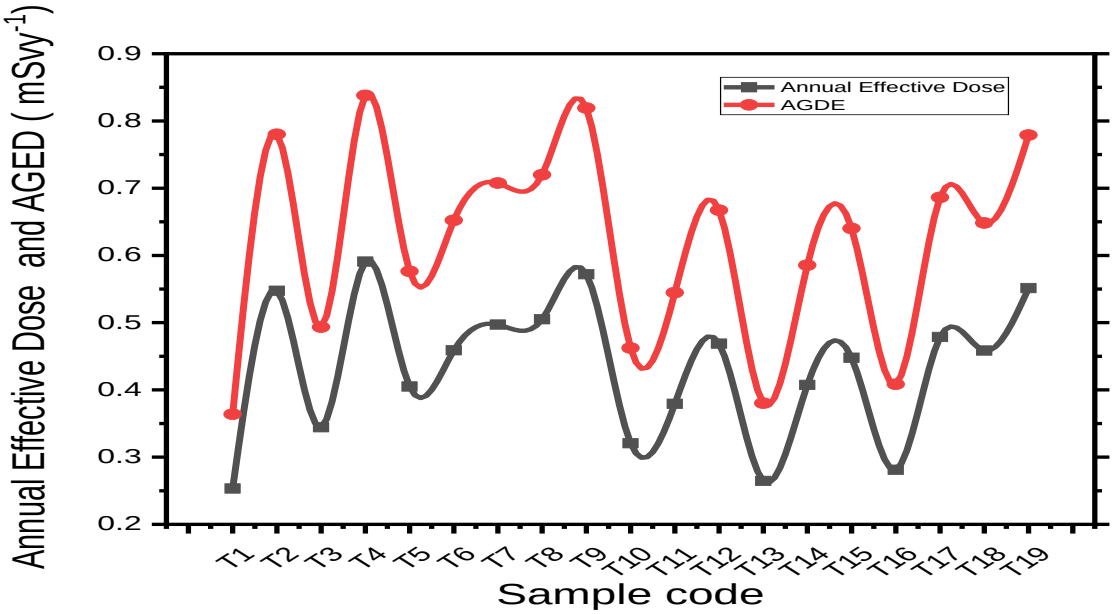

Figure 4.7: Variation of Annual effective Dose and AGED in the selected floor tiles samples.

4.6.2 Annual Gonadal Equivalent Dose due to radiation in the Cement Samples

From Table 4.5, the average value of AGED for the studied cement samples was $0.501 \pm 0.015\ mSvy^{-1}$, with a range of $0.279 \pm 0.010\ mSvy^{-1}$, in C_7 to $0.706 \pm 0.025\ mSvy^{-1}$ in C_1. This is higher than the recommended global mean value of 0.3 $mSvy^{-1}$ (Ndour et al., 2020; Penabei et al., 2018). This implies that the radiation effects in cement samples studied are significant and harmful since they exceed the global mean value limit (Commission, 2004; Nations et al., 1989). It was noted that all the individual cement samples analyzed save for C_7 (OPC 42.5R), had the annual gonadal equivalent dose values higher than the permissible level of 0.3 $mSvy^{-1}$. Similar high average value (0.340 $mSvy^{-1}$) of AGED was reported by O. Ndour (Ndour et al., 2020)

4.7 Estimation of the Radiological Hazard Indices by Gamma Rays in the Samples

The present study examines the radiological internal and external hazard indices caused by gamma rays in tile and cement samples. The global dose limit of unity (1.00), set by the ICRP, was used to compare the hazard levels in the analyzed samples (Commission, 2004).

The external hazard index (E_H) was calculated using equation 4.6 (Mammba et al., 2021; Purnama & Damayanti, 2020).

$$E_H = \frac{A_{Ra}}{370} + \frac{A_{Th}}{259} + \frac{A_K}{4810} \leq 1 \qquad 4.6$$

The internal hazard index (I_H) was calculated using equation 4.7

$$I_H = \frac{A_{Ra}}{185} + \frac{A_{Th}}{259} + \frac{A_K}{4810} \leq 1 \qquad 4.7$$

where, A_{Ra}, A_{Th} ,$and\ A_K$ are the activity concentrations due to Radium-226, Thorium-232 and potassium -40 radionuclides, respectively, in the selected cement and tiles samples.

4.7.1 External and Internal Radiological Hazard Indices by Gamma Rays in the Floor Tile Samples

The calculated external hazard index and internal hazard index values are presented in Table 4.6 and Figure 4.7. The values of E_H ranged from 0.305 ± 0.008 for T_1 (Twyford, Tanzania) to 0.737 ± 0.018 for T_1 (Twyford, Kenya). The external hazard indexes of all the studied tile

samples are less than unity, and accordingly they can safely be used for construction (IAEA, 1989; Nations et al., 2000). Considering that the value of E_H and I_H must not exceed the unit limit (≤ 1), for all the tile samples, the internal hazard indices are lower than unity. Therefore , the use of both locally made and imported floor tiles have no immediate negative health implications on the inhabitants, However, it is necessary to observe and study the long-term cumulative effects on the inhabitants of buildings furnished with tiles (White & Mallya, 2012).

Table 4.6: The radiation hazard indices from the floor tile samples

Sample code	**E_H**	**I_H**	**ELCR ($x10^{-3}$)**
T_1	0.305±0.0.008	0.254±0.010	0.89±0.00235
T_2	0.685±0.018	0.618±0.020	1.92±0.00499
T_3	0.421±0.012	0.362±0.015	1.21±0.00337
T_4	0.737±0.018	0.616±0.023	2.07±0.00495
T_5	0.496±0.015	0.390±0.020	1.42±0.00418
T_6	0.572±0.015	0.487±0.019	1.61±0.00412
T_7	0.619±0.014	0.536±0.018	1.74±0.00395
T_8	0.630±0.013	0.563±0.017	1.77±0.00375
T_9	0.714±0.014	0.683±0.016	2.00±0.00384
T_{10}	0.383±0.012	0.320±0.015	1.12±0.00338
T_{11}	0.454±0.016	0.368±0.022	1.33±0.00449
T_{12}	0.583±0.015	0.506±0.018	1.64±0.00410
T_{13}	0.314±0.011	0.238±0.014	0.93±0.00304
T_{14}	0.497±0.013	0.443±0.016	1.43±0.00369
T_{15}	0.546±0.014	0.451±0.018	1.57±0.00404
T_{16}	0.331±0.011	0.287±0.014	0.98±0.00312
T_{17}	0.587±0.015	0.523±0.012	1.68±0.00438
T_{18}	0.576±0.016	0.476±0.021	1.60±0.00441
T_{19}	0.696±0.018	0.585±0.024	1.93±0.00512
AVG	**0.534±0.014**	**0.458±0.018**	**1.52±0.00396**
Min value	0.305±0.008	0.238±0.010	0.886±0.0024
Max value	0.737±0.018	0.683±0.024	2.068±0.00510

According to Figure 4.8, there is a similar trend in the variation of external and internal hazard indices and in each analyzed sample, the value of internal hazard index was less than the external hazard index. This different could be due to radioactive material distribution and tile composition. The internal hazard index primarily concerns radon gas and its progeny, which can be inhaled and pose internal health risks. The external hazard index, on the other hand, relates to gamma radiation exposure from the tile. If the concentration of radon-emitting radionuclides (like uranium-238) is low relative to other gamma-emitting radionuclides (like thorium-232 or

potassium-40), the internal hazard index might be lower than the external hazard index. Also different tiles may have different compositions, leading to varied levels of radon emissions and gamma radiation. For example, tiles with a higher content of potassium-40 or thorium-232 may have a higher external hazard index, while those with lower radium-226 (which decays into radon) may have a lower internal hazard index (Dizman & Keser, 2019; Ochen et al., 2021).

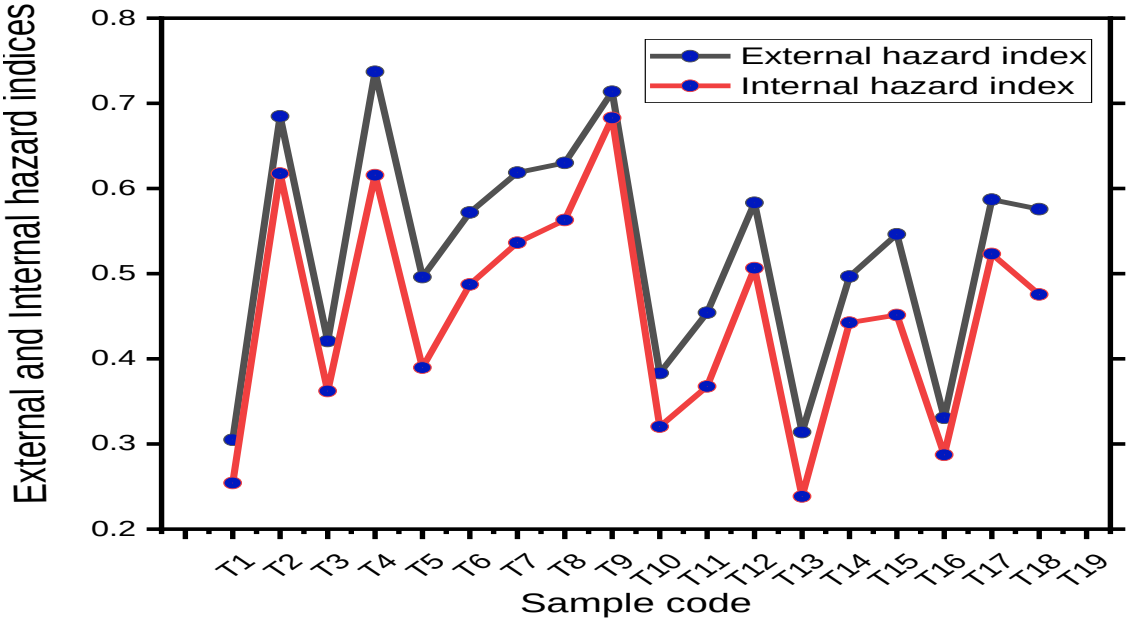

Figure 4.8: Comparative variations of external and internal hazard indices from the tile samples.

4.7.1 External and Internal Radiological Hazard Indices by Gamma Rays in the Cement Samples

The calculated values of the external hazard index and internal hazard index for the studied cement samples are presented in Table 4.7. All the cement samples that were studied had external hazard and internal hazard indices values that are less than unity, meaning that they can be used for construction with safety (UN, 2013). Similar low values of hazard indices were reported by E.Sidique, J.S Nalianya and H.P.Mammba (El-Gamal et al., 2018; Mammba et al., 2021; Nalianya et al., 2022).The values of the external hazard index ranged from 0.23±0.01 for C_7 (Ordinary Portland, Simba Cem -I 42.5N, Uganda) to 0.60±0.02 for C_1 (Portland cem –I 42.5N –OPC, Tororo, Uganda). Therefore , the use of both homemade and imported cement have no immediate negative health implications on the inhabitants, However, it is necessary to

observe and study the long-term cumulative effects on the inhabitants of buildings constructed using the selected cement brands in this study.

Table 4.7: The radiation hazard indices in the selected cement samples

Sample code	E_H	I_H	ELCR($x10^{-3}$)
C_1	0.60±0.02	0.83±0.03	1.75±0.00635
C_2	0.59±0.02	0.75±0.03	1.68±0.00523
C_3	0.31±0.01	0.39±0.02	0.93±0.00342
C_4	0.47±0.01	0.53±0.02	1.36±0.00398
C_5	0.25±0.01	0.31±0.01	0.76±0.00299
C_6	0.45±0.01	0.48±0.02	1.29±0.00391
C_7	0.23±0.01	0.26±0.01	0.67±0.00244
C_8	0.27±0.01	0.32±0.01	0.81±0.00249
C_9	0.38±0.01	0.45±0.01	1.11±0.00335
C_{10}	0.52±0.01	0.60±0.02	1.48±0.00390
C_{11}	0.46±0.01	0.57±0.02	1.33±0.00430
C_{12}	0.35±0.01	0.42±0.01	1.05±0.00316
C_{13}	0.58±0.01	0.65±0.02	1.65±0.00410
AVG	**0.42±0.01**	**0.50±0.02**	**1.22±0.00383**
Min Value	**0.23±0.01**	**0.26±0.01**	**0.67±0.00244**
Max Value	**0.60±0.02**	**0.83±0.03**	**1.75±0.00635**
GDL	**1**	**1**	**0.29**

4.8 Calculation of the Excess Life Time Cancer Risk (ELCR)

ELCR estimates the additional risk of developing cancer over a lifetime due to exposure to radiation (Mattsson & Hoeschen, 2013). ELCR provides a quantitative measure of the potential increase in cancer risk from radiation exposure, helping regulators assess whether the use of certain materials poses an acceptable risk. The measure of the risk that cancer development can happen during a person`s life time by the gamma rays from exposure to the selected samples was determined using equation 4.8 (Elgazzar & Kazem, 2015).

$$ELCR = D_{AE} x DL x RF \qquad 4.8$$

where; $ELCR$, D_{AE} , DL and RF is the excess life time cancer risk, annual Effective Dose, duration of life (70 years) and Risk factor (Sv^{-1}) or Fatal cancer risk per Sievert. For stochastic effects, ICRP uses values of RF = $0.05x10^{-3}mSv^{-1}$ for the public. The ELCR value obtained in this study was compared with the global recommended value of $0.29x10^{-3}$ (Commission, 2004; UN, 2013) .

4.7.1 Excess Lifetime Cancer Risk by the Gamma Rays from the Selected Floor Tile Samples

Figure 4.9 and the last column of Table 4.6 provides a summary of the excess life time cancer risk (ELCR) values obtained for the analyzed floor tile samples. The average of ELCR value was found to be $(1.52 \pm 0.0396)x\ 10^{-3}$, with values ranging from $(0.89 \pm 0.024)x\ 10^{-3}$ to $(2.068 \pm 0.051)x\ 10^{-3}$.The upper recommended value of $0.29x\ 10^{-3}$ was 5.24 times lower than the average excess lifetime cancer risk of the studied floor tile samples (Agbalagba et al., 2014; Commission, 2004; Mammba et al., 2021; Nations et al., 1989; Vañó et al., 2015). Consequently, it is best to avoid using floor tiles with such high ELCR values for construction as they can pose a radiation risk in the long run and increase the likelihood that people living in this environment would develop cancer. The high value of ELCR obtained in this study is also in agreement with the results reported by H.P. Mammba (Mammba et al., 2021)

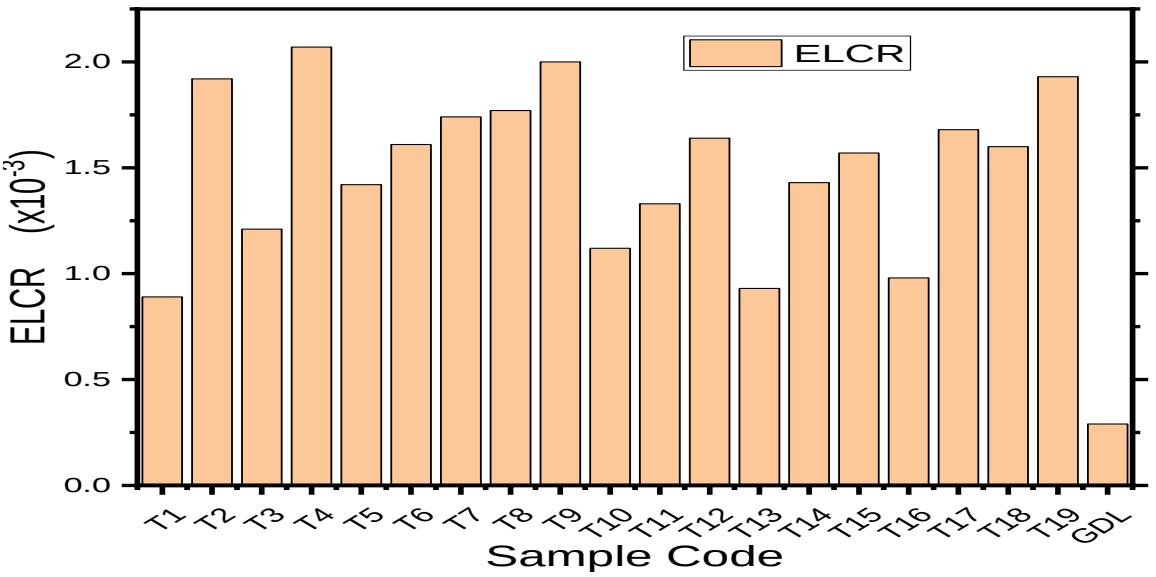

Figure 4.9: Comparative analysis of the ELCR of the studied tile samples with the global dose limit (GDL).

From the figure 4.9, all the studied sample exhibited ELCR dose above the agreed global dose limit (GDL) of $0.29x10^{-3}$. The difference between the lowest value $0.89x10^{-3}$ of the ELCR and the world agreed value of $0.29x10^{-3}$ is $0.6x10^{-3}$, which is 2.1 times the GDL. Therefore with continuous absorption of such doses, the chances of developing cancer are very high (White & Mallya, 2012).

4.7.2 Excess Lifetime Cancer Risk by Gamma Rays from the Selected Cement Brands Samples

The graphical representation in figure 4.10 and the last column of Table 4.7 provide a summary of the ELCR values obtained for the analyzed cement brand samples. The average ELCR value was found to be $(1.22 \pm 0.0383)x\ 10^{-3}$, with values ranging from $(0.67 \pm 0.0244)x\ 10^{-3}$ to $(1.75 \pm 0.0635)x\ 10^{-3}$. The upper recommended value of $0.29x\ 10^{-3}$ is 4.21 times lower than the average excess lifetime cancer risk obtained in this study (Al-Kaabi & Hmood, 2019; Nations et al., 2010; Penabei et al., 2018). Consequently, it is best to minimize using the selected cement brands with such high ELCR values for construction as they can pose a radiation risk and increase the likelihood that people living in this environment would develop cancer.

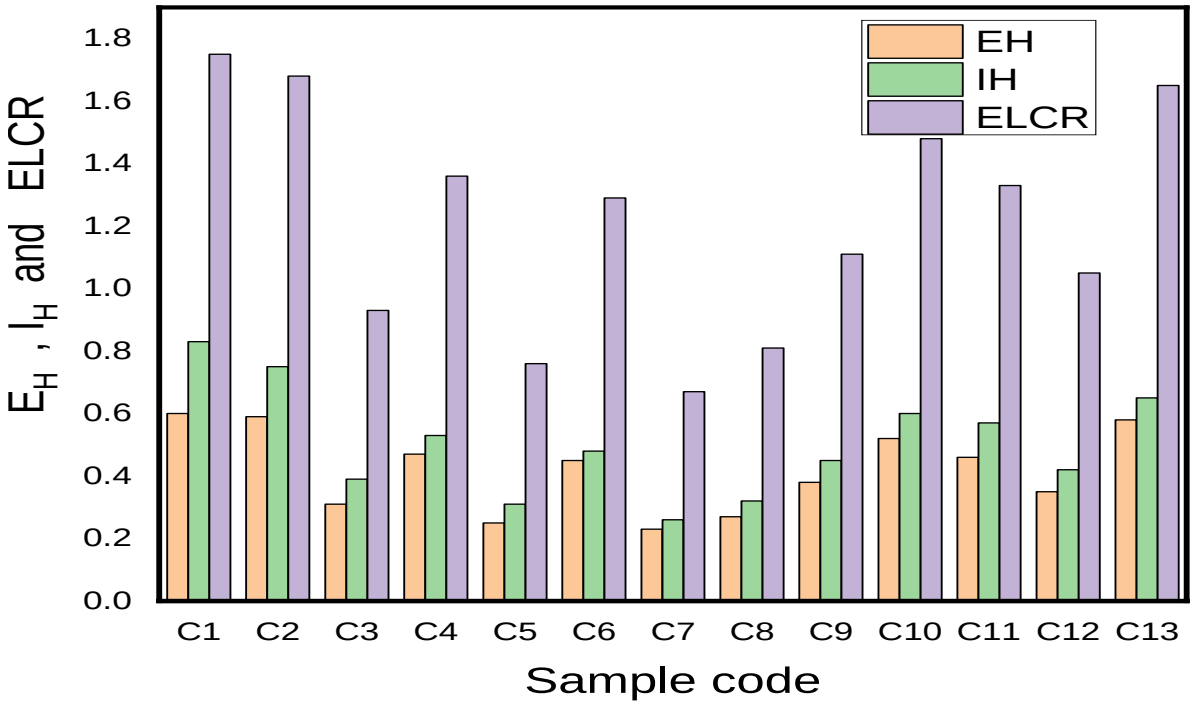

Figure 4.10: Variation of radiological hazard indices and ELCR in the analyzed cement samples.

4.8 Comparison of the Activity concentration in Samples from different countries

Table 4.8 shows the reported specific activities and radium equivalent activity in tiles and cement samples studied in different nations. The highest values for specific activities of Ra-226, Th-232, K-40, and Ra_{eq} for the cement and tiles samples were 109.00, 1574.00, 288.00, and

100.00, respectively. The variations can be ascribed, among other things, to variations in radioactive mineral contents as well as in the geological, geochemical, and geographic origin of the raw materials (Kapanadze et al., 2019b). Because potassium, thorium, and radium are not evenly distributed in the soil and rocks from which most of the building materials are made, their activity concentrations often vary significantly over a distance (Penabei et al., 2018).

Table 4.8: Specific activities and radium equivalent activity of cement and tile samples from different regions (Countries) with the current studies.

Material	**Country**	**Activity concentration ($BqKg^{-1}$)**				**Reference**
		Ra-226	**Th-232**	**K-40**	**Ra_{eq}**	
Tiles	Kenya	11.00	109.00	1574.00	288.00	(Nalianya et al., 2022)
	Egypt	38.23	42.54	439.33	-----	(Sidique et al., 2022)
	India	41.88	57.38	527.53	164.56	(Senthilkumar et al., 2014)
	China	73.00	62.00	480.00	199.00	(Xhixha et al., 2013)
	Italy	20.00	33.00	504.00	93.00	(Righi et al., 2009)
	Spain	100.00	50.00	500.00	------	(Maxwell et al., 2019)
	Uganda	**30.80**	**95.80**	**388.60**	**197.70**	**This study**
Cement	Kenya	35.80	52.70	432.00	-----	(Mulwa et al., 2023)
	Tanzania	46.00	28.00	228.00	-----	(Mammba et al., 2021)
	Egypt	47.40	57.70	312.40	57.70	(Lyngkhoi & Nongkynrih, 2020)
	Cameroon	27.01	15.24	276.53	70.10	M.Ngachin
	India	35.73	37.75	159.83	161.95	(Senthilkumar et al., 2013)
	China	68.30	51.70	173.80	162.00	(Xinwei, 2004)
	Italy	41.00	63.00	357.00	-----	(Trevisi et al., 2012)
	Uganda	**31.20**	**61.90**	**463.10**	**155.30**	**This study**
	World limit	40.00	35.00	400.00	370.00	(Commission, 2004)

It is significant to remember that the values as in Table 4.8 are not representative values for the mentioned countries, but rather relate to the regions from which the samples were taken. These comparisons demonstrate that the cement and tiles commonly used in Tororo town, Uganda, have specific activities and radium equivalent activities that, on average, are lower and some are higher than those of certain other countries included in the comparison.

Figures 4.11 and 4.12 shows the comparison of the radiation levels from cement and tiles samples in different countries. It was observed that the K-40 content was the highest as compared to other radionuclides of Ra-226 and Th-232. Kenya has the highest K-40 activity in

tiles, with 1574 $BqKg^{-1}$, followed by India, then Egypt, China, Italy, Spain, and Uganda. Spain has the highest concentration of radium (Ra-226) in its tiles (100.00 $BqKg^{-1}$), followed by China (73.00 $BqKg^{-1}$). In cement samples, Uganda has the highest value of K-40 activity with 463.10 $Bqkg^{-1}$ followed by Kenya, Italy, Egypt, Cameroon, Tanzania, china and India.

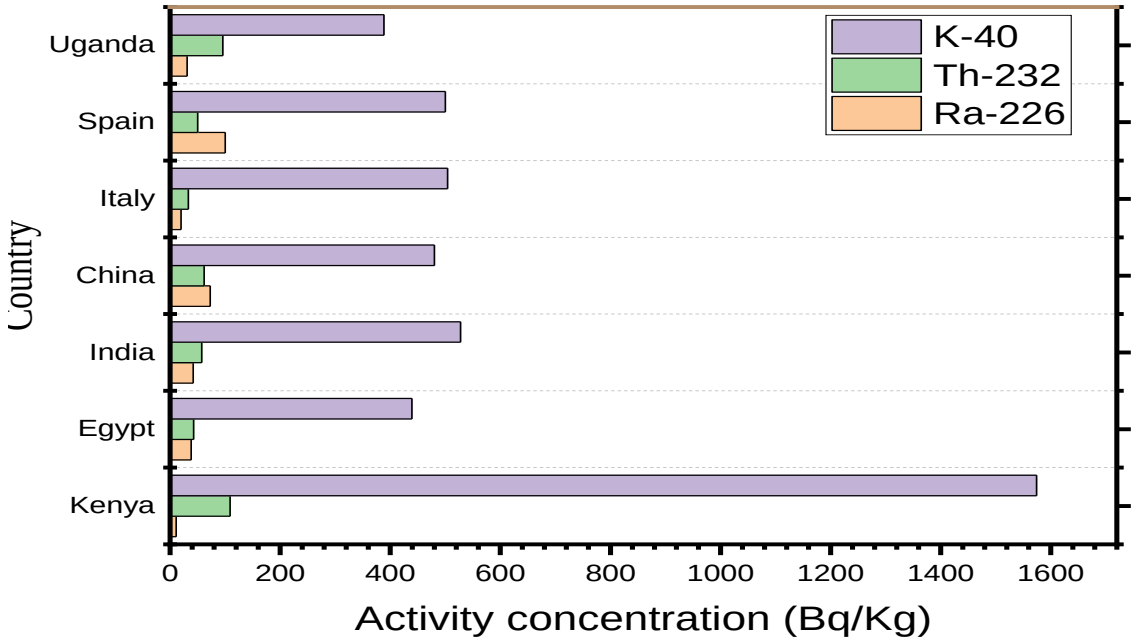

Figure 4.11: Comparison of the Activity concentration of radiations from tiles from different countries.

This comparison demonstrates how regional variations exist in the concentration of radionuclides in materials originating from the Earth's crust. Related Studies conducted in different countries show that some building materials derived from the earth's crust contain significant radioactivity (Mammba et al., 2021; Trevisi et al., 2012; Xinwei, 2005). This provides an explanation for the activity concentrations of the natural radionuclides in the tile and cement samples being higher than the global average values (Mulwa et al., 2023).

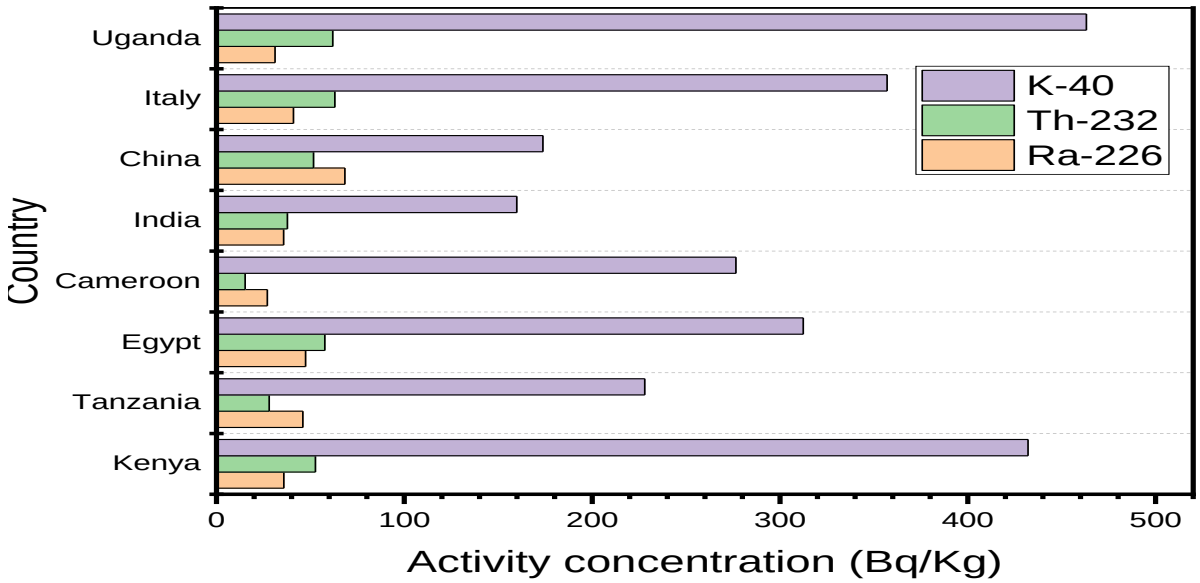

Figure 4.12: Comparison of the Activity concentration from cement samples from different countries.

CHAPTER FIVE: CONCLUSION AND RECOMMENDATIONS

5.0 Introduction

The study has essentially produced results regarding the radionuclides that emit gamma rays that are present in the floor tile and cement samples, as well as their activity concentrations, absorbed dose rates, annual effective dose equivalent, radium equivalent activity, internal and external radiological hazard indices, excess lite time cancer risk, and annual gonadal equivalent dose. Additionally, the study's results have been compared to global average activity concentrations of radionuclides, global average absorbed dose rates, global dose limit of excess life-time cancer risk, global internal and external exposure limit value of unity, and annual gonadal equivalent dose. The conclusions drawn and suggestions made are presented below.

5.1 Conclusion

The natural radionuclide content of the Ra-226, Th-232, and K-40 in the cement and floor tile samples were identified by using the technique of gamma-ray spectroscopy by NaI detector. The results may be useful in the assessment of the exposures and the radiation doses due to the natural radioactive element contents in floor tiles and cement samples used in building construction in Tororo district, Uganda.

The mean activity concentrations of Ra-226, Th-232, and K-40 were $30.8 \pm 2.3\ \mathrm{Bqkg^{-1}}$, $95.8 \pm 2.3\ \mathrm{Bqkg^{-1}}$ and $388.6 \pm 6.2\ \mathrm{Bqkg^{-1}}$in the floor tile samples and $31.2 \pm 1.7\ \mathrm{Bqkg^{-1}}$, $61.9 \pm 1.9\ \mathrm{Bqkg^{-1}}$ and $463.1 \pm 7.5\ \mathrm{Bqkg^{-1}}$ in cement samples, respectively. When compared to the world agreed means values, the average activity concentration of Th-232 in floor tiles, Ra-226, Th-232 and K-40 cement samples exceeded the recommended limit of $40\ \mathrm{Bqkg^{-1}}$, 35 $\mathrm{Bqkg^{-1}}$ and 400 $\mathrm{Bqkg^{-1}}$ respectively.

The calculated mean radium equivalent activity ($Ra_{eq} = 197.7 \pm 5.2\ \mathrm{Bqkg^{-1}}$), the absorbed gamma dose rate ($D_A = 88.3 \pm 2.3\ \mathrm{nGyh^{-1}}$), the annual effective dose ($D_{AE} = 0.43 \pm 0.011\ \mathrm{mSvy^{-1}}$) external hazard index ($E_H = 0.534 \pm 0.014$) and internal hazard index ($I_H = 0.458 \pm 0.018$) in floor tile samples were lower than the recommended limits save for absorbed gamma dose whose mean value obtained was above the recommended limit of 84 $\mathrm{nGyh^{-1}}$.

The calculated radiological parameters Ra_{eq}, D_A, D_{AE}, E_H and I_H in cement samples were 155.3 ± 5.1 Bqkg^{-1}, 71.1 ± 2.2 nGyh^{-1}, 0.349 ± 0.011 mSvy^{-1}, 0.42 ± 0.01, , 0.50 ± 0.02, respectively. These values were lower than the recommended limits, therefore, the use of these cement brands in the construction of buildings is considered to be safe for the dwellers.

The results of the present study could be a valuable database for future estimations of the impact of radioactive pollution as well as improving the specific requirements for cements and tiles in the Uganda.

5.2 Recommendations

Based on the results of this study, it is recommended that the Atomic Energy Council (AEC) and the Ministry of Works, in collaboration with the Ministry of Health, conduct an epidemiological study using common building materials to determine the dwellers' later-life radiological gonadal and cancer risk. Also, the scope of the study should be expanded to include more building materials other than cement and floor tiles only such that first level data of radionuclide contamination in the building materials is obtained. To verify the findings of this study about the radiological hazards levels of gamma-ray emitting radionuclides to the population, particularly in the samples where the radiological dosage levels were found to be higher than the world average limit, a comparable study should be conducted in other Towns in Uganda.

REFERENCES

. A. M. (2016). Radioactivity Levels and Dose Rates From Rocks in Selected Mining Areas and Quarries in Eastern Uganda. *International Journal of Research in Engineering and Technology*, *05*(03), 5–11. https://doi.org/10.15623/ijret.2016.0503002

Abbas, M. I., Noureddeen, S. F., Abbas, M. I., Distance, S., Efficiency, P., & Detector, T. (2015). *Calibration of well-type NaI(Tl) detector using a point sources measured out the detector well at different axial distances*. https://doi.org/10.1088/1748-0221/10/03/P03022

Ademola, A. K., Abodunrin, O. P., Fatai, M. A., & ... (2017). Assessment of natural radioactivity levels in cement samples commonly used for construction in Lagos and Ogun states, Nigeria. *Elixir Nucl. Radiat …*, *May 2019*. https://www.researchgate.net/profile/Oluwasayo-Abodunrin/publication/333486086_Assessment_of_natural_radioactivity_levels_in_cement_samples_commonly_used_for_construction_in_Lagos_and_Ota_environments_Nigeria/links/5ceff0874585153c3da686d3/Assessment-of-n

Ademola, J. A., & Oguneletu, P. O. (2005). Radionuclide content of concrete building blocks and radiation dose rates in some dwellings in Ibadan, Nigeria. *Journal of Environmental Radioactivity*, *81*(1), 107–113. https://doi.org/10.1016/j.jenvrad.2004.12.002

Adewoyin, O. O., Omeje, M., Joel, E. S., & Odetunmibi, O. A. (2019). Comparative assessment of natural radioactivity and radiological hazards in building tiles and sharp sand sourced locally and those imported from China and India. *International Journal of Radiation Research*, *17*(3), 455–463. https://doi.org/10.18869/acadpub.ijrr.17.3.455

Agbalagba, E. O., Osakwe, R. O. A., & Olarinoye, I. O. (2014). Comparative assessment of natural radionuclide content of cement brands used within Nigeria and some countries in the world. *Journal of Geochemical Exploration*, *142*, 21–28. https://doi.org/10.1016/j.gexplo.2013.12.002

Agency, H. P., Jr, J. D. B., Clarke, R. H., Cousins, C., Gonza, A. J., Lee, J., Lindell, B., Sasaki, Y., Meinhold, C. B., Shandala, N., Sinclair, W. K., Streffer, C., Sugier, A., Pan, Z., Pentreath, R. J., Preston, R. J., Alexakhin, R. M., Cousins, C., Aires, B., … Dicus, G. J. (n.d.). *Annals of the ICRP*.

Akhtar, N., Tufail, M., Ashraf, M., & Iqbal, M. M. (2005). Measurement of environmental radioactivity for estimation of radiation exposure from saline soil of Lahore, Pakistan. *Radiation Measurements*, *39*(1), 11–14. https://doi.org/10.1016/j.radmeas.2004.02.016

Al-Kaabi, M. A., & Hmood, A. N. (2019). Study of the Radiological Doses in Karbala city. *International Journal of Radiation Research*, *17*(1), 171–176. https://doi.org/10.18869/acadpub.ijrr.17.1.171

Al-Sewaidan, H. A. (2019). Natural radioactivity measurements and dose rate assessment of selected ceramic and cement types used in Riyadh, Saudi Arabia. *Journal of King Saud University - Science*, *31*(4), 987–992. https://doi.org/10.1016/j.jksus.2019.04.001

Amakom, M. C., Orji, E. C., Iroegbu, C., Eke, C. B., Nkwoada, U. A., Madu, D. A., Ugochuwu, G. K., & Oforma, J. T. (2018). Radionuclide concentration: The coal ash effect. *International Journal of Physical Sciences*, *13*(15), 230–234. https://doi.org/10.5897/ijps2018.4718

Aneke, F. I., & Shabangu, C. (2021). Green-efficient masonry bricks produced from scrap plastic waste and foundry sand. *Case Studies in Construction Materials*, *14*, e00515. https://doi.org/10.1016/j.cscm.2021.e00515

Assembly, G. (2016). *UNSCEAR 2016 Report Report to the General Assembly*.

Assessment, I. (n.d.). *Iaea tecdoc series* (Issue 1716).

Badawi, M. S., Gouda, M. M., El-khatib, A. M., Thabet, A. A., Salim, A. A., & Abbas, M. I. (2015). *NaI (Tl) Detector Efficiency Computation Using Radioactive Parallelepiped Sources Based on Efficiency Transfer Principle*. *2015*. https://doi.org/10.1155/2015/451932

Bediako, M., & Amankwah, E. O. (2015). Analysis of chemical composition of Portland cement in Ghana: A key to understand the behavior of cement. *Advances in Materials Science and Engineering*, *2015*. https://doi.org/10.1155/2015/349401

Bhattacharjee, P., & Sigl, G. (2000). Origin and propagation of extremely high-energy cosmic rays. *Physics Report*, *327*(3–4), 109–247. https://doi.org/10.1016/S0370-1573(99)00101-5

Biira, S., Kisolo, A. W., & D'ujanga, F. M. (2014). Concentration levels of radon in mines, industries and dwellings in selected areas of Tororo and Busia districts, Eastern Uganda. *Advances in Applied Science Research*, *5*(6), 31–44.

Biira, S., Ochom, P., & Oryema, B. (2021). Evaluation of radionuclide concentrations and average annual committed effective dose due to medicinal plants and soils commonly consumed by pregnant women in Osukuru, Tororo (Uganda). *Journal of Environmental Radioactivity*, *227*(June 2020), 106460. https://doi.org/10.1016/j.jenvrad.2020.106460

Birge, R. T. (1939). The Propagation of Errors. *American Journal of Physics*, *7*(6), 351–357. https://doi.org/10.1119/1.1991484

Blackadar, C. B. (2016). Historical review of the causes of cancer. *World Journal of Clinical Oncology*, *7*(1), 54–86. https://doi.org/10.5306/wjco.v7.i1.54

Buregyeya, A., Nwaubani, S., Schmidt, W., Kerali, A. G., & Bagampadde, U. (2018). Pozzolanic and hydration properties of kamafugites and carbonatitic lavas as supplementary cementitious materials in Portland cement. *African Journal of Science, Technology, Innovation and Development*, *10*(7), 845–859. https://doi.org/10.1080/20421338.2018.1527539

Census, H. (2006). 2002 UGANDA POPULATION AND Analytical Report. *Distribution*, *October*.

Chiozzi, P., De Felice, P., Fazio, A., Pasquale, V., & Verdoya, M. (2000). Laboratory application of NaI(Tl) γ-ray spectrometry to studies of natural radioactivity in geophysics. *Applied Radiation and Isotopes*, *53*(1–2), 127–132. https://doi.org/10.1016/S0969-8043(00)00123-8

Christiana O., N., Yohanna, A., Osagie, I., & Eric J., A. (2019). Experimental Evaluation of Radiological Hazards in Ceramic Tiles Used in the Jos-South, Area of Plateau State, Nigeria. *International Journal of Advances in Scientific Research and Engineering*, *05*(12), 01–08. https://doi.org/10.31695/ijasre.2019.33571

Clement, C. H., Stewart, F. A., Akleyev, A. V., Hauer-Jensen, M., Hendry, J. H., Kleiman, N. J., Macvittie, T. J., Aleman, B. M., Edgar, A. B., Mabuchi, K., Muirhead, C. R., Shore, R. E.,

& Wallace, W. H. (2012). ICRP publication 118: ICRP Statement on Tissue Reactions and Early and Late Effects of Radiation in Normal Tissues and Organs Ã¢â‚¬â€• Threshold Doses for Tissue Reactions in a Radiation Protection Context. *Annals of the ICRP*, *41*(1–2), 1–322. https://doi.org/10.1016/j.icrp.2012.02.001

Commission, I. (2004). *2004 Annual Report International Commission on Radiological Protection*.

Consultation, P., Steen, J. Van Der, Steel, T., Cowie, M., Janssens, A., Miyazaki, S., Tinto, R., & Services, H. (2020). *Occurring Radioactive Material (NORM) in Industrial Processes*. 1–5.

Dairiki, J. (1982). Radioactive Decay Data Tables: A Handbook of Decay Data for Application to Radiation Dosimetry and Radiological Assessments. In *Nuclear Science and Engineering* (Vol. 82, Issue 4). https://doi.org/10.13182/nse82-a21463

Dizman, S., & Keser, R. (2019). Natural radioactivity in ceramic tiles and associated radiological hazards. *International Journal of Radiation Research*, *17*(2), 245–252. https://doi.org/10.18869/acadpub.ijrr.17.2.245

Doroudiani, S., Doroudiani, B., & Doroudiani, Z. (2012). Materials that release toxic fumes during fire. In *Toxicity of Building Materials*. https://doi.org/10.1016/B978-0-85709-122-2.50009-7

Döse, M. (2016). *Ionizing Radiation in Concrete and Concrete Buildings – Empirical Assessment*.

Durusoy, A., & Yildirim, M. (2017). Determination of radioactivity concentrations in soil samples and dose assessment for Rize Province, Turkey. *Journal of Radiation Research and Applied Sciences*, *10*(4), 348–352. https://doi.org/10.1016/j.jrras.2017.09.005

El-Gamal, H., Sidique, E., El-Haddad, M., & Farid, M. E. A. (2018). Assessment of the natural radioactivity and radiological hazards in granites of Mueilha area (South Eastern Desert, Egypt). *Environmental Earth Sciences*, *77*(19). https://doi.org/10.1007/s12665-018-7880-x

Elgazzar, A. H., & Kazem, N. (2015). *Table 23.1. Sources of ionizing radiation*. 540–548.

Engineer, P., & Chemicals, O. F. (2015). Cement additives. In *Petroleum Engineer's Guide to Oil Field Chemicals and Fluids*. https://doi.org/10.1016/b978-0-12-803734-8.00010-2

Eštoková, A., & Palaš, L. (2013). *Assessment of Natural Radioactivity Levels of Cements and Cement Composites in the Slovak Republic*. 7165–7179. https://doi.org/10.3390/ijerph10127165

Evitt, S., Kingdom, U., Kingdom, U., Application, F., Data, P., Examiner, P., Bell, M. L., Examiner, A., & Sample, D. (2000). *United States Patent (19). 19*, 4–9.

Goodhead, D. T. (1989). The initial physical damage produced by ionizing radiations. *International Journal of Radiation Biology*, *56*(5), 623–634. https://doi.org/10.1080/09553008914551841

Granger, D. E., Lifton, N. A., & Willenbring, J. K. (2013). A cosmic trip: 25 years of cosmogenic nuclides in geology. *Bulletin of the Geological Society of America*, *125*(9–10), 1379–1402. https://doi.org/10.1130/B30774.1

He, J., Xiao, H., Yang, Y., Qu, J., Xu, H., & Lin, L. (2015). *A Study of Background Subtraction Method for NaI (Tl) Instrument Spectrum Based on Adaptive FWHM*. *Icmeis*, 462–468.

Higley, K. A., Kocher, D. C., Real, A. G., & Chambers, D. B. (2012). Relative biological effectiveness and radiation weighting factors in the context of animals and plants. *Annals of the ICRP*, *41*(3–4), 233–245. https://doi.org/10.1016/j.icrp.2012.06.014

Huntzinger, D. N., & Eatmon, T. D. (2009). A life-cycle assessment of Portland cement manufacturing: comparing the traditional process with alternative technologies. *Journal of Cleaner Production*, *17*(7), 668–675. https://doi.org/10.1016/j.jclepro.2008.04.007

IAEA. (2018). *Radiation Protection and Safety in Medical Uses of Ionizing Radiation : Specific Safety Guide.* 340.

IAEA. (1989). "Measurement of radionuclides in food and the environment." Technical Reports Series No. 295 (Vienna: IAEA). In *Journal of Environmental Radioactivity*.

IAEA. (2013). The Behaviours of Cementitious Materials in Long Term Storage and Disposal of

Radioactive Waste: Results of a Coordinated Research Project. In *Iaea-Tecdoc-1701*. https://www-pub.iaea.org/MTCD/Publications/PDF/TE-1701_web.pdf

IAEA ANNUAL REPORT 2010. (2010).

IAEA ANNUAL REPORT 2016 IAEA Annual Report 2016. (2016).

Janouˇ, S. (2016). *Sustainable Development Goals : A need for relevant indicators*. *60*, 565–573.

Joel, E. S., Maxwell, O., Adewoyin, O. O., Adagunodo, T. A., Olawole, O. C., Akinyemi, M. L., Arijaje, T. E., & Embong, Z. (2019). Radiological risk assessment in some imported tiles from China and its possible health implication for Nigerian users. *Journal of Physics: Conference Series*, *1299*(1). https://doi.org/10.1088/1742-6596/1299/1/012091

Joel, E. S., Maxwell, O., Adewoyin, O. O., Ehi-Eromosele, C. O., Embong, Z., & Oyawoye, F. (2018). Assessment of natural radioactivity in various commercial tiles used for building purposes in Nigeria. *MethodsX*, *5*, 8–19. https://doi.org/10.1016/j.mex.2017.12.002

Joel, E. S., Maxwell, O., Adewoyin, O. O., Ehi-eromosele, C. O., Embong, Z., & Saeed, M. A. (2018). Assessment of natural radionuclides and its radiological hazards from tiles made in Nigeria. *Radiation Physics and Chemistry*, *144*(November 2017), 43–47. https://doi.org/10.1016/j.radphyschem.2017.11.003

Kapanadze, K., Magalashvili, A., & Imnadze, P. (2019a). A study of distribution of natural radionuclides in soils and assessment of exposure hazards from terrestrial -radiation in the region of Tsalka (Georgia). *European Chemical Bulletin*, *8*(8), 274–281. https://doi.org/10.17628/ecb.2019.8.274-281

Kapanadze, K., Magalashvili, A., & Imnadze, P. (2019b). Distribution of natural radionuclides in the soils and assessment of radiation hazards in the Khrami Late Variscan crystal massif (Georgia). *Heliyon*, *5*(3), e01377. https://doi.org/10.1016/j.heliyon.2019.e01377

Klaver, M., Klemme, S., Liu, X. N., Hin, R. C., Coath, C. D., Anand, M., Lissenberg, C. J., Berndt, J., & Elliott, T. (2024). Titanium-rich basaltic melts on the Moon modulated by reactive flow processes. *Nature Geoscience*, *17*(2), 118–123. https://doi.org/10.1038/s41561-023-01362-5

Łukaszek-Chmielewska, A., Girard, M., Wojtkowski, K., Isajenko, K., & Piotrowska, B. (2018). Analysis of natural radionuclide concentrations in selected building materials available on the domestic market. *SHS Web of Conferences*, *57*, 02003. https://doi.org/10.1051/shsconf/20185702003

Lyngkhoi, B., & Nongkynrih, P. (2020). Radioactivity in building materials and assessment of risk of human exposure in the East Khasi Hills District, Meghalaya, India. *Egyptian Journal of Basic and Applied Sciences*, *7*(1), 194–209. https://doi.org/10.1080/2314808X.2020.1781747

Mammba, H. P., Balobegwa, V. A., Muhulo, A. P., Pantaleo, P. A., & Kawala, R. A. (2021). Assessment of natural radioactivity and radiation hazards of building materials in Kinondoni District, Dar es Salaam, Tanzania. *Tanzania Journal of Science*, *47*(2), 664–673. https://doi.org/10.4314/tjs.v47i2.22

mapping using gamma ray. (2003). *July*.

Mattsson, S., & Hoeschen, C. (2013). Radiation protection in nuclear medicine. *Radiation Protection in Nuclear Medicine*, 1–165. https://doi.org/10.1007/978-3-642-31167-3

Maxwell, O., Emmanuel, J. S., Olusegun, A. O., Cyril, E. E. O., Ifeanyi, A. T., & Embong, Z. (2019). A STUDY of NATURAL RADIOACTIVITY in SOME BUILDING MATERIALS in NIGERIA. *Radiation Protection Dosimetry*, *183*(3), 332–335. https://doi.org/10.1093/rpd/ncy121

Meindinyo, R. K., Agbalagba, E., & Olali, S. A. (2017). Assessment of Natural Radionuclide Content of Common Brands of Cement Used in Nigeria. *IOSR Journal of Research & Method in Education (IOSRJRME)*, *07*(02), 56–61. https://doi.org/10.9790/7388-0702025661

Michele, D., Guia, G., Sonia, C., Chiara, M., Roberto, S., & Chiara, Z. (2019). Deposits, composition and technological behavior of fluxes for ceramic tiles. *Periodico Di Mineralogia*, *88*(3), 235–257. https://doi.org/10.2451/2019PM861

Mittal, S., Rani, A., & Mehra, R. (2016). Estimation of radon concentration in soil and

groundwater samples of Northern Rajasthan, India. *Journal of Radiation Research and Applied Sciences*, *9*(2), 125–130. https://doi.org/10.1016/j.jrras.2015.10.006

Mulwa, V., Linturi, J. ., & Riara, M. (2023). Natural Radioactivity Levels of Selected Cement Brands Used in Kenya Using Gamma Ray Spectroscopy. *Journal of Environment Pollution and Human Health*, *11*(2), 46–50. https://doi.org/10.12691/jephh-11-2-4

Nalianya, J. S., Waswa, M. N., Maingi, F., & Wanyama, C. K. (2022). *Assessment of Radiation Dose Levels in Tiles Used for Decoration in Bungoma County , Kenya*. *IX*(Iii), 3–7.

National Planning Authority. (2020). Third National Development Plan (NDPIII) 2020/21-2024/25. *National Planning Authority, January*, 1–310. http://envalert.org/wp-content/uploads/2020/06/NDP-3-Finale.pdf

Nations, U., Committee, S., & Radiation, A. (2000). *SOURCES AND EFFECTS United Nations Scientific Committee on the Effects of Atomic Radiation: Vol. I*.

Nations, U., Committee, S., & Radiation, A. (2010). *Report of the United Nations Scientific Committee on the Effects of Atomic Radiation 2010 UNSCEAR 2010 Report*.

Nations, U., Committee, S., & Radiation, A. (2013a). *UNSCEAR 2013 Report: Vol. I*.

Nations, U., Committee, S., & Radiation, A. (2013b). *UNSCEAR 2013 Report: Vol. II*.

Nations, U., Sales, P., Ix, N. E., & Isb, P. (1989). *Book review UNSCEAR Report (1988) Sources , Effects and Risks of Ionising Radiation . United Nations Scientific Committee on the Effects of Atomic Radiation , 1988 . Report to the General Carcinogenesis Book review been called into question . The questi*.

Ndour, O., Thiandoume, C., Traore, A., Cagnat, X., & Mbaye, P. (2020). Assessment of natural radioactivity and its radiological hazards in several types of cement used in Senegal. *SN Applied Sciences*, *2*(12), 1–8. https://doi.org/10.1007/s42452-020-03904-7

Ng, K. -hoon. (2003). Non-Ionizing Radiations - Sources, Biological Effects, Emissions and Exposures. *Proceedings of the International Conference on Non-Ionizing Radiation at UNITEN, October*, 1–16.

Nicoletti, G. M., Notarnicola, B., & Tassielli, G. (2002). Comparative Life Cycle Assessment of flooring materials: Ceramic versus marble tiles. *Journal of Cleaner Production*, *10*(3), 283–296. https://doi.org/10.1016/S0959-6526(01)00028-2

Notation, S. H., & Compounds, R. (1824). *Chapter 2: Portland Cement (cont.)*. *2*.

Ochen, W., D'ujanga, F. M., Oruru, B., & Olupot, P. W. (2021). Physical and mechanical properties of porcelain tiles made from raw materials in Uganda. *Results in Materials*, *11*, 100195. https://doi.org/10.1016/j.rinma.2021.100195

Of, C., & Establishments, B. (2011). *UGANDA BUREAU OF STATISTICS REPORT ON THE*. *256*.

Of, H., & Extensions, D. (2008). *INDC International Nuclear Data Committee HANDBOOK OF NUCLEAR DATA FOR SAFEGUARDS : August*.

Okello, T. (2013). Use of Local brewery Waste and Bitter Cassava Flour as a Partial Replacement of Cement for Plastering Eco Houses. *Journal of Chemical Information and Modeling*, *53*(9), 1689–1699.

Özdiş, B. E., Çam, N. F., & Canbaz Öztürk, B. (2017). Assessment of natural radioactivity in cements used as building materials in Turkey. *Journal of Radioanalytical and Nuclear Chemistry*, *311*(1), 307–316. https://doi.org/10.1007/s10967-016-5074-0

Panzi Mukhokosi, E., Mukwaya, G. W., & Enjiku, B. (2023). Structural and Mechanical Properties of Non-Glazed Ceramic Tiles Developed from Selected Mineral Deposits in Uganda. *Nano-Horizons*, *2*(2), 1–14. https://doi.org/10.25159/nanohorizons/13816

Patrick, D. O., Kefas, H. M., John, Y. M., & Ameh, V. I. (2015). *Investigation of the physical properties of tiles produced with Otukpo clay*. *May 2016*.

Penabei, S., Bongue, D., Maleka, P., Dlamini, T., Saïdou, Guembou Shouop, C. J., Halawlaw, Y. I., Ngwa Ebongue, A., & Kwato Njock, M. G. (2018). Assessment of natural radioactivity levels and the associated radiological hazards in some building materials from Mayo-Kebbi region, Chad. *Radioprotection*, *53*(4), 265–278. https://doi.org/10.1051/radiopro/2018030

Petoussi-Henss, N., Bolch, W. E., Eckerman, K. F., Endo, A., Hertel, N., Hunt, J., Pelliccioni, M., Schlattl, H., & Zankl, M. (2010). Conversion Coefficients for Radiological Protection Quantities for External Radiation Exposures. *Annals of the ICRP*, *40*(2–5), 1–257. https://doi.org/10.1016/j.icrp.2011.10.001

Population, N., & Profiles, A. S. (2017). *Area Specific Profiles Tororo District*. *April*.

Portland Cement, Third edition. (2011). In *Portland Cement, Third edition*. https://doi.org/10.1680/pc.36116

Prise, K. M., Belyakov, O. V., Newman, H. C., Patel, S., Schettino, G., Folkard, M., & Michael, B. D. (2002). Non-targeted effects of radiation: Bystander responses in cell and tissue models. *Radiation Protection Dosimetry*, *99*(1–4), 223–226. https://doi.org/10.1093/oxfordjournals.rpd.a006768

Protection, R., Basic, I., & Standards, S. (n.d.). *Radiation Protection and Safety of Radiation Sources : International Basic Safety Standards General Safety Requirements Part 3*.

Protection, R., Minerals, I., & Materials, R. (n.d.). *Safety Reports Series N o . 4 9 Assessing the Need for Radiation Protection Measures in Work Involving Minerals and*.

Publication, I. (2015). *Annals o f the ICRP* (Vol. 44, Issue 2).

Publication, S. (1977). *Special publication 461*.

Publications, L. (2007). *Learn- More Weblinks CHEMISTRY PAPER No . 4 : Environmental Chemistry MODULE No . 14 : Soil composition , micro and macronutrients CHEMISTRY PAPER No . 4 : Environmental Chemistry MODULE No . 14 : Soil composition , micro and macronutrients*. *4*.

Purnama, D. ., & Damayanti, T. (2020). Determination of internal and external hazard index of natural radioactivity in well water samples. *Journal of Physics: Conference Series*, *1436*(1), 012090. https://doi.org/10.1088/1742-6596/1436/1/012090

Report, I. A. (2011). *IAEA ANNUAL REPORT 2011*.

Ridha, A. A., & Hasan, H. A. (2016). Cancer Risk Due to the Natural Radioactivity in Cigarette

Tobacco. *Detection*, *04*(03), 54–65. https://doi.org/10.4236/detection.2016.43008

Righi, S., Guerra, R., Jeyapandian, M., Verità, S., & Albertazzi, A. (2009). Natural radioactivity in Italian ceramic tiles. *Radioprotection*, *44*(5), 413–419. https://doi.org/10.1051/radiopro/20095078

Scherer, P. O. J. (2017). *Graduate Texts in Physics Computational Physics*.

Senthamizhchelvan, S., Bravo, P. E., Esaias, C., Lodge, M. A., Merrill, J., Hobbs, R. F., Sgouros, G., & Bengel, F. M. (2010). Human biodistribution and radiation dosimetry of 82Rb. *Journal of Nuclear Medicine*, *51*(10), 1592–1599. https://doi.org/10.2967/jnumed.110.077669

Senthilkumar, G., Raghu, Y., Sivakumar, S., Chandrasekaran, A., Prem Anand, D., & Ravisankar, R. (2014). Natural radioactivity measurement and evaluation of radiological hazards in some commercial flooring materials used in Thiruvannamalai, Tamilnadu, India. *Journal of Radiation Research and Applied Sciences*, *7*(1), 116–122. https://doi.org/10.1016/j.jrras.2013.12.009

Senthilkumar, G., Ravisankar, R., Vanasundari, K., Vijayalakshmi, I., Vijayagopal, P., & Jose, M. T. (2013). Assessment of radioactivity and the associated hazards in local cement types used in Tamilnadu, India. *Radiation Physics and Chemistry*, *88*, 45–48. https://doi.org/10.1016/j.radphyschem.2013.03.002

Shahbazi-Gahrouei, D., Setayandeh, S., & Gholami, M. (2013). A review on natural background radiation. *Advanced Biomedical Research*, *2*(1), 65. https://doi.org/10.4103/2277-9175.115821

Sharma, N., Singh, J., Esakki, S. C., & Tripathi, R. M. (2015). ScienceDirect A study of the natural radioactivity and radon exhalation rate in some cements used in India and its radiological significance. *Journal of Radiation Research and Applied Sciences*, *9*(1), 47–56. https://doi.org/10.1016/j.jrras.2015.09.001

Sheppard, M. I., Allan, C. J., Lupton, L. R., Taylor, T., Tonner, P. D., River, C., & Laboratories, N. (1980). The Environment Behaviour of Uranium and Thorium. *Atomic Energy of*

Canada Limited, *Whiteshell Nuclear Research Establishment-AECL-6795*, 51.

Siddeeg, S. M., Suliman, M. A., Rebah, F. Ben, Mnif, W., Ahmed, A. Y., & Salih, I. (2018). Comparative study of natural radioactivity and radiological hazard parameters of various imported tiles used for decoration in Sudan. *Symmetry*, *10*(12), 1–10. https://doi.org/10.3390/sym10120746

Sidique, E., Hassan, S. H. A., & Dawoud, M. M. (2022). Natural Radioactivity Measurements and Radiological Hazards Evaluation for Some Egyptian Granites and Ceramic Tiles. *Sustainability (Switzerland)*, *14*(21), 1–19. https://doi.org/10.3390/su142114611

Sjostedt, S., & Bezak, E. (2010). Non-targeted effects of ionising radiation and radiotherapy. *Australasian Physical and Engineering Sciences in Medicine*, *33*(3), 219–231. https://doi.org/10.1007/s13246-010-0030-8

Smith, G. (2014). UNSCEAR 2013 Report. Volume I: Report to the General Assembly, Annex A: Levels and effects of radiation exposure due to the nuclear accident after the 2011 great east-Japan earthquake and tsunami. *Journal of Radiological Protection*, *34*(3), 725–727. https://doi.org/10.1088/0952-4746/34/3/b01

Strong, A. W., Moskalenko, I. V., & Ptuskin, V. S. (2007). Cosmic-ray propagation and interactions in the galaxy. *Annual Review of Nuclear and Particle Science*, *57*, 285–327. https://doi.org/10.1146/annurev.nucl.57.090506.123011

Tiles, W., Tiles, F., Tiles, G. P., Glazed, G., Lappato, F., Products, S., Products, L. S., Matt, M. M., Products, O. S., First, S., Stages, A., & Ground, E. (n.d.). *2 . SELECTION OF APPROPRIATE TILE 3 . APPLICATION METHODS AND INFORMATION FOR USE*.

To, R., & General, T. H. E. (2021). *UNSCEAR 2020 / 2021 Report Volume I: Vol. I*.

Trevisi, R., Risica, S., D'Alessandro, M., Paradiso, D., & Nuccetelli, C. (2012). Natural radioactivity in building materials in the European Union: A database and an estimate of radiological significance. *Journal of Environmental Radioactivity*, *105*, 11–20. https://doi.org/10.1016/j.jenvrad.2011.10.001

UBOS. (2017). Area Specific Profiles Kamuli District. *The National Population and Housing*

Census 2014, *April*, 84.

UBOS. (2020). The Uganda national household survey. *Uganda Bureau of Statistics*, 76. https://www.ubos.org/wp-content/uploads/publications/09_2021Uganda-National-Survey-Report-2019-2020.pdf

UBOS. (2022). *Monthly Merchadise Trade Statistics Bulletin*. *April*, 4.

Uganda Bureau of Statistics, (UBOS). (2016). *"National population and housing census 2014—main report," Uganda Bureau of Statistics (UBOS): Kampala, Uganda, 2016.*

UN. (2013). UNSCEAR 2013 Report. *Andystaging.Rwdev.Org*, *II*. http://andystaging.rwdev.org/sites/reliefweb.int/files/resources/UNSCEAR_2013_Report_Annex_B_Children.pdf

UNBS. (2017). Final Draft Uganda Standard: Cement-Part1: Composition, Specification and conformity criteria for common cements. *Uganda Standards*.

UNSCEAR 1993 Report.pdf. (n.d.).

USGS. (2022). *2019 Minerals Yearbook The Mineral Industry of Cambodia*. *July*.

Vañó, E., Miller, C. J., Rehani, M. M., Kang, K., Rosenstein, M., Ortiz-López, P., Mattsson, S., Padovani, R., & Rogers, A. (2015). Annals o f the ICRP. In *Protection, International Commission on Radiological* (Vol. 44, Issue 1). www.icrp.org

Volume, R. (2006). *EFFECTS OF United Nations Scientifi c Committee on the Effects of Atomic Radiation: Vol. I*.

Wallbrink, P., Scientific, T. C., & Walling, D. E. (2007). *Radionuclide Measurement Using HPGe Gamma Spectrometry*. *November 2014*. https://doi.org/10.1007/0-306-48054-9

White, S. C., & Mallya, S. M. (2012). Update on the biological effects of ionizing radiation, relative dose factors and radiation hygiene. *Australian Dental Journal*, *57*, 2–8. https://doi.org/10.1111/j.1834-7819.2011.01665.x

Windows, M., & Professional, X. P. (n.d.). *ORTEC MAESTRO-32 v7 User's Manual 777800P*.

777800.

World Health Organization. (2016). Chapter 2 : Radiation protection concepts and principles. *Communicating Radiation Risk in Pediatric Imaging*, 29–48.

Xhixha, G., Ahmeti, A., Bezzon, G. P., Bitri, M., Broggini, C., Buso, G. P., Caciolli, A., Callegari, I., Cfarku, F., Colonna, T., Fiorentini, G., Guastaldi, E., Mantovani, F., Massa, G., Menegazzo, R., Mou, L., Prifti, D., Rossi Alvarez, C., Kuqi, D. S., … Zyfi, A. (2013). First characterisation of natural radioactivity in building materials manufactured in Albania. *Radiation Protection Dosimetry*, *155*(2), 217–223. https://doi.org/10.1093/rpd/ncs334

Xinwei, L. (2004). Radioactivity level in Chinese building ceramic tile. *Radiation Protection Dosimetry*, *112*(2), 323–327. https://doi.org/10.1093/rpd/nch396

Xinwei, L. (2005). Natural radioactivity in some building materials of Xi'an, China. *Radiation Measurements*, *40*(1), 94–97. https://doi.org/10.1016/j.radmeas.2005.01.003

Yoder, R. C., Dauer, L. T., Balter, S., Boice, J. D., Grogan, H. A., Mumma, M. T., Passmore, C. N., Rothenberg, L. N., & Vetter, R. J. (2022). Dosimetry for the study of medical radiation workers with a focus on the mean absorbed dose to the lung, brain and other organs. *International Journal of Radiation Biology*, *98*(4), 619–630. https://doi.org/10.1080/09553002.2018.1549756

Youk, J., Kwon, H. W., Lim, J., Kim, E., Kim, T., Kim, R., Park, S., Yi, K., Nam, C. H., Jeon, S., An, Y., Choi, J., Na, H., Lee, E. S., Cho, Y., Min, D. W., Kim, H. J., Kang, Y. R., Choi, S. H., … Ju, Y. S. (2024). Quantitative and qualitative mutational impact of ionizing radiation on normal cells. *Cell Genomics*, *4*(2), 100499. https://doi.org/10.1016/j.xgen.2024.100499

APPENDICES

Appendix A-1

Basic Data for Cement Samples

Sample	Prominent photo peak	Centroid Energy (keV)	FWHM (keV)	Sample Mass (kg)	Time (s)	Net count (s^{-1})	Activity ($Bqkg^{-1}$)	Radionuclide
C_1	1	252.8	3.37	0.500	6000	23.791	102.90	Pb-214(Ra-226)
	2	521.24	11.27	0.500	6000	39.497	90.63	TI-208(Th-232)
	3	769.76	7.2	0.500	6000	16.031	69.26	Bi-214(Ra-226)
	4	1291.72	23.83	0.500	6000	61.221	459.60	K-40
C_2	1	244.8	2.58	0.500	6000	658	119.63	Pb-214(Ra-226)
	2	352.04	1.0	0.500	6000	48	1.78	Pb-214(Ra-226)
	3	492.24	6.29	0.500	6000	1456	84.59	TI-208(Th-232)
	4	759.24	1.04	0.500	6000	239	64.42	Bi-214(Ra-226)
	5	1279.72	3.02	0.500	6000	3586	439.74	K-40
C_3	1	484.48	4.29	0.500	6000	548	31.83	TI-208(Th-232)
	2	625.56	3.16	0.500	6000	413	11.95	Bi-214(Ra-226)
	3	779.76	1.57	0.500	6000	217	58.49	Bi-214(Ra-226)
	4	1331.72	14.7	0.500	6000	4130	506.44	K-40
C_4	1	245.84	1.7	0.500	6000	197	35.82	Pb-214(Ra-226)
	2	352.12	1.05	0.500	6000	101	3.73	Pb-214(Ra-226)
	3	491.24	6.77	0.500	6000	1415	82.20	TI-208(Th-232)
	4	1287.52	15.72	0.500	6000	4018	492.70	K-40
C_5	1	252.8	1.58	0.500	6000	197	35.81	Pb-214(Ra-226)
	2	521.2	4.81	0.500	6000	501	29.11	TI-208(Th-232)
	3	606.48	1.0	0.500	6000	55	1.59	Bi-214(Ra-226)
	4	1188	3.28	0.500	6000	3334	408.83	K-40
	5	1750.32	1.18	0.500	6000	307	26.45	Bi-214(Ra-226)
C_6	1	240.04	1.0	0.500	6000	56	10.18	Pb-214(Ra-226)
	2	481.24	8.01	0.500	6000	1407	81.74	TI-208(Th-232)
	3	1185.12	13.67	0.500	6000	4147	508.5	K-40
C_7	1	357.96	1.85	0.500	6000	42	1.55	Pb-214(Ra-226)
	2	482	2.5	0.500	6000	570	33.12	TI-208(Th-232)
	3	625.56	2.18	0.500	6000	708	20.49	Bi-214 (Ra-226)
	4	1278.8	13.88	0.500	6000	2725	334.15	K-40
	5	1750.32	5.88	0.500	6000	142	12.24	Bi-214(Ra-226)
C_8	1	492.72	1.58	0.500	6000	498	28.93	TI-208(Th-232)
	2	620.96	4.16	0.500	6000	630	18.23	Bi-214(Ra-226)
	3	1293.12	14.83	0.500	6000	4126	505.95	K-40
C_9	1	490	4.91	0.500	6000	983	57.11	TI-208(Th-232)
	2	620.96	1.32	0.500	6000	146	4.23	Bi-214(Ra-226)
	3	1187.52	11.65	0.500	6000	3547	434.95	K-40
	4	1750.32	13.88	0.500	6000	550	47.93	Bi-214(Ra-226)
C_{10}	1	490.6	6.74	0.500	6000	1520	88.31	TI-208(Th-232)
	2	625.56	4.58	0.500	6000	990	28.66	Bi-214(Ra-226)
	3	1365.12	15.15	0.500	6000	3762	461.31	K-40

	4	1717.6	2.02	0.500	6000	356	30.68	Bi-214(Ra-226)
C_{11}	1	252.8	2.83	0.500	6000	268	48.72	Pb-214(Ra-226)
	2	515.04	4.47	0.500	6000	1232	71.58	TI-214(Th-232)
	3	914.2	1.41	0.500	6000	1124	53.04	Ac-228(Th-232)
	4	1218.8	15.02	0.500	6000	4040	495.40	K-40
	5	1729.96	11.31	0.500	6000	397	34.21	Bi-214(Ra-226)
C_{12}	1	357.96	2.95	0.500	6000	304	11.24	Pb-214(Ra-226)
	2	493.64	3.76	0.500	6000	844	49.03	TI-208(Th-232)
	3	625.56	6.3	0.500	6000	643	18.61	Bi-214(Ra-226)
	4	1185.12	14.74	0.500	6000	4013	492.09	K-40
	5	1733.4	6.28	0.500	6000	464	39.98	Bi-214(Ra-226)
C_{13}	1	515.04	6.79	0.500	6000	1812	105.27	TI-208(Th-232)
	2	642.44	1.42	0.500	6000	553	16.00	Bi-214(Ra-226)
	3	1186.8	14.67	0.500	6000	3924	481.18	K-40
	4	1729.96	4	0.500	6000	433	37.31	Bi-214(Ra-226)

Note: FWHM = Full Width at Half Maximum

Appendix A-2

Basic Data for Floor Tile Samples

Sample	**Prominent photo peaks**	**Sample mass**	**FWHM** (keV)	**Centroid Energy (keV)**	**Time (s)**	**Net count rate(s^{-1})**	**Activity ($Bqkg^{-1}$)**	**Radio nuclide**
T_1	1	0.500	6.90	465.04	6000	1555	90.34	TI-208(Th-232))
	2	0.500	2.15	579.6	6000	67	2.87	TI-208(Th-232))
	3	0.500	1.19	642.44	6000	703	20.35	Bi-214(Ra-226)
	4	0.500	15.32	1178.8	6000	5363	657.64	K-40
	5	0.500	1.25	1424.08	6000	130	15.94	K-40
T_2	1	0.500	8.12	465.04	6000	1501	272.89	TI-208(Th-232))
	2	0.500	1.00	580.76	6000	104	4.45	TI-208(Th-232))
	3	0.500	2.23	642.44	6000	920	26.63	Bi-214(Ra-226)
	4	0.500	15.01	1217.2	6000	5740	703.87	K-40
	5	0.500	2.80	1394.32	6000	332	40.71	K-40
T_3	1	0.500	1.74	349.2	6000	132	4.88	Pb-214 (Ra-226)
	2	0.500	7.50	470	6000	1244	72.27	TI-208(Th-232))
	3	0.500	1.48	655.68	6000	572	16.56	Bi-214(Ra-226)
	4	0.500	14.27	1028.8	6000	5876	720.54	K-40
	5	0.500	3.88	1493	6000	189	23.18	K-40
	6	0.500	10.49	1729.96	6000	582	50.15	Bi-214(Ra-226)
T_4	1	0.500	8.27	512	6000	2375	137.98	TI-208(Th-232))
	2	0.500	13.64	1128.8	6000	5476	671.49	K-40

	3	0.500	2.84	1457.96	6000	156	19.13	K-40
	4	0.500	15.24	1729.96	6000	569	49.03	Bi-214(Ra-226)
T_5	1	0.500	8.59	517.2	6000	2164	125.72	TI-208(Th-232))
	2	0.500	1.68	965.12	6000	403	32.46	Ac-228 (Th-232)
	3	0.500	14.92	1180.84	6000	5481	672.11	K-40
	4	0.500	3.54	1433.6	6000	312	38.25	K-40
	5	0.500	1.37	1738.24	6000	501	43.17	Bi-214(Ra-226)
T_6	1	0.500	1.40	349.2	6000	609	22.52	Pb-214 (Ra-226)
	2	0.500	7.22	517.2	6000	1862	108.18	TI-208(Th-232))
	3	0.500	13.39	1198.8	6000	4609	565.18	K-40
	4	0.500	2.26	1409.32	6000	241	29.55	K-40
	5	0.500	14.28	1738.24	6000	531	45.76	Bi-214(Ra-226)
T_7	1	0.500	9.03	511.24	6000	3630	210.89	TI-208(Th-232))
	2	0.500	3.44	532.08	6000	436	25.33	TI-208(Th-232))
	3	0.500	5.25	642.44	6000	1063	30.77	Bi-214(Ra-226)
	4	0.500	14.95	1191.72	6000	4945	606.38	K-40
	5	0.500	2.27	1394.32	6000	777	95.28	K-40
	6	0.500	5.08	1759.56	6000	413	35.59	Bi-214(Ra-226)
T_8	1	0.500	1.98	349.6	6000	127	4.69	Pb-214 (Ra-226)
	2	0.500	8.31	506.24	6000	4132	240.06	TI-208(Th-232))
	3	0.500	1.00	517.2	6000	160	9.29	TI-208(Th-232))
	4	0.500	15.07	1187.52	6000	5035	617.42	K-40
	5	0.500	5.84	1457.96	6000	835	102.39	K-40
	6	0.500	10.46	1750.32	6000	580	49.98	Bi-214(Ra-226)
T_9	1	0.500	1.04	352.12	6000	171	6.33	Pb-214 (Ra-226)
	2	0.500	8.30	471.24	6000	4906	285.03	TI-208(Th-232))
	3	0.500	1.00	547.44	6000	241	14.00	TI-208(Th-232))
	4	0.500	5.19	620.44	6000	1018	29.47	Bi-214(Ra-226)
	5	0.500	12.27	1037.52	6000	3949	484.25	K-40
	6	0.500	3.45	1750.32	6000	232	19.99	Bi-214(Ra-226)
T_{10}	1	0.500	1.00	344.24	6000	161	5.96	Pb-214 (Ra-226)
	2	0.500	6.08	472.72	6000	955	55.48	TI-208(Th-232))
	3	0.500	13.25	1285.12	6000	3902	478.49	K-40
	4	0.500	10.81	1750.32	6000	528	45.50	Bi-214(Ra-226)
	1	0.500	1.00	245.84	6000	126	22.91	Pb-214 (Ra-226)
	2	0.500	3.46	512.72	6000	1099	63.85	TI-208(Th-232))

T_{11}	3	0.500	3.11	756	6000	133	35.85	Bi-214(Ra-226)
	4	0.500	12.54	1085.12	6000	4238	519.69	K-40
	5	0.500	15.4	1738.24	6000	601	51.79	Bi-214(Ra-226)
T_{12}	1	0.500	8.06	490	6000	1916	111.31	TI-208(Th-232))
	2	0.500	3.37	620.44	6000	850	24.60	Bi-214(Ra-226)
	3	0.500	13.37	1191.72	6000	4934	605.04	K-40
	4	0.500	8.87	1451.2	6000	518	63.52	K-40
	5	0.500	9.50	1759.56	6000	435	37.48	Bi-214(Ra-226)
T_{13}	1	0.500	2.11	512.72	6000	666	38.69	TI-208(Th-232))
	2	0.500	3.50	625.56	6000	791	22.89	Bi-214(Ra-226)
	3	0.500	14.22	1091.72	6000	5790	710.00	K-40
	4	0.500	9.93	1424.08	6000	639	78.36	K-40
	5	0.500	4.79	1759.56	6000	443	38.17	Bi-214(Ra-226)
T_{14}	1	0.500	1.57	324.28	6000	100	3.69	Pb-214 (Ra-226)
	2	0.500	5.09	511.04	6000	1496	86.91	TI-208(Th-232))
	3	0.500	3.42	625.56	6000	654	18.93	Bi-214(Ra-226)
	4	0.500	15.68	1085.12	6000	3979	487.93	K-40
	5	0.500	12.71	1750.32	6000	505	43.52	Bi-214(Ra-226)
T_{15}	1	0.500	4.67	465.04	6000	1543	89.64	TI-208(Th-232))
	2	0.500	2.84	650.64	6000	1368	39.60	Bi-214(Ra-226)
	3	0.500	13.74	1285.12	6000	3832	469.90	K-40
	4	0.500	8.47	1750.32	6000	419	36.10	Bi-214(Ra-226)
T_{16}	1	0.500	1.00	245.84	6000	25	4.55	Pb-214 (Ra-226)
	2	0.500	4.20	515.04	6000	766	44.50	TI-208(Th-232))
	3	0.500	2.61	622.44	6000	535	15.49	Bi-214(Ra-226)
	4	0.500	13.95	1335.12	6000	4295	526.68	K-40
	5	0.500	2.33	1750.32	6000	405	34.89	Bi-214(Ra-226)
T_{17}	1	0.500	1.00	252.8	6000	155	28.18	Pb-214 (Ra-226)
	2	0.500	6.51	462.72	6000	1820	105.74	TI-208(Th-232))
	3	0.500	4.59	610.96	6000	719	20.81	Bi-214(Ra-226)
	4	0.500	14.51	1078.8	6000	4171	511.47	K-40
	5	0.500	16.88	1738.24	6000	363	31.279	Bi-214(Ra-226)
T_{18}	1	0.500	1.00	245.84	6000	211	38.36	Pb-214 (Ra-226)
	2	0.500	4.43	492.72	6000	759	38.91	TI-208(Th-232))
	3	0.500	1.61	625.56	6000	1144	33.11	Bi-214(Ra-226)
	4	0.500	13.15	958.8	6000	2251	181.29	Ac-228 (Th-232)

	5	0.500	2.65	1194.32	6000	2308	283.02	K-40
	6	0.500	3.89	1429.56	6000	838	102.76	K-40
	7	0.500	10.62	1733.4	6000	593	51.09	Bi-214(Ra-226)
T_{19}	1	0.500	1.89	252.8	6000	243	44.18	Pb-214 (Ra-226)
	2	0.500	7.61	512.72	6000	1316	76.46	TI-208(Th-232))
	3	0.500	11.27	625.56	6000	1210	35.02	Bi-214(Ra-226)
	4	0.500	14.57	965.12	6000	2486	200.23	Ac-228 (Th-232)
	5	0.500	1.33	1194.32	6000	1582	193.99	K-40
	6	0.500	9.28	1738.24	6000	640	55.15	Bi-214(Ra-226)

Note: FWHM = Full Width at Half Maximum

Appendix B

Energy Window of the Radionuclides

Energy (Kev)	**Decay series radionuclide**	**Parent radionuclide**
>84	X-Rays	X-Rays
186	226_{Ra}	Ra-226
242	214_{Pb}	
295		
352		
609	212_{Bi}	
768		
1120		
1764		
238.6	212_{Pb}	Th-232
510.8	208_{TI}	
583.2		
2614.5		
338.3	228_{Ac}	
911.2		
968.97		
1188.83	40_{K}	40_{K}
1574.42		